AD-A080 850 UNIVERSITY OF SOUTHERN CALIFORNIA LOS ANGELES DEPT O--ETC F/G 20/2
REPORT ON WORK PERFORMED FOR OFFICE OF NAVAL RESEARCH.(U)
OCT 79 N P ONG N00014-77-C-0473

UNCLASSIFIED NL

1 OF 1
AD
A080 850

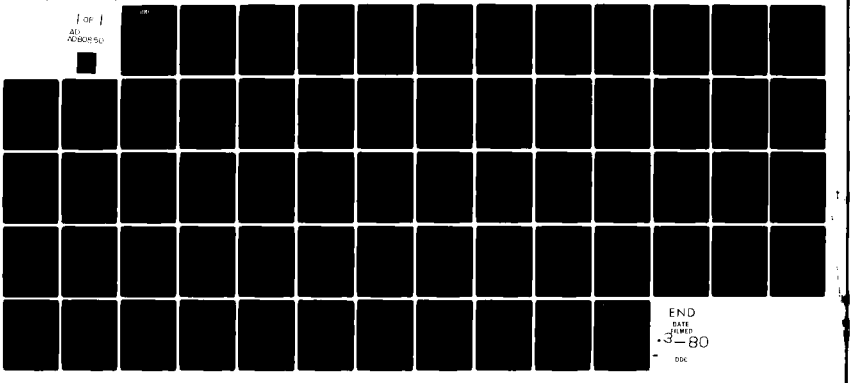

END
DATE FILMED
3-80
DDC

NR 319-122

L

1-28-80

SCB

LEVEL II 2

AD A080850

DDC FILE COPY

DDC
RECEIVED
FEB 11 1980
E

(6) REPORT ON WORK PERFORMED

FOR

OFFICE OF NAVAL RESEARCH,

CONTRACT ~~N 000-14-C0437~~ N00014-77-C-0472

(6/1/77 - 10/31/79)

(15)

(11) 31 [illegible]

Principal Investigator
Dr. N. P. Ong
Assistant Professor of Physics
Department of Physics
Los Angeles, Ca. 90007

80 2 7 007

CONTENTS

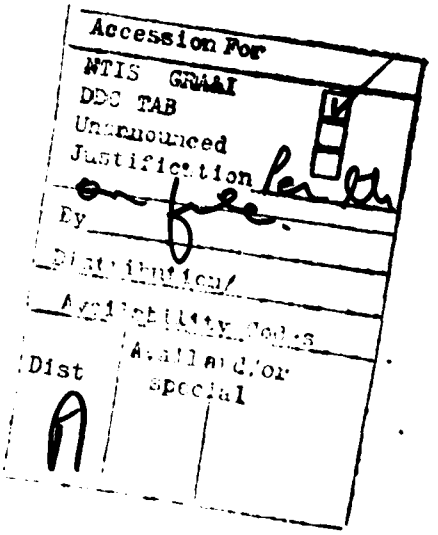

I. INTRODUCTION

In the field of quasi-one-dimensional conductors much interest has been generated by the recent discovery[1,2] of anomalous electronic transport properties in the linear-chain metal $NbSe_3$. This interest is two-fold.

First, from the theoretical point of view the observed properties give every indication that a new many-body effect involving coherent electronic charge transport is being excited in $NbSe_3$ below the phase transition where charge-density-waves (CDW) form. The theory that the coupled electron-and-lattice condensate should display conduction processes such as sliding conductivity and phase oscillations has been discussed by many workers[3-5] following the original work of Frohlich[6]. Attempts to apply these ideas to real solids have been controversial in the recent past[7] because the experimental evidence is often marginal or not reproducible. In most cases conventional single-particle theory can accommodate the observed transport properties. In $NbSe_3$ many-body effects on the electronic transport are so predominant that they were inferred to be the signature of the Frohlich mechanism long before it was experimentally established that the phase transitions were, in fact, caused by CDW formation. These anomalous transport properties are easily observed, reproducible from sample to sample, and indisputably at variance with (by orders of magnitude) the predictions of single-particle theory. The dynamics of CDW metals provide a third situation where many-body effects dominate the electronic transport. (The other two are superconductivity and the Kondo effect.)

The second viewpoint is from the applications aspect. Much of the impetus behind activity in this field has come from the hope that the Frohlich mechanism[6] may lead to high temperature superconductivity. This hope has dimmed considerably, partly because none of the one-dimensional conductors studied exceed 3,000 $(\Omega cm)^{-1}$ in conductivity at room temperature or show great conductivity enhancement in the CDW phase. However, study of the (non-Ohmic) mechanism in $NbSe_3$ (which is by far the strongest candidate for the Frohlich mechanism) will increase our understanding of the Frohlich mechanism (especially on the question of its pinning to the host lattice or suppression in most CDW systems.) Quite apart from such considerations the non-linear I-V characteristics in the CDW phase may be exploited for device applications. The strong dispersion of the Ohmic conductivity in $NbSe_3$ in the GHz region together with the I-V non-linearities may also find useful applications in signal detection at these frequencies. (Doping studies show that the dispersion can be pushed into the 100GHz region.)

II. PHYSICS OF PHASE TRANSITIONS AND ANOMALOUS TRANSPORT IN $NbSe_3$

As a background for the following report in III on the work performed on $NbSe_3$ we present here a brief discussion of the physics underlying the various experiments.

PEIERLS DISTORTION[8]: A strictly one-dimensional electron gas confined to a chain of atoms of spacing a is inherently unstable to the following distortion. The ions move to new equilibrium positions which are described by a static, longitudinal sinusoidal wave.

This superlattice distortion presents a new periodic potential which induces new gaps in the electronic band. If the superlattice periodicity is such that the new gaps occur at the Fermi level of the original band then the electron gas gains energy, because the opening of the gaps lowers the energy of the single-particle states below the gap. A phase transition[9] into the distorted phase occurs when the gain in electronic energy offsets the cost in strain energy coming from the periodic lattice distortion. In most systems the transition occurs as a function of temperature because a decrease in temperature sharpens the Fermi-Dirac distribution and enhances the gain in electronic energy. Conversely, the effect of pressure is to increase the strain energy cost of the lattice which favors the normal phase. This leads to a decrease of the transition temperature with increasing pressure.

In the condensed phase the static lattice distortion appears as faint superlattice Bragg spots[10] in x-ray and electron scattering experiments. The charge density of the condensed electrons is also modulated by the same periodicity (hence the name charge-density-wave (CDW)). Since the periodicity is tied to the Fermi Surface dimension, the CDW can either be commensurate with the original host lattice (CCDW) or incommensurate (ICDW). The conditions under which the CDW is commensurate or incommensurate, or changes from one to the other, is at present an active area of research[11].

ELECTRON TRANSPORT IN CDW STATE. In the foregoing picture the CDW transition converts a partially filled band (metal) to a filled-band (below the CDW gap). Thus in a one-dimensional system the transition is from metal to semi-conductor, as is in fact observed in KCP, TTF-TCNQ and its analogs and in TaS_3. However, in the two-dimensional layered-compounds[10] ($TaSe_2$, $NbSe_2$ etc.) and in $NbSe_3$ the transition is from metal-to-metal. Presumably, other electronic bands which do not participate in the transition survive to provide metallic conduction in the low temperature phase. In the higher-dimensional systems there exist flat portions of the Fermi surface (FS) which are sufficiently parallel[12] ("nesting" criterion) to drive the CDW instability. The superlattice periodicity is then determined by the wave vector ("spanning vector") which -- by translation in k-space -- brings one portion of the FS into coincidence with its nesting partner. Gaps occur over these nesting portions only. Other pockets of the FS are not affected by the CDW transition. To clarify the discussion of the conduction mechanisms in the CDW state we shall distinguish the uncondensed (free) carriers from the carriers in the bands that

develop a gap. The latter will be called collectively the condensate. Note that very near the transition temperature T_{CDW} free carriers can be thermally generated from the condensate as well if $kT \geq \Delta_{CDW}$. Further, to distinguish the anomalous transport properties next to be discussed, we shall call the transport by the uncondensed and thermally generated carriers "normal" conductivity (even though we are in the CDW phase). Thus, in the normal phase ($T > T_{CDW}$) current is carried by all portions of the FS. Below T_{CDW} gaps occur over the nesting portions. The gaps grow from 0 to their maximum value in analogy to the case in superconductivity. Thermal generation of quasi-particles across the growing gap leads to a semiconducting-type conductivity contribution from the nesting portions. At very low temperatures when the gaps are fully developed these quasi-particles are frozen out leaving only the uncondensed carriers to carry the current. The normal conductivity decreases to a value appropriate to the reduced FS area, but remains metallic down to the lowest temperature.

MANY-BODY EFFECTS: FROHLICH MODE, DISCOMMENSURATIONS. If the CDW is commensurate with the host lattice, the phase of the sinusoidal electronic charge density (relative to the host) can be adjusted so that peaks in the electronic density occur between adjacent metal ions. This enhances the gain in bonding energy. The CCDW is said to be "locked-in" to the host. In the incommensurate case "lock-in" is not possible if the ICDW is rigid because the gain in bonding energy averages to zero over the whole crystal. This implies that the phase ϕ has no preferred value in the ground state if the host lattice is

free of defects. In particular ϕ can be made to vary linearly in time with no cost in energy. This would correspond to the condensate sliding relative to the host lattice, and is the basis for charge transport in the Fröhlich model[4,6].

In a real solid this sliding mode is impeded by pinning to impurities and lattice defects[3]. Fukuyama and Lee[13], and Lee and Rice[5] have studied the pinning effects of impurities on an ICDW. They distinguish between the two cases of strong and weak pinning. In the strong pinning case the impurity potential is sufficiently strong that ϕ adjusts itself locally at each impurity site. In the weak pinning case the pinning energy gained by local phase deformation at each site is not sufficient to overcome the cost in strain energy. However, pinning still occurs as follows. The ICDW breaks up into finite domains. Within each domain the phase is more or less uniform and assumes an optimum value determined by all the weak impurities within the domain. The total pinning energy gained from this collection of impurities now becomes sufficient to overcome the strain energy in the domain walls (where ϕ changes rapidly). The ICDW is therefore pinned by the collection of impurities. Moreover, the pinning energy is expected to increase with the concentration of weak impurities. When an electric field is applied the condensate does not move until the field exceeds some threshold value required to dislodge the domain. Such a stick-slip process is expected to give rise to strong nonlinearities in the conductivity. Lee and Rice[5] have studied this problem and predict that the threshold field E_0 should increase as

$$E_0 \propto c^2 \qquad (1)$$

where c is the concentration of weak impurities.

The impurities also affect the ac response of the condensate. The pinned condensate will in general have a characteristic pinning frequency so that an applied weak ac field near the pinning frequency will induce segments of the condensate to undergo forced oscillations. The pinning frequency may be quite low if the pinning is weak. Again, since the pinning energy increases with impurity concentration the pinning frequency should also increase with c.

In summary, over and above the normal conductivity carried by the uncondensed carriers the CDW state should display two conductivity mechanisms which are manifestations of the Fröhlich mode. These are non-Ohmicity in the dc conductivity at relatively low fields, and excess absorption at a relatively low rf frequency. Since these are mechanisms involving collective motion of the charged condensate they cannot be described by the single-particle models, and their effects on the transport may manifest themselves as spectacular departures from conventional Drude behavior.

III. SUMMARY OF EXPERIMENTS DONE ON $NbSe_3$ AT USC

The report on the experiments performed on $NbSe_3$ at USC in the last two years (and funded by the Office of Naval Research) follows more or less the chronological order in which the experiments were done. This sequence of presentation will show in a more transparent way the evolution of the physical ideas used to describe $NbSe_3$. Some significant work performed at other institutions will be mentioned where appropriate.

1) Non-Ohmic Conductivity

Following the original observation by Monceau, Ong, and coworkers[1] at U.C. Berkeley that $NbSe_3$ is non-Ohmic below the two phase transitions at T_1 (142 K) and T_2 (58 K), as well as anomalous in its microwave absorption[2] at 9.8 GHz, we set out to measure more systematically the temperature dependence of the non-Ohmic parameters. Monceau, et al.[1], had found that the non-Ohmicity obeyed the relation

$$\sigma(E, T) = \sigma_a(T) + \sigma_b(T)\, e^{-E_0(T)/E} \qquad (2)$$

The temperature dependence of σ_a, σ_b and E_0 for both transitions were measured by us[2,14] and interpreted in terms of the CDW model as follows. Arguing from the separability of the Ohmic conductivity into two parts, one coming from the non-nesting FS portions and the other from the condensate through thermal generation of carriers, we formed the parameter[14]

$$\alpha(T) \equiv \sigma_b(T)/(\sigma_a(T) + \sigma_b(T)) \ , \qquad (3)$$

and related it to the CDW gap Δ by

$$\alpha(T) = \alpha(0) \tanh \beta\Delta/2 \ , \quad \beta = (k_B T)^{-1} \ . \qquad (4)$$

Data on α confirmed that it rapidly saturated to a constant value as T decreased, as required by Eq. (4). Moreover, by fitting Eq. (4) to the data we extracted values for the gap at both the T_1 and T_2 transition. This was the first measurement of the CDW gap in $NbSe_3$, and lent strong support to the unconfirmed (at that time) CDW model.

2) Young's Modulus

The CDW transition may also be regarded as the softening and condensation of the longitudinal phonon with $q = 2k_F$. There is therefore some likelihood that acoustic or mechanical probes may be sensitive to the transition. Working with Dr. Brill at Stanford we measured[15] the Young's Modulus in $NbSe_3$ and detected an elastic anomaly at the T_1 transition. However, no anomaly was seen to the limits of our uncertainty (10^{-4}) at the T_2 transition. The modulus was measured using a vibrating reed technique.

3) Hall Effect

One of the consequences of the appearance of a gap over portions of the FS is the loss of carriers. If the CDW model is valid in $NbSe_3$ the loss of carriers at both T_1 and T_2 should have a drastic effect on the Hall constant. We succeeded in attaching transverse probes to the small samples and were able to measure

the Hall constant both as a function of magnetic field and temperature[16]. The Hall constant does change significantly at both T_1 and T_2. However, the relative change is much larger than what one might have inferred (on the basis of a single-band model) from the conductivity data. The Hall constant also changes sign at low temperature indicating the presence of both holes and electrons. Clearly a full two-band analysis would be required to relate the measured Hall constant directly to the carrier concentrations.

4) Conductivity Anisotropy, Magnetoresistance and Two-Band Model

The conductivity anisotropy and transverse magnetoresistance were measured[17] to provide enough data for a full two-band analysis. Together with the Hall data, these measurements provided six experimental numbers to fix the six parameters of the two-band model[18] at each temperature below T_2. Finally we were able to extract the number of electrons and holes and their respective mobilities along the chain and transverse directions. This rather complete analysis provides full information on the mobilities and concentrations in the CDW phase below T_2. To our knowledge no such analysis has been carried out for any other CDW system.

5) Superlattice Measurement

At about this time various groups reported the successful detection of superlattice spots associated with the T_1 and T_2 transitions. Tsutsumi et al.[19], (Hokkaido University) using electron diffraction measured the spanning vector of the T_1 CDW to be (in units of a*, b*, c*)

$$Q_1 = (0, 0.25, 0) . \quad (5)$$

Fleming and co-workers (Bell Labs)[20] using diffuse x-ray scattering determined Q_2 (for the T_2 CDW) to be

$$Q_2 = (0.5, 0.26, 0.5) . \quad (6)$$

In addition, Fleming et al.[20], measured the superlattice spot intensity in the presence of a strong electric field and found no decrease in the spot intensity. In other words, the non-Ohmicity is not associated with a break-up of the CDW condensate.

6) Effect of Impurities on the Anomalous Transport Properties

We next inquired whether the Fröhlich mechanism, which can successfully account for the non-Ohmicity as well as the excess microwave absorption mode, was capable of making predictions which can be tested. Since the Fröhlich mode is sensitive to the presence of impurities the first obvious test is to dope the nominally pure compund with weak impurities and observe their effect on both the non-Ohmicity and microwave absorption. Specifically, Lee and Rice[5] predict that the threshold field E_0 should increase as c^2 (Eq. (1)). The excess microwave absorption should also decrease rapidly as the impurities stiffen the effective spring constant and drive up the pinning frequency. These predictions have been verified by our impurity studies[21]. The nominally pure compound was doped with Ta in the 1000 ppm range and both the dc Ohmic breakdown and the excess microwave absorption were measured as a function of c, the Ta concentration. Preliminary measurements

showed that both effects are dramatically suppressed by increasing c. The microwave absorption mode at 9.3 GHz decreases monotonically with increasing c, consistent with the pinning frequency increasing with c. The effect on the depinning field E_0 in the dc non-Ohmic measurements is even more pronounced. E_0 rises rapidly as c increases. Measurements on 17 samples showed that E_0 increases as c^2 in striking agreement with the predictions of Lee and Rice.

In some samples Ti was used as dopant instead of Ta. Since Ti is group IV it enters the lattice as a charged impurity and is expected to behave as a strong pinning center. Our results show that its effectiveness in suppressing both the non-Ohmicity and the excess microwave absorption is ten times larger than for Ta in the same concentration. This confirms that charged defects are much more effective in pinning the condensate than uncharged ones.

7) Thermopower

In collaboration with Drs. Dee and Chaikin[22] at UCLA we have measured the thermopower in the regime where non-Ohmicity appears. This was accomplished by applying a strong low-frequency ac field to the sample. In the absence of a thermal gradient across the length of the sample no dc voltage develops across the sample. When a temperature gradient ΔT is applied a dc voltage proportional to ΔT appears. If the applied ac field is zero this dc voltage gives the familiar thermopower S. In the presence of the strong ac field we measure an enhancement of S which is quite unexpected. The simple Fröhlich model would predict a decrease in S when the condensate is made to slide. At present the con-

tradictory results are not understood and further work is underway.

8) Far-Infrared Magnetoabsorption

Dr. R. Wagner (NRL, Wahsington, D.C.) in collaboration with our group has detected[23] cyclotron resonance lines in $NbSe_3$. The absorption lines occur in the far-infrared at fields of the order of 8 Tesla. Sample inhomogeneities so far have prevented a complete analysis of the line shapes despite the good reproducibility of the data. This is also a continuing project.

Present Status and Future Directions

Two and a half years ago, the nature of the phase transitions in $NbSe_3$ and the intriguing anomalous transport properties associated with the new phases was unknown. In the intervening period much work, mainly transport measurements, has been done to study the transitions as well as the anomalous properties. The CDW model has been placed on a firm footing with the discovery of two incommensurate superlattices. Furthermore, rather complete measurements on the galvanomagnetic properties in the Ohmic (normal) regime have been done, and analyzed in terms of a two-band model. All the transport measurements in the anomalous (non-Ohmic, high frequency) regimes support the Fröhlich model of a sliding CDW. This model has been shown to have impressive predictive powers in the study of impurity effects, although in the thermopower measurements it contradicts experiment. If the Fröhlich model turns out to be the correct one, $NbSe_3$ will represent the only system (so far) in which this new mechanism of charge transport (sliding conductivity) can be conveniently studied.

The questions to be addressed in future programs are:

1) What limits the conductivity of the sliding condensate? This problem clearly requires a better understanding of the pinning mechanism of various kinds of defects. The study of T and Ti impurities is a start in this direction. A related issue is the viscous coupling between the uncondensed carriers and the condensate. This may ultimately limit the maximum conductivity.

2) What is the galvanomagnetic response of the sliding condensate? Hall and magnetoresistance measurements are feasible in the anomalous regimes (non-Ohmic and microwave frequencies). The response of the condensate current to high magnetic fields should be novel and interesting.

3) What is the transient response of the condensate? The anomalously low pinning frequency of the condensate implies that the (low-current) conductivity has a measurable frequency dependence in the MHz region. Such long time constants in the electronic response have not been previously encountered in a bulk, homogeneous metal.

IV. REFERENCES

1. P. Monceau, N. P. Ong, A. M. Portis, A. Meershacut and J. Rouxel, Phys. Rev. Lett. 37, 602 (1976).
2. N. P. Ong and P. Monceau, Phys. Rev. B 16, 3443 (1977).
3. P. A. Lee, T. M. Rice and P. W. Anderson, Solid State Commun. 14, 703 (1974).
4. D. Allender, J. W. Bray, and J. Bardeen, Phys. Rev. B 9, 119 (1974); J. Bardeen, preprint 1979.
5. P. A. Lee and T. M. Rice, Phys. Rev. B 15, April 1979.
6. H. Frohlich, Proc. Roy. Soc. (London) A 223, 296 (1954).
7. See for e.g., G. A. Thomas, et al., Phys. Rev. B 13, 5105 (1976), and M. J. Cohen, et al., ibid. 13, 5111 (1976).
8. R. Peierls, Quantum Theroy of Solids, (Oxford Univ. Press, London, 1955), Ch. 5.
9. M. J. Rice and S. Strassler, Solid State Commun. 13, 1389 (1973).
10. For a review see, J. A. Wilson, F. J. DiSalvo, andF. Mahajan, Adv. Phys. 24, 117 (1975).
11. W. L. McMillan, Phys. Rev. B 14, 1496 (1976).
12. W. M. Lomer, Proc. Phys. Soc. Lond. 80, 489 (1962).
13. H. Fukuyama and P. A. Lee, Phys. Rev. B 17, 535 (1978).
14. N. P. Ong, Phys. Rev. B 17, 3243 (1978).
15. J. W. Brill and N. P. Ong, Solid State Commun. 25, 1075 (1978).
16. N. P. Ong and P. Monceau, Solid State Commun. 26, 487 (1978).
17. N. P. Ong and J. W. Brill, Phys. Rev. B 18, 5265 (1978).
18. N. P. Ong, Phys. Rev. B 18, 5272 (1978).

19. T. Tsutsumi, T. Takagaki, M. Yamamoto, Y. Shiozaki, M. Ido and T. Sambongi, Phys. Rev. Lett. 39, 1675 (1977).

20. R. M. Fleming, D. E. Moncton and D. B. McWhan, Phys. Rev. B 18, 5560 (1978).

21. N. P. Ong, J. W. Brill, J. C. Eckert, J. W. Savage, S. K. Khanna and R. B. Somoano, Phys. Rev. Lett. 42, 811 (1979).

22. R. H. Dee, P. M. Chaikin and N. P. Ong, Bull, Am. Phys. Soc. 24, 386 (1979), and Phys. Rev. Lett. (to appear).

23. R. J. Wagner and N. P. Ong, Bull. Am. Phys. Soc. 24, 388 (1979).

V. PUBLICATIONS

The publications resulting from this contract are listed chronologically.

1. "Young's Modulus of $NbSe_3$", J. W. Brill and N. P. Ong Solid State Commun. 25, 1075 (1978).

2. "Transport Studies near phase transitions in $NbSe_3$", N. P. Ong, Phys. Rev. B17, 3243 (1978).

3. "Hall effect of a linear-chain metal $NbSe_3$", N. P. Ong and P. Monceau, Solid State Commun. 26, 487 (1978).

4. "Conductivity Anisotropy and transverse magnetoresistance of $NbSe_3$", N. P. Ong and J. W. Brill, Phys. Rev. B18, 5265 (1978).

5. "Two-Band Model for $NbSe_3$ (Ohmic Regime)", N. P. Ong, Phys. Rev. B18, 5272 (1978).

6. "Effect of Impurities on the Anomalous Transport Properties of $NbSe_3$", N. P. Ong, J. W. Brill, J. C. Eckert, J. W. Savage, S. K. Khanna and R. B. Somoano, Phys. Rev. Lett. 42, 811 (1979).

7. "Electric-Field-Dependent Thermopower of $NbSe_3$", R. H. Dee, P. M. Chaikin and N. P. Ong, Phys. Rev. Lett. 42, 1234 (1979).

8. "Superconductivity in $Nb_{.95}Ta_{.05}Se_3$", W. W. Fuller, P. M. Chaikin and N. P. Ong, Solid State Commun. 30, 689 (1979).

9. "Specific Heat of $NbSe_3$ and other trichalcogenides", J. C. Eckert and N. P. Ong, manuscript in preparation.

Solid State Communications, Vol. 25, pp. 1075–1078, 1978. Pergamon Press. Printed in Great Britain

YOUNG'S MODULUS OF $NbSe_3$*

J.W. Brill†

Physics Department, Stanford University, Stanford, CA 94305, U.S.A.

and

N.P. Ong

Physics Department, University of Southern California, Los Angeles, CA 90007, U.S.A.

(*Received* 28 *October* 1977 *by A.A. Maradudin*)

Using the Barmatz vibrating reed technique we have measured the Young's modulus of $NbSe_3$. An anomaly is observed at T_1 (142 K) but not at T_2 (58 K). Taken together with published specific heat data our results provide upper (lower) bounds for the anisotropy of the transition-temperature-stress-dependence at T_1 (T_2).

1. INTRODUCTION

THE TRANSITION-METAL-TRICHALCOGENIDE $NbSe_3$ has aroused much interest because of its unusual transport properties [1, 2]. The resistivity is metallic and shows two giant anomalies [3] indicative of phase transitions occuring at T_1 (142 K) and T_2 (58 K). At temperatures below 142 K, the conductivity is highly non-Ohmic and has been shown to behave [2] as

$$\sigma = \sigma_{an} + \sigma_{bn}\, e^{-\epsilon_{0n}/\epsilon}, \quad n = 1, 2 \qquad (1)$$

where ϵ is the applied electric field and σ_{an} and σ_{bn} are field-independent quantities. In equation (1), the second subscript n labels the phase transition. The activation field ϵ_{0n} diverges close to the transition temperature and the quantity $\alpha_n \equiv \sigma_{bn}/(\sigma_{an} + \sigma_{bn})$ has been shown [4] to behave like an order parameter.

$NbSe_3$ undergoes a third transition to the superconducting state [5] when hydrostatic pressure is applied (T_c is 6 K at 10 K bar) and recent Hall effect [6] measurements show a striking loss of carriers at T_1 and T_2 which correlates with the rapid rise in the resistivity at these temperatures. The frequency dependence of the resistivity is also anomalous [2]. Both anomalies are sharply reduced at 10 GHz. The transitions have been tentatively associated [1–3] with charge-density-wave [7] (CDW) formation; the non-Ohmic behavior and anomalous frequency dependence of the conductivity have been described [2, 8] in terms of excitations in the CDW condensate. However, this hypothesis remains unverified by direct X-ray evidence.

Since CDW formation involves the softening and freezing of a phonon mode, a super-lattice distortion corresponding to the condensed mode appears below the CDW transition. It is natural to investigate the elastic properties of the system to detect anomalies at these transitions. In the layered dichalcogenides 2H-$TaSe_2$ and 2H-$NbSe_2$, where CDW formation has been experimentally established [7], strong anomalies in the Young's modulus were detected [9, 10] at the CDW transitions. The internal friction also showed striking changes near these phase transitions. Anomalies have also been observed at the Peierl's distortion temperatures in the one-dimensional conductors TTF–TCQN [11] and tri-methyl-ammonium-iodide-TCNQ [12]. To acquire more information on the transitions in $NbSe_3$, we have performed Young's modulus measurements on single crystals, utilizing the Barmatz [13] vibrating reed technique.

The results for the two samples investigated show a small anomaly in the modulus at 142 K, but no evidence of the 58 K transition was detected. Using Testardi's theory [14], we show from our results that the stress dependence of T_2 is highly anisotropic. The T_1 transition is less anisotropic, but a numerical estimate is not available until the specific heat anomaly at T_1 is measured.

2. EXPERIMENTAL

The flexural resonant frequency of a cantilevered beam of length l and thickness t is given by [9, 13]

$$f_n = \left(\frac{\kappa}{2\pi}\right)\left(\frac{\kappa_n}{l}\right)^2\left(\frac{E}{\rho}\right)^{1/2}, \qquad (2)$$

* Work supported in part by a grant from the Office of Naval Research (N00014-77-C-0473) and by the Stanford Center for Materials Research, NSF Contract No. DMR-72-03022.

† Present address: Physics Dept., University of Southern California, Los Angeles, CA 90007, U.S.A.

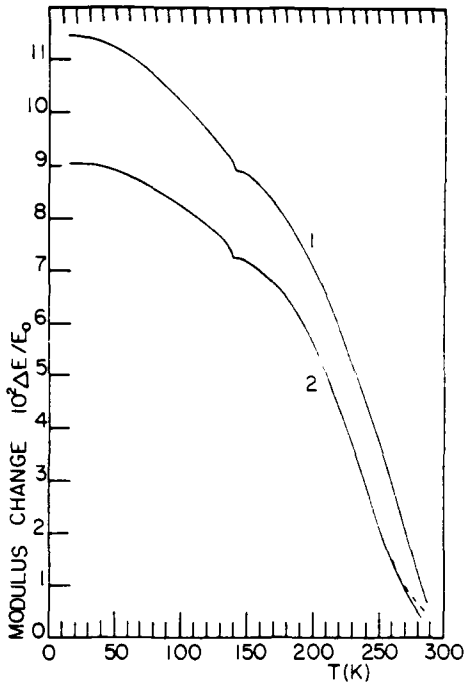

Fig. 1. The change in Young's modulus E vs temperature for two samples. The two curves for sample No.2 near room temperature indicate hysteresis between cooling (solid line) and warming (dashed line) attributed to creep in the clamp. The anomaly near 141 K is identified with the large resistivity anomaly observed at $T_1 = 142$ K. $E_0(300\text{ K}) \sim 3 \times 10^{12}$ dyne cm^{-1}.

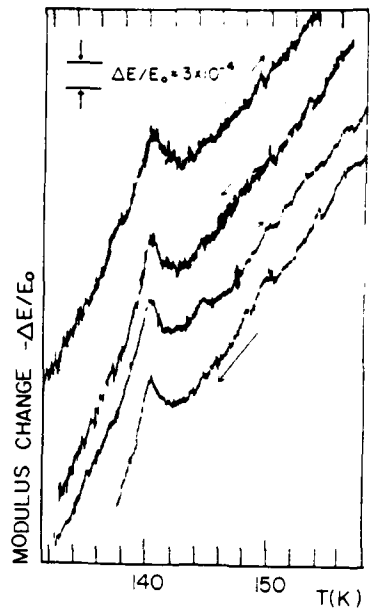

Fig. 2. XY recorder trace for four runs through the T_1 transition in sample No. 2; increasing modulus is toward bottom of figure. The upper two curves were obtained using a d.c. bias of 50 V and driving voltage of 6 V. The third and fourth curves have a.c. and d.c. voltages respectively doubled. The arrows indicate warming or cooling. The lack of hysteresis is consistent with the second order nature of transition.

where $\kappa = t/(12)^{1/2}$ is the radius of gyration, the κ_n are constants 1.875, 4.694, . . . , E is the Young's modulus in the axial direction, and ρ is the density.

Single crystals of $NbSe_3$ were mounted on the end of copper rods using low temperature solder [15]. The free end of the crystal was placed between two electrodes ~ 3 mm apart. An a.c. voltage applied to one of the electrodes excited flexural oscillations of the reed at twice the applied frequency [13]. Typical strains used at resonance were $\epsilon \lesssim 10^{-6}$. A d.c. bias was applied through 10 GΩ to the second electrode, which picked up the signal due to the modulated capacitance to the grounded reed. A MOSFET mounted directly on the pick up electrode limited the static capacitance to ground to ~ 3 pf. The signal was detected by a PAR 129A lock-in amplifier operating in the $2f$ mode. The output of the lock-in was used to phase lock the drive signal to the resonance. The measurement technique is described in more detail elsewhere [9, 12]. The lock-in output, and therefore the change in resonant frequency (and relative change in modulus) and temperature are monitored continuously on an XY recorder.

The sample is cooled with a closed-cycle helium refrigerator [16]. The temperature of the sample is measured using a copper wire thermometer [17]. A thermostatted heater allows the sample chamber temperature to be held constant (fluctuations < 1/10 K) [13] at any temperature between ambient and 20 K.

The crystals used were typically a few microns thick, 50–100 μm wide, and a few mm long. Because the width ≫ thickness, the thickness was very difficult to measure, making absolute values of the modulus very uncertain; the small thickness also made crystal mounting difficult. The measured Q's of the resonances, typically ~ 1000, were strain dependent and probably limited by friction at the clamp.

For crystal No. 1, the length equals 0.49 cm, the thickness (3.3 ± 1.0) μm, and the room temperature resonant frequency 110 Hz, giving a modulus value $E = (1.5 \pm 1.0) \times 10^{12}$ dyne cm^{-2}. Crystal No. 2 was 0.35 cm long with a resonant frequency = 670 Hz; the thickness was not determined. A third crystal (which was not cooled) was 0.16 cm long, 2.8 ± 0.7 μm thick, and had a resonant frequency = 1660 Hz, giving a modulus value $E = (5.5 \pm 2.8) \times 10^{12}$ dyne cm^{-2}. The disparity of modulus values may be due to the failure to obtain a rigid clamp (which would lower the resonant

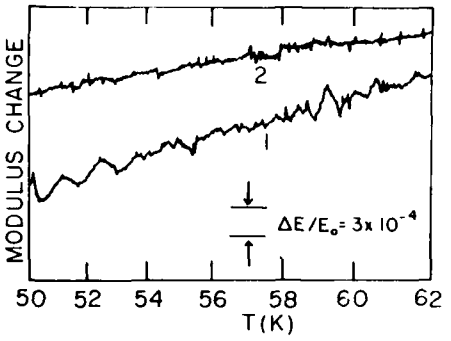

Fig. 3. *XY* recorder trace for both samples near the T_2 transition; increased modulus is toward bottom of figure. An upper limit of 10^{-4} is obtained for the anomaly size $\Delta E/E_0$.

frequency), or slightly warping a crystal when mounting (which would increase the frequency). (These conditions could also explain the slightly different slopes, $d \ln E/dT$, observed in crystals Nos. 1 and 2 when cooled, although this might also be a frequency dependent effect [9].) These ambient values of the modulus should be compared to that of 1.8×10^{12} dyne cm^{-2} for 2H-$NbSe_2$ [9].

3. RESULTS

Figure 1 shows the change in E as a function of temperature (taking the room temperature value as the base line). Although an anomaly in E appears at 142 K, no anomaly or abrupt change in slope is discernible near 58 K. The curve for sample No. 2 shows some hysteresis (broken curve) near 300 K between warming and cooling runs, probably arising from creep in the clamp. No hysteresis was detected for sample No. 1. In Fig. 2, four runs through the T_1 transition in sample 2 are displayed (with the sign of ΔE reversed from that in Fig. 1). The upper two curves were taken with a d.c. bias = 50 V and an a.c. drive of 6 V. For the third run, the a.c. voltage was increased to 12 V, and for the fourth the d.c. was increased to 100 V. The arrows indicate cooling or warming runs. The four curves demonstrate that the anomaly at T_1 is not affected by the small strains and fields used, and that there is no hysteresis effects to the accuracy of our measurements. This is consistent with non-Ohmic measurements, which show that the transitions at T_1 and T_2 are both 2nd order. [In 2H-$TaSe_2$, the first-order commensurate transition near 90 K shows [9] strong elastic hysteresis (> 5 K).] The curves in Fig. 2 were obtained at a drift rate of ~ 0.5 K min^{-1}. During each run the temperature was allowed to stabilize at several points to eliminate the possibility of non-equilibrium effects inside the sample chamber. Aside from the elastic anomaly, the T_1 transition manifests itself as a slight change in the slope of E vs T. For sample No. 1 we measure $\Delta(dE/E_0)/dT = + 1.26 \times 10^{-4}$ K^{-1} across the transition, while for sample No. 2 the change in relative slope is $+ 1.09 \times 10^{-4}$ K^{-1}. The size of the T anomaly, $\Delta E/E_0$ (defined as the difference in the value of E at the minimum and the extrapolation of the pre-transition behavior) is equal to 8.0×10^{-4} (sample No. 1) and 9.3×10^{-4} (sample No. 2).

In Fig. 3 we have plotted the recorder trace of the modulus change against temperature near 58 K for both samples. To the level of uncertainty in the measurements, $\delta E/E_0 \sim 10^{-4}$, no anomaly or slope change is detected.

As discussed above, the measured Q's of the resonance were dominated by losses at the clamp. No structure in the Q was observed at either transition for either sample. An upper limit on the internal friction due to either phase transition is $\tan \delta < 3 \times 10^{-4}$.

4. DISCUSSION

At a second-order phase transition, the change in Young's modulus, E_i (measured along the ith direction) is related to the specific heat anomaly, ΔCp, by [14]

$$(\delta T_c/\delta \sigma_i)^2 = -\frac{\Delta E}{E_i^2} T_c/\Delta Cp \tag{3}$$

where σ_i is the uniaxial stress in the ith direction and T_c is the transition temperature. Although the stress dependence of T_1 and T_2 in $NbSe_3$ have not been measured directly, it is of interest to compare the value obtained from equation (3) with published values of $\delta T_1/\delta p$, where p is the hydrostatic pressure. The pressure dependence is related to the stress dependence by:

$$\delta T_c/\delta p = -\left(\frac{\delta T_c}{\delta \sigma_a} + \frac{\delta T_c}{\delta \sigma_b} + \frac{\delta T_c}{\delta \sigma_c}\right) \tag{4}$$

where a, b and c are the three crystallographic directions. Monceau and co-workers [18] have measured $\delta T_c/\delta p$ to be -4 K $kbar^{-1}$ at both T_1 and T_2. The specific heat anomaly at T_1 has not been determined but is known to be smaller than the reported value of 6×10^5 erg cm^{-3} K^{-1} for the T_2 transition [19]. Using this value and the value of $\Delta E_b/E_b$ reported here, we obtain from equation (3) a lower bound for $|\delta T_1/\delta \sigma_b|$, (taking $E \sim 3 \times 10^{12}$ dyne cm^{-2}),

$$|\delta T_1/\delta \sigma_b| > 0.26 \text{ K kbar}^{-1}. \tag{5}$$

Assuming $\delta T_1/\delta \sigma_b$ is positive, equation (5) places an upper limit to the anisotropy in the stress dependence of T_1,

$$\tfrac{1}{2}(K_{1a} + K_{1c}) < 6.4, \tag{6}$$

where

$$K_{1i} \equiv |\delta T_1/\delta \sigma_i|/|\delta T_1/\delta \sigma_b|. \tag{7}$$

More accurate measurements to obtain ΔCp at T_1 are necessary to get specific values for K_{1a} and K_{1c}.

The present measurements detect no modulus anomaly at T_2. Thus we have an upper bound of $\Delta E_b/E_b < 10^{-4}$ at the lower transition. Using the reported specific heat anomaly value of $0.5\,R$, we may compute an upper bound for $\delta T_2 \delta\sigma_b$:

$$|\delta T_2/\delta\sigma_b| < 0.051 \text{ K kbar}^{-1}. \quad (8)$$

This implies that the stress dependence of T_2 is highly anisotropic. With the same assumptions as those that led to equation (7), we have

$$\tfrac{1}{2}(K_{2a} + K_{2c}) > 37. \quad (9)$$

In equation (9), K_{2a} is the T_2-analogue of the anisotropy factor defined in equation (7).

5. CONCLUSION

By measuring the flexural resonance frequency of two $NbSe_3$ crystals clamped at one end, we have observed an anomaly in the Young's modulus near T_1. The absence of elastic hysteresis is consistent with the second order nature of the transition. From the observed $\Delta E_b/E_b$, we have observed an upper bound [equation (7)] to the anisotropy of the stress dependence of T_1. The refining of this value must await more accurate measurements on the specific heat near T_1. The absence of any manifestation of the T_2-transition has been interpreted as a lower bound to the anisotropy of the T_2-stress dependence. It appears that this anisotropy is an order of magnitude larger than that at T_1, and may correlate with the larger size of the resistivity anomaly at T_1.

Acknowledgement – One of the authors (JWB) would like to thank W.A. Little for many useful ideas and suggestions. We are grateful to P. Monceau for early communication of results.

REFERENCES

1. MONCEAU P., ONG N.P., PORTIS A.M., MEERSCHAUT A. & ROUXEL J., *Phys. Rev. Lett.* **37**, 602 (1976).
2. ONG N.P. & MONCEAU P., *Phys. Rev. B* **16**, 3443 (1977).
3. HAEN P., MONCEAU P., TISSIER B., WAYSAND G., MEERSCHAUT A., MOLINIE P. & ROUXEL J., *Proc. 14th Int. Con. Low Temp. Phys.* (Edited by KRUSIUS & VUORIO), p. 445. North-Holland, Otaniemi, Finland (1975).
4. ONG N.P. (unpublished).
5. MONCEAU P., PEYRARD J., RICHARD J. & MOLINIE P., *Phys. Rev. Lett.* **39**, 161 (1977).
6. ONG N.P. & MONCEAU P., (unpublished).
7. For a review see WILSON J.A., DISALVO F.J. & MAHAJAN S., *Adv. Phys.* **24**, 117 (1975).
8. MAKI K., *Phys Rev. Lett.* **39**, 46 (1977).
9. BARMATZ M., TESTARDI L.R. & DISALVO F.J., *Phys. Rev.* **B12**, 4367 (1975).
10. BARMATZ M., TESTARDI L.R., DISALVO F.J. & HARPER J.M.E., *Phys. Rev.* **B13**, 4637 (1976).
11. BARMATZ M., TESTARDI L.R., GARITO A.F. & HEEGER A.J., *Solid State Commun.* **15**, 1299 (1974).
12. BRILL J.W., Unpublished Ph.D. thesis, Stanford University (1977).
13. BARMATZ M., LEAMY H.J. & CHEN H.S., *Rev. Sci. Instrum.* **42**, 885 (1971).
14. TESTARDI L.R., *Phys. Rev.* **B12**, 3849 (1975).
15. Cerrolow 117, Cerro Metal Products, Bellefonte, Pa.
16. Cryodyne Model 350, Croygenic Technology Inc., Waltham, Mass.
17. DAUPHINEE T.M. & PRESTON-THOMAS H., *Rev. Sci. Instrum.* **25**, 884 (1954).
18. CHAUSSY J., HAEN P., LASJAUNAIS J.C., MONCEAU P., WAYPARD G., WAINTAL A., MEERSCHAUT A., MOLINIE P. & ROUXEL J., *Solid State Commun.* **20**, 759 (1976).
19. MONCEAU P. (private communication).

NOTE ADDED IN PROOF

Superlattice spots have been recently observed in $NbSe_3$ by electron diffraction [19]. Recent efforts to measure the specific heat show that the T_2 anomaly is much smaller than the reported value in [18]. This alters our conclusions in equations (8) and (9).

PHYSICAL REVIEW B VOLUME 17, NUMBER 8 15 APRIL 1978

Transport studies near phase transitions in $NbSe_3$

N. P. Ong

Department of Physics, University of Southern California, Los Angeles, California 90007

(Received 8 August 1977)

The non-Ohmic transport properties of $NbSe_3$ are studied near the two phase transitions at T_1 and T_2. From the non-Ohmic data a parameter α is obtained which provides information on the fraction of Fermi surface affected by the phase transitions. By relating α to a BCS-type gap and modifying the calculations of Fedders and Martin on the spin-density-wave state in Cr we have obtained a theoretical curve for α which agrees well with the experimental data. This good agreement provides new indirect evidence for the charge-density-wave (CDW) state in $NbSe_3$. The derivative of the low-field resistivity versus temperature has also been measured and is shown to be divergent at T_1 and T_2. The index of this divergence is presented and its significance to the dimensionality of the system is discussed. Finally, we briefly discuss the possibility of explaining the non-Ohmicity below T_1 in terms of nonlinear excitations in a CDW condensate.

I. INTRODUCTION

The transition-metal trichalcogenide[1-3] $NbSe_3$ undergoes two phase transitions at the temperatures T_1 (142 K) and T_2 (58 K). The electronic conductivity is greatly perturbed by processes which set in at T_1 and T_2, as evidenced by the appearance of two giant anomalies in the resistivity. The conductivity within these anomalies has been shown[3,4] to be highly non-Ohmic, with the conductivity increasing rapidly as the applied electric field is increased. The frequency dependence of the conductivity is also anomalous.[3] At a frequency of 9 GHz, no evidence of the T_2 transition appears in the microwave resistivity while the T_1 anomaly is sharply reduced in size compared to the dc case. In conjunction with other indirect experimental evidence which will be discussed in Sec. IV A, the two transitions have been tentatively identified with the formation of charge-density waves (CDW's). If this hypothesis is valid, the non-Ohmic behavior and the anomalous frequency dependence raise the intriguing possibility that nonlinear excitations are being observed in a CDW condensate. Such excitations have been the subject of much theoretical discussion. In particular, Rice, Bishop, Krumhansl and Trullinger[5] have described the excitation of solitonlike ϕ particles in a one-dimensional (1D) CDW system. Maki[6] has also discussed the electric-field generation of solitons as a possible source of non-Ohmicity. The lack of direct experimental evidence (from x-ray or neutron scattering) for superlattice formation in $NbSe_3$ makes the CDW model rather provisional and it is entirely possible that the phase transitions are caused by a different instability. (See note added in proof.) However, all experimental evidence obtained to date is consistent with the CDW model and recent Hall-effect measurements[7] have provided direct evidence of a large loss of carriers at both T_1 and T_2. This is to be expected from a theory in which sections of the Fermi surface (FS) are destroyed by gap formation.

In this paper the behavior near T_1 and T_2 of the various parameters associated with the non-Ohmicity are presented and the results are analyzed using a model in which a fraction of the carriers are removed by gap formation at the FS. The temperature dependence of the parameter α [defined in Eq. (2)] is interpreted in terms of thermal excitations of carriers across a growing gap. An equation is derived relating α to the gap function Δ and good agreement between experiment and theory is obtained, using appropriately scaled Bardeen-Cooper-Schrieffer (BCS)[8] values for the gap Δ. To obtain the transition temperatures, the derivative of the low-electric-field resistivity with respect to temperature has been measured and shown to diverge at the two transitions. The critical index of this divergence provides an indication of the conductivity anisotropy but the conclusions are not firmly established because of the rounding off of the divergence very near T_1 and T_2 in the present data.

Below T_1 and T_2, the non-Ohmicity of the conductivity obeys the equation[3]

$$\sigma(E,T)=\sigma_{an}(T)+\sigma_{bn}(T)e^{-E_{0n}/E}, n=1,2, \quad (1)$$

where E is the applied electric field, T is the temperature, and the subscripts 1 and 2 identify the transitions. The activation field E_{0n} is strongly temperature dependent. Its temperature dependence as well as that of σ_a and σ_b have been described in Ref. 3, where the parameter α_n defined by

$$\alpha_n=\sigma_{bn}/(\sigma_{an}+\sigma_{bn}), \quad n=1,2 \quad (2)$$

was introduced. Arguing from the fact that the conductivity is proportional to the FS area we in-

terpreted[3] α_n as measuring the fraction of FS destroyed by gap formation. α_n was shown to grow from zero at T_n and saturate to a constant value at temperatures below that at which the low-field resistivity peaks. However, insofar as the above interpretation of α_n is not unique, we shall discuss a slightly different interpretation of α_n here. The new interpretation considers the α_n (suitably normalized) to measure the number of carriers thermally excited across a growing gap. As opposed to the interpretation in Ref. 3, the fraction of FS destroyed by gap formation is considered to be temperature independent. The loss of carriers is still a smooth function of temperatures because the size of the gap increases smoothly from zero, and thermal excitation of carriers across this gap decreases in relation to the size of the gap.

II. EXPERIMENTAL

All the measurements were done in the four-probe configuration with the leads attached to the sample by silver paint. The non-Ohmic data were taken using pulsed currents with a pulse width of 2 μsec and a duty cycle of 10^{-4}. Typically the maximum power dissipation across a sample of 30 Ω was 5×10^{-7}W. This was inferred to be well within the thermal capacity of the cryogenic system because a dc current dissipating the same power in the sample revealed no signs of temperature increase in the sample. Pulse heights were measured by means of a bucking variable-voltage reference as described in Ref. 3. The uncertainty and reproducibility of the measurements were 1 in 10^3, decreasing to 1 in 10^2 for the smallest pulses. To ensure that there was no hysteresis in the measured conductivity (as the E field was varied at a fixed temperature) dc measurements using a 10-μA current were performed before and after each pulse measurement. In samples which were inadvertently damaged by excessively heavy pulses (typically 25 mA into a 30-Ω sample) the measured conductivity showed large hysteresis and was not reproducible. Microscopic examination of these damaged samples invariably showed the presence of broken strands which separate from the main body of the sample. For undamaged samples no hysteresis under field variation or thermal cycling was observed to the accuracy of the measurements and results were reproducible after a warm-up to room temperature and subsequent cool down. The temperature was measured by a calibrated silicon diode sensor and the stability was maintained to ±20 mK for the 20 min required to complete the non-Ohmic measurement at each temperature point.

In the measurements of the low-field-resistivity derivative the temperature was allowed to drift at a rate of 0.1 K/min pass the transitions, and the voltage across the sample was measured in 70-mK steps with an HP standard differential voltmeter. The derivative was computed by differentiating the best quadratic fit to the resistance at five adjacent temperature points. There was a hysteresis of approximately 0.1 K between cooling and warming runs, but the two transitions were inferred to be second order because the displacement between cooling and warming curves was temperature independent to ±20 mK.

III. RESULTS

From Eq. (1) we have the conductivity in the two limits of weak and strong fields

$$\sigma(E\to 0)=\sigma_{an}, \tag{3}$$

$$\sigma(E\to\infty)=\sigma_{an}+\sigma_{bn}. \tag{4}$$

In Eq. (3), σ_{an} is just the low-field conductivity. If Eq. (1) is valid then by plotting $\ln(\sigma-\sigma_a)$ vs $1/E$, we should obtain a straight line. From the slope and intercept of this straight line the values of E_0 and σ_{bn} may be obtained. The parameter α_n is then computed from Eq. (2). In Ref. 3 preliminary measurements showed α_n to increase from zero at T_n and then saturate to a temperature-independent value at lower temperatures. E_{0n} appears to attain a large value just below T_n, decrease to a minimum, and then increase rapidly as the temperature is lowered. In this paper more extensive data on α_n and E_{0n} are reported, in particular near T_1 and T_2. Figure 1 shows α_2 and E_{02} at temperatures near T_2. α_2 (solid circles) grows smoothly from zero as $(T_2-T)^{1/2}$ close to T_2. The solid line obeys the equation $2.05\,(1-T/T_2)^{1/2}$. At lower temperatures, the experimental points deviate from the solid line. This behavior, reminiscent of the behavior of the gap function Δ in the BCS theory of superconductivity, has prompted us to relate α_n to Δ. This will be discussed in Sec. IV B. The open circles represent the measured activation field E_{02}. It may be seen to diverge as T approaches T_2^*. The source of this divergence is still unclear. The broken line indicates the low-field resistivity ρ (zero suppressed). It may be seen that deviation from the pretransition linear behavior occurs 2 K above T_2. This is ascribed to scattering from fluctuations in the gap in analogy to the case in itinerant antiferromagnets (see Sec. IV D). Figure 2 displays the same quantities α_1 and E_{01} close to the T_1 transition. The larger error bars reflect the greater uncertainty in the measurements caused by the smaller change in σ induced by a given field. (The activation field near T_1 is about an order of magnitude larger than that near T_2

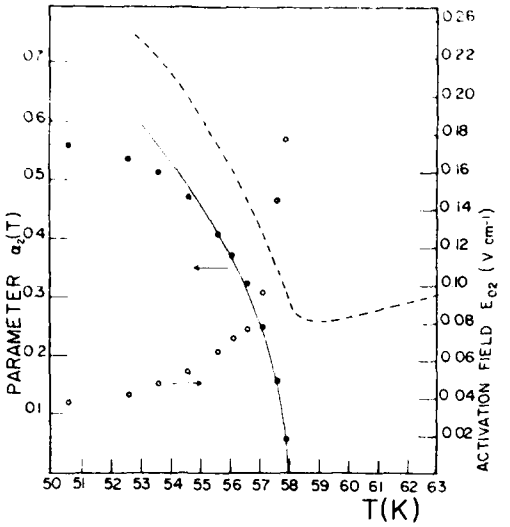

FIG. 1. Behavior of the parameter α_2 (solid circles) and activation field E_{02} (open circles) near T_2. The solid line is the mean-field prediction of the temperature dependence $(T_c - T)^{1/2}$. The broken line is the low-field resistivity (zero suppressed).

while the maximum relative increase in σ is three times smaller near T_1.) Nevertheless, behavior similar to that of α_2 and E_{02} is obtained for α_1 and E_{01}. The solid line has the equation $0.849(1 - T/T_1)^{1/2}$.

In Figs. 3 and 4 the critical behavior of α_n and

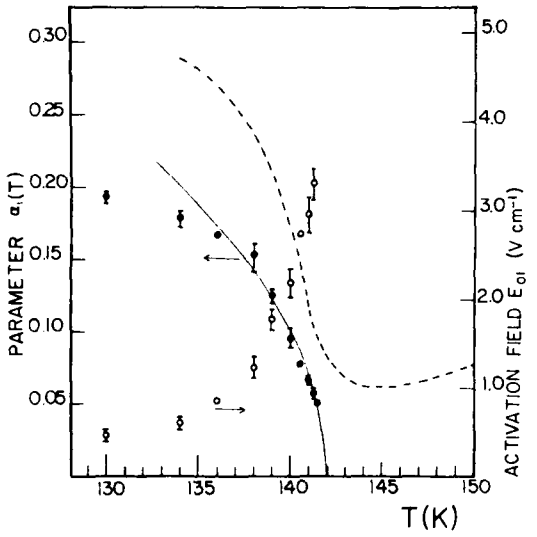

FIG. 2. Behavior of the parameter α_1 (solid circles) and activation field E_{01} (open circles) near T_1. The solid line is mean-field behavior. The broken line is the low-field resistivity with zero suppressed.

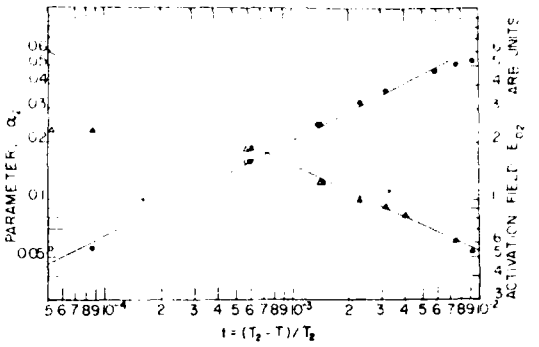

FIG. 3. Log-log plot of α_2 (circles) and E_{02} (triangles) versus the reduced temperature $t = 1 - T/T_2$. The open (solid) circles and triangles are for values of t with $T_2 = 57.94$ K (57.96 K). From the slope of the straight lines the exponent of $\alpha_2(E_{02})$ is $+0.50 \pm 0.03$ (-0.45 ± 0.03).

E_{0n} is shown. The data for both α_n and E_{0n} at the two transitions may be fitted to straight lines in the log-log plot against the reduced temperature $t = (T/T_n - 1)$. The slope of the straight lines passing through α_1 and α_2 (circles) is

$$\beta_1 = 0.50 \pm 0.07, \tag{5a}$$

$$\beta_2 = 0.50 \pm 0.03, \tag{5b}$$

where $\alpha_n \propto |t|^{\beta_n}$. In anticipation of the discussion which relates α_n to the order parameter the critical index of α_n has been identified[9] with β. The slope of the E_{0n} lines is -0.45 ± 0.05 (for E_{01}) and -0.45 ± 0.03 (for E_{02}). Due to the larger error bars in the E_{0n} data the case for a power-law behavior near T_n is less firmly established than for α_n. As is well known in the interpretation of such data the slope of the "best fit" is affected by the choice of the critical temperature T_n. In Fig. 3 the solid circles correspond to choosing T_2 as 57.96 K while the open circles correspond to $T_2 = 57.94$ K. How-

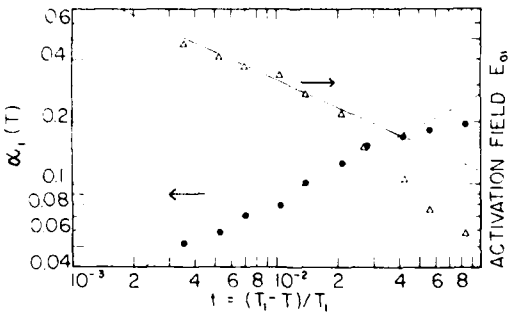

FIG. 4. Log-log plot of α_1 (circles) and E_{01} (triangles) versus the reduced temperature $t = 1 - T/T_1$. From the two lines the exponents for α_1 and E_{01} are $+0.50 \pm 0.07$ and -0.45 ± 0.05, respectively.

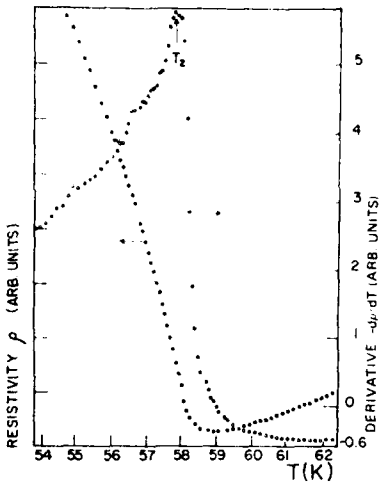

FIG. 5. Resistivity (solid circles) and its derivative with respect to temperature (open circles) near T_2. T_2 is taken to be where $d\rho/dT$ peaks.

ever, precision resistivity measurements[10] on the ferromagnetics near the Néel point have shown that the derivative of the resistivity is divergent at the Néel point. Recently, similar measurements[11,12] on the one-dimensional CDW metal tetrathiafulvalene-tetracyanoquinodimethane (TTF-TCNQ) and its selenium analog have shown the existence of a divergence in the derivative of the resistivity with respect to temperature. The transition temperature T_c in these systems is taken to be where the divergence occurs and it is found experimentally that the derivative of the resistivity behaves as a power law in the reduced temperature on either side of T_c. The critical index is different on both sides of the transition. As an aid to locating T_1 and T_2 in $NbSe_3$ the low-(electric)-field resistivity has been measured at 70 mK intervals near the two transitions. Figures 5 and 6 show for the T_2 and T_1 transitions the derivative

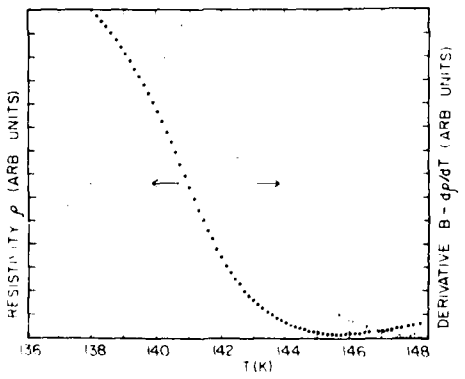

FIG. 6. Resistivity (solid circles) and its derivative with respect to temperature (open circles) near T_1.

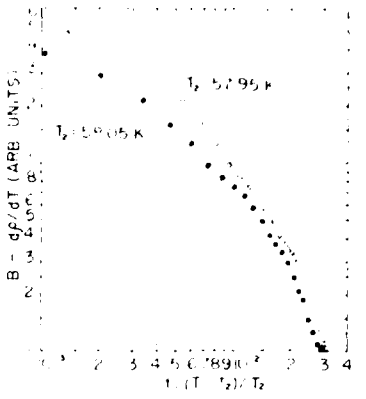

FIG. 7. Log-log plot of the derivative of the low-field resistivity (with background subtracted) vs the reduced temperature $t = (T - T_2)T_2$. The solid (open) circles correspond to choosing T_2 equal to 58.05 K (57.95 K). The slopes of the two lines are −1.0 and −1.5.

(open circles) after the subtraction of the flat pretransition background B. As may be seen, the derivative peaks at a temperature below where the derivative changes sign. In both figures the solid circles represent the low-field resistivity (with zero suppressed). Unfortunately, substantial rounding of the divergence occurs, especially at T_1, and it is not possible to ascertain the transition points to better than 0.1 K. For the T_2 transition the divergence is at 58.00 ± 0.05 K. Although this is consistent with the value of T_2 (57.96 K) used in

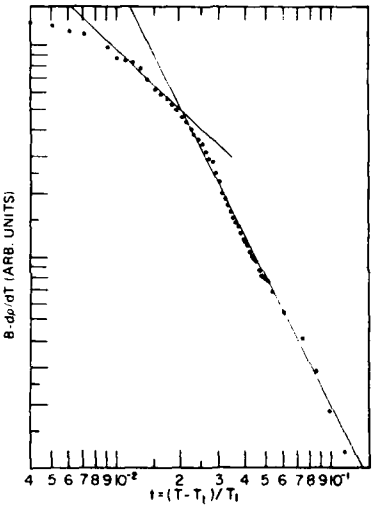

FIG. 8. Log-log plot of the derivative of the resistivity (with background subtracted) versus the reduced temperature near the T_1 transition. As discussed in the text the rounding of the divergence prevents an unambiguous measurement of the critical exponent near T_1. But at temperatures several K above T_1, the exponent is −2.0. This extends to about 15 K above T_1.

studying the critical behavior of α_2 the uncertainty of 100 mK prevents an unambiguous determination of the critical index of $d\rho/dT$. In Fig. 7 the derivative (after background subtraction) is plotted against the reduced temperature t in log-log scale. (The open circles are for $T_2 = 57.95$ K and the solid circles are for $T_2 = 58.05$ K.) The critical index lies between -1.0 and -1.5 depending on the choice of T_2. The flattening of the curves for $t < 3 \times 10^{-3}$ reflects the rounding off of the divergence. A similar situation obtains for the T_1 transition. The peak determined by the derivative data occurs at 141.0 ± 0.1 K. This is substantially lower than the value of 142 K used in the analysis of the critical behavior of α_1. This discrepancy is larger than the uncertainty in both measurements and is not understood. Figure 8 shows the log-log plot of the derivative versus t. As in Fig. 7 substantial rounding occurs near T_2 and it is not possible to extract a critical index in this region. However, for $t > 2 \times 10^{-2}$ the derivative obeys $d\rho/dT \propto t^{-2.0}$ over an interval of 15 K above T_1. The index is insensitive to any reasonable choice of T_1. This fluctuation contribution to the resistivity over such a wide range of temperature makes the T_1 transition appear much "broader" than the T_2 transition in the resistivity-temperature profile.

IV. THEORETICAL AND DISCUSSION

A. Charge-density-wave model

The arguments in favor of the CDW model in $NbSe_3$ have been reviewed in some detail in Ref. 3. Briefly, these are based on data from the pressure dependence[2] of T_1 and T_2, the detection of a heat-capacity anomaly[2] at T_2, the rapid rise of the superconducting transition temperature[13] T_c under pressure, and the extraction of the parameters[3] α_n which are consistent with gap formation at the FS. Recently, the Hall effect[7] and Young's modulus[14] have been measured. The Hall constant R_H shows an abrupt rise at both T_1 and T_2, indicating a decrease in carrier concentration at these transitions. The elastic modulus along the chain direction shows a small anomaly at T_1 (but none was detected at T_2). Both these experiments are consistent with the CDW model, since the Young-modulus measurement indicates a structural change (at least at T_1) while the Hall measurement provides direct evidence for a loss of carriers associated with these structural transitions. In the face of the accumulated indirect evidence it appears worthwhile to pursue the CDW hypothesis further even though more direct evidence (x-ray or neutron-scattering data) is not available.

We consider the Fröhlich electron-phonon (e-p) Hamiltonian

$$H = \sum_{\vec{k}} \epsilon_{\vec{k}} c_{\vec{k}}^{\dagger} c_{\vec{k}} + \sum_{\vec{q}} \hbar\omega_{\vec{q}} b_{\vec{q}}^{\dagger} b_{\vec{q}} + \frac{1}{\sqrt{N}} \sum_{\vec{k},\vec{q}} g_{\vec{q}} c_{\vec{k}+\vec{q}}^{\dagger} c_{\vec{k}} (b_{\vec{q}} + b_{-\vec{q}}^{\dagger}) , \tag{7}$$

where $c_{\vec{k}}^{\dagger}$ and $b_{\vec{q}}^{\dagger}$ are the creation operators for electrons and phonons, respectively, N is the number of ions, and $\omega_{\vec{q}}$ is the unrenormalized phonon frequencies. Within the random-phase approximation (RPA) the phonon frequencies will be renormalized[15] to

$$\Omega_{\vec{q}}^2 = \omega_{\vec{q}}^2 \left(1 + \frac{g_{\vec{q}}^2}{\hbar\omega_{\vec{q}} N} \sum_{\vec{k}} \frac{f(\epsilon_{\vec{k}}) - f(\epsilon_{\vec{k}-\vec{q}})}{\epsilon_{\vec{k}} - \epsilon_{\vec{k}-\vec{q}}}\right) . \tag{8}$$

In Eq. (8) the second term is proportional to the electronic susceptibility and $f(\epsilon_{\vec{k}})$ is the Fermi-Dirac distribution. Equation (8) may be derived by[15] computing the lowest-order contribution to the phonon self-energy and examining the pole of the phonon propagator computed within RPA. In most metals the correction is small except at $\vec{Q} \approx 2\vec{k}_F$ where the derivative of the correction with respect to q becomes infinite and Eq. (8) gives rise to the Kohn anomaly.[16] A much larger effect may arise in some systems if band pathologies allow the susceptibility to diverge for certain values of $\vec{q}$. As first pointed out by Lomer,[17] the existence of large portions of FS that are parallel (nest) would cause the denominator of the summand in Eq. (8) to vanish over a large fraction of phase space, for the value of $\vec{q}$ (called the spanning vector $\vec{Q}$) that brings about this nesting condition. This has been established as the mechanism which stabilizes spin-density wave[18] (SDW) state in Cr, and is also presumably the case in the layered compounds where CDW's occur.

The stability criterion may be taken as the condition $\Omega_{\vec{Q}} = 0$. From Eq. (8) this is equivalent to

$$1 + \frac{g_{\vec{Q}}^2}{\hbar\omega_{\vec{Q}} N} \sum_{\vec{k}} \frac{f(\epsilon_{\vec{k}}) - f(\epsilon_{\vec{k}-\vec{Q}})}{\epsilon_{\vec{k}} - \epsilon_{\vec{k}-\vec{Q}}} = 0 . \tag{9}$$

Extensive calculations on the SDW state exist in the literature. With a slight modification the results may be applied to CDW systems as well. From the paper by Fedders and Martin[19] (FM) the stability criterion for the SDW state is

$$1 + \frac{V(0)\gamma^2}{\Omega} \sum_{\vec{k}} \frac{f_a(\epsilon_{\vec{k}}) - f_b(\epsilon_{\vec{k}-\vec{Q}})}{E_a(\vec{k}) - E_b(\vec{k}-\vec{Q})} = 0 , \tag{10}$$

$$V(0) = 4\pi e^2 / \mathcal{S}_{\mathrm{FT}}^2 , \tag{11}$$

where Ω is the volume, $V(0)$ is the long-wavelength screened Coulomb interaction, γ is a matrix element, e is the electronic charge, and $\mathcal{S}_{\mathrm{FT}}$ is the Fermi-Thomas screening length. The subscripts

a, b refer to the electron and hole bands, respectively. The occurrence of two (or more) types of carriers is indicated in $NbSe_3$ by the Hall effect[7] which reverses sign at 15 K. It is possible that nesting may occur between hole and electron pockets as in Cr. In any case, the results we shall use from the FM calculation will not be affected by this assumption. The energies measured from the FS are given by

$$\epsilon_a(k) = E_a(k) - E_F = v_a(k - k_c), \tag{12}$$

$$\epsilon_b(k) = E_b(k + Q) - E_F = v_b(k - k_c), \tag{13}$$

where v_a, v_b are velocities at the FS in the two bands and k_c is an average Fermi momentum. The FM results are analogous to those of the BCS theory[8] of superconductivity. They obtain for the transition temperature T_c,

$$k_B T_c = (2\gamma_e \bar{v} \bar{k}_c f/\pi) e^{-1/\lambda_{SDW}}, \tag{14}$$

where

$$\ln f = (K^2 + 2Kk_c - 6k_c^2)/4k_c^2, \tag{15}$$

$$\lambda_{SDW} = [\gamma^2 V(0) k_c^2/2\pi^2 v], \quad \ln\gamma_e = 0.577\ldots, \tag{16}$$

$$\bar{k}_c^2 = k_c(K - k_c), \quad \bar{v} = (v_a v_b)^{1/2}, \quad v = \tfrac{1}{2}(v_a + v_b). \tag{17}$$

The assumptions made in evaluating Eq. (10) are that the surfaces of constant energy in both bands are spherical and congruent. The first Brillouin zone has also been approximated by a sphere of radius K. FM also derive an equation for the gap function Δ. In the two limits $T \to 0$, $T \to T_c$, Δ is given by

$$\Delta(T \to 0) = \pi v k_B T_c/\gamma_e \bar{v} = 1.76(v/\bar{v}) k_B T_c, \tag{18}$$

$$\Delta(T \to T_c^-) = 3.06(v/\bar{v})(k_B T_c)(1 - T/T_c)^{1/2}. \tag{19}$$

The results in Eqs. (14)–(20) may be applied to a CDW system provided we change the coupling constant λ_{SDW}. Comparing Eqs. (9) and (10) we may define the equivalent coupling constant given by

$$\lambda_{CDW} = g_Q^2 \Omega k_c^2/\hbar\omega_Q N 2\pi^2 v. \tag{20}$$

In Eq. (19) the gap increases as $(1 - T/T_c)^{1/2}$ near T_c. This may also be derived from the Landau expansion[20] of the free energy

$$F_{CDW} - F_N = a\psi^2 + (\tfrac{1}{2}b)\psi^4, \quad \psi \propto \Delta, \quad a = a'(T - T_c). \tag{21}$$

Minimizing $(F_{CDW} - F_N)$ with respect to ψ we have

$$\Delta \propto \psi = [a'(T_c - T)/b]^{1/2}. \tag{22}$$

The specific-heat discontinuity is given by

$$C_V/\Omega = T_c a'^2/b = -2T_c(F_{CDW} - F_N)/(T_c - T)^2. \tag{23}$$

Using FM's result[19] for the decrease in the free energy near the transition

$$F_{CDW} - F_N = -(k_c^2 \bar{v}^2/4\pi^4 v^3 k_B^2 T_c^2)[\tfrac{7}{8}\zeta(3)]\Delta^4, \tag{24}$$

we have for the specific-heat discontinuity

$$C_v/\Omega = [4/7\zeta(3)](k_c^2 v/\bar{v}^2)(k_B^2 T_c). \tag{25}$$

B. α parameter and the energy gap

In $NbSe_3$ the non-Ohmic results reported here indicate a strong correlation between the behavior of α_n in Figs. 1 and 2 and the order parameter described by Eq. (22). In the following, arguments will be developed to establish the relationship of α with the gap Δ. Although the non-Ohmic behavior is still not understood it is possible to extract information on the FS by examining the $E = 0$ and $E = \infty$ limits of the conductivity. We make the assumption that the drop in conductivity at T_1 and T_2 is due to the loss of FS area which results from gap formation over the nesting fraction. Since the gap is very small for temperatures near T_c there will be substantial thermal excitation of carriers across the gap at these temperatures. As the gap increases, these excitations will drop rapidly in number. In the low E-field limit we may express the conductivity as[21] (suppressing the n subscript)

$$\sigma(E \to 0) = \sigma_N + \sigma_G 2f(\beta\Delta), \tag{26}$$

$$f(\beta\Delta) = (e^{\beta\Delta} + 1)^{-1}. \tag{27}$$

In Eq. (26), $\beta = (k_B T)^{-1}$, Δ is the gap size, and σ_N (σ_G) represents the conductivity associated with the FS area not affected by the gap (destroyed by the gap). Comparing Eq. (26) with Eq. (3) we have

$$\sigma_a = \sigma_N + 2f\sigma_G. \tag{28}$$

In the strong-field limit excitations induced by the infinite field saturate the non-Ohmic mechanism and we recover the pretransition behavior [obtained by setting $\Delta = 0$ in Eq. (26)]. From Eq. (4) we have

$$\sigma_a + \sigma_b = \sigma_N + \sigma_G. \tag{29}$$

Using Eqs. (28) and (29) in Eq. (2), α may be written

$$\alpha = [\sigma_G/(\sigma_N + \sigma_G)] \tanh(\tfrac{1}{2}\beta\Delta). \tag{30}$$

Insofar as σ_N and σ_G have the same temperature dependence, the coefficient of $\tanh(\frac{1}{2}\beta\Delta)$ in Eq. (30) will be only weakly temperature dependent. Near T_c we may expand [using Eq. (19)]

$$\alpha(T)/\alpha(0) \simeq \tfrac{1}{2}\beta_c\Delta \simeq 1.53(1 - T/T_c)^{1/2}(v/\bar{v}). \tag{31}$$

This accounts for the behavior of $\alpha(T)$ shown in Figs. 1–4. In Eq. (31), $\alpha(0)$ is the value of $\alpha(T)$ at $T = 0$ and $\beta_c = (kT_c)^{-1}$. Taking the experimental values appropriate to the T_2 transition

$$\alpha_2(0) = 0.63 \pm 0.01 \tag{32}$$

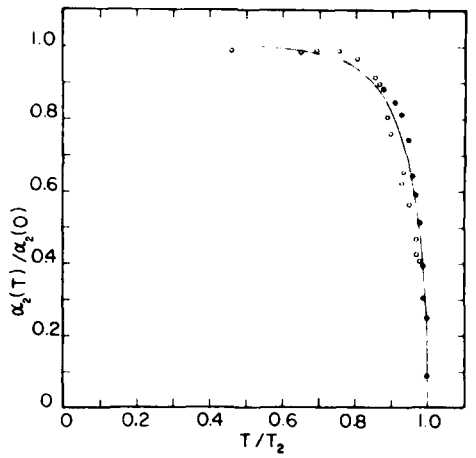

FIG. 9. Temperature dependence of $\alpha_2(T)/\alpha_2(0)$. The line is the theoretical expression $\tanh(\frac{1}{2}\beta\Delta)$ [see Eq. (30)] with $\Delta = 2.12\,\Delta_{BCS}$. The solid circles are the data from Fig. 1 while the open circles, which have more scatter, are from previously published measurements (Ref. 3) on another sample.

and

$$\alpha_2(T) = 2.05(1 - T/T_2)^{1/2}, \quad T \to T_2^-, \tag{33}$$

we have for $(v/\bar{v})_2$ the value [using Eq. (33) in Eq. (31)]

$$(v/\bar{v})_2 = 2.12 \pm 0.05. \tag{34}$$

Equation (34) expresses the ratio of the gap measured in $NbSe_3$ (at T_2) and the BCS gap. From Eqs. (18) and (34) we derive a theoretical value for the zero-temperature gap,

$$\Delta_2(0) = 3.73 k_B T_2 = 19 \text{ meV}. \tag{35}$$

At the T_1 transition the corresponding numbers are

$$(v/\bar{v})_1 = 2.8, \quad \Delta_1(0) = 60 \text{ meV}. \tag{36}$$

In Fig. 9 we compare the experimental data on α_2 with the BCS-FM model. The measured values of $\alpha_2(T)/\alpha_2(0)$ for two samples are compared with Eq. (30). The line is the theoretical curve $\tanh(\frac{1}{2}\beta\Delta)$. Values of Δ were obtained by multiplying the values of Δ_{BCS} provided by Mühlschlegel[22] by the scale factor $(v/\bar{v})_2$ given in Eq. (34). The solid circles are the data in Fig. 1 while the open circles which show more scatter are from earlier published results[3] on another sample.

The Landau-type mean-field theory predicts that the electronic specific heat shows a discontinuity at T_2 with a contribution given by Eq. (25). Although thermal measurements on $NbSe_3$ are sparse we may venture a comparison with the early results of Chaussy *et al.*[2] The specific heat shows a large anomaly (6×10^5 erg/cm^{3}K) at 52 K. This is to be compared with the 1.7×10^5 erg/cm^{3}K anomaly at the CDW transition[23] in $2H$-$NbSe_2$. Using Eq. (34) in Eq. (35) we compute a discontinuity in C_v/Ω of 9×10^3 (3×10^4) erg/cm^{3}K assuming a carrier density of 10^{20} cm^{-3} (10^{22} cm^{-3}), and an effective mass of 0.3 times the free-electron mass.[24] The electronic contribution is clearly too small to account for the large observed anomaly, and one has to include the lattice contribution. However, a large lattice contribution would appear to be inconsistent with the Young's modulus (ϵ) measurements[14] which detected no change in ϵ to 3 parts in 10^4 at T_2. More-accurate measurements of the heat capacity at both transitions are necessary before a realistic estimate of the electronic contribution can be made.

C. Activation field E_0 and nonlinear excitations

In many ways the non-Ohmicity of the conductivity below T_1 is the most interesting and puzzling property of $NbSe_3$. Efforts to interpret the observed behavior of σ given by Eq. (1) have not been successful. The activated form of σ strongly suggests an electric-field induced quantum tunneling process. However, the very small E-field values (0.1–1 V/cm) needed to induce non-Ohmicity have posed great difficulties in comparing theoretical expressions with experimental data. The simplest theory which reproduces Eq. (1) is that of Zener tunneling[4] across a gap at the FS. However, the magnitude of the gap arrived at using measured values of E_0 is two orders of magnitude smaller than $k_B T$. The E-field creation of soliton-antisoliton pairs in a one-dimensional CDW condensate has been discussed by Maki.[6] In this model the electric field induces a tunneling from a region in ϕ space (where ϕ is the CDW phase) to another region which corresponds to the appearance of a soliton-antisoliton pair. Interpreting Eq. (1) in terms of Maki's mechanism again leads to values of the soliton rest energy two orders of magnitude smaller than $k_B T$. Thus, the thermal creation of these solitons would appear to overwhelm the quantum creation at temperatures near T_1 and T_2. Recently, Larkin and Lee[25] (LL) have considered the problem of a one-dimensional CDW pinned by impurities, and the nonlinear conductivity arising from the quantum tunneling between impurity sites. In the strong pinning case they obtain for the non-Ohmic resistivity

$$\rho \propto \exp\{[2\pi v_F (m^*/m)^{1/2} \ln\epsilon]/eEl^2\}, \quad \epsilon = Vl/v_F, \tag{37}$$

where v_F is the characteristic velocity related to the elastic energy for deformation of ϕ, E is the electric field, V is the impurity strength, and l the

average distance between impurities. Applying their calculations to $NbSe_3$ LL conclude that the observed value of E_0 would require l to be extremely large. Furthermore, as in the previous two cases, thermal energy would dominate the energy supplied by the field. LL conclude that their impurity-pinning model is inapplicable to $NbSe_3$.

D. Critical divergence of $d\rho/dT$

The divergence of the derivative of the resistivity in pure metals and alloys at a phase transition appears to be very widespread. In ferromagnetics[10] such as Ni the derivative of ρ diverges logarithmically at the critical point T_N. In antiferromagnetic materials the divergence has a higher critical index). Fisher and Langer[26] (FL) have proposed that the divergence is due to critical scattering by the short-range spin fluctuations and have proposed a divergence $|t|^{-\alpha}$ (where α is the specific-heat index) above the Néel point T_N. Below T_N the scattering is dominated by the growing order parameter and $d\rho/dt \propto t^{2\beta-1}$ (where β is the order-parameter critical index). This agrees with what is experimentally observed in Ni. However, in antiferromagnetics the divergence above T_N has a higher critical index. Suezaki and Mori[27] (SM) have pointed out that the long-range spin fluctuations are dominant (above T_N) in the case of antiferromagnetics, where fluctuations occur around the wave vector $\vec{Q}$, leading to large angle scattering of conduction electrons. This is particularly true in SDW metals such as Cr where $\vec{Q} = 2\vec{k}_F$. The microscopic calculations of Takada[28] point to the same conclusion, namely, long-range fluctuations are dominant in antiferromagnetics while short-range fluctuations are dominant in ferromagnetics. Recently Horn and Guidotti[12] (HG) have studied the divergence of $d\rho/dT$ in the pseudo-one-dimensional organic metals [TTF-TCNQ and tetraselenafulvalene-tetracyanoquinodimethane (TSeF-TCNQ)] at the Peierls transition T_P. They found that (above T_P) the critical index is -1.0 along both axes in TTF-TCNQ and -1.5 along the b axis in TSeF-TCNQ. These indices are substantially larger than those found in the magnetic materials (0.0 to -0.3). To explain their results they considered the effect on $d\rho/dT$ of restricting the allowed final states for scattering due to the reduced dimensionality d of the metal. Using mean-field values for the critical exponents HG obtain the results[27]

$$\frac{d\rho}{dT} \propto \begin{cases} t^{-1.5} & (d=1), \\ t^{-1.0} & (d=2), \\ t^{-0.5} & (d=3). \end{cases} \tag{38}$$

The derivative of the resistivity arising from the long-range fluctuations may be written as [cf. Eq. (3.9) of Ref. 27]

$$\frac{d\rho_{\mu T}}{dT} \propto Q_\mu Q_\tau g_{\vec{Q}}^2 \sum_{\vec{q}} f_{\vec{q}}(1 - f_{\vec{Q}+\vec{q}}) \times \mathrm{Re}\int_0^\infty dt \exp(-i\omega_{\vec{Q}+\vec{q}} t - \Gamma t) \times \sum_{\vec{k}} \Psi_{\vec{Q}+\vec{k}}(t), \tag{39}$$

where $\vec{Q}$ is the spanning vector of the CDW, $g_{\vec{Q}}$ is the electron-phonon coupling constant, $f_{\vec{q}}$ is the Fermi-Dirac distribution, Γ^{-1} is the lifetime of the electrons, and

$$\Psi_{\vec{R}}(t) = -\frac{\partial \chi_{\vec{R}}(t)}{\partial T}. \tag{40}$$

In Eq. (40), $\chi_{\vec{R}}$ is the density-density correlation function which diverges at $T = T_c$ for $\vec{K} = \vec{Q}$. To evaluate Eq. (39) the assumption of critical slowing down is made so that we may neglect[27] the time dependence of $\Psi_{\vec{k}}$ in Eq. (40) and it is valid to use the static scaling laws,[9]

$$\chi_{\vec{Q}+\vec{k}}(0) = t^{-\gamma} F(k/\kappa). \tag{41}$$

In Eq. (41), γ is the susceptibility critical index, F is an unknown function, and κ is the inverse correlation length which behaves as (for $T \to T_c$)

$$\kappa \propto t^{\nu}. \tag{42}$$

The dimensionality d of the electron gas enters when we evaluate $\sum_{\vec{k}} \Psi_{\vec{Q}+\vec{k}}$. Using Eqs. (41) in Eq. (40) and performing the sum over $\vec{k}$ we have

$$\sum_{\vec{k}} \Psi_{\vec{Q}+\vec{k}}(0) \propto t^{-\gamma-1} \kappa^d \int_0^\infty dx\, x^d G(x). \tag{43}$$

Substituting Eq. (43) in Eq. (39) we finally have [using Eq. (42)]

$$\frac{d\rho_{\mu T}}{dT} \propto Q_\mu Q_\tau t^{-\gamma-1+\nu d}. \tag{44}$$

Using mean-field values ($\gamma = 1$, $\nu = \frac{1}{2}$) we have HG's results [Eq. (38)].

In $NbSe_3$ the critical exponent lies between -1 and -1.5 at the T_2 transition. Using the above theory this implies that the dimensionality of the system is 2 or 1, the data being insufficiently unambiguous to decide between the two. However, a value of -0.5 or smaller for the critical exponent can be excluded rather definitely. At the T_1 transition the rounding of the divergence very near T_1 prevents an extraction of the index. For $t > 2 \times 10^{-2}$, however, an exponent of 2 is obtained. This is larger than the result in Eq. (44) using reasonable values of γ, ν, and d. It is possible that the assumptions underlying the derivation of Eq. (44) no longer hold at temperatures well above T_1. In particular the

critical slowing-down assumption is expected to be invalid far above T_1 and one needs to examine the dynamics of the fluctuations without this simplifying assumption.

V. SUMMARY AND CONCLUSION

The non-Ohmic conductivity of $NbSe_3$ has been measured at temperatures in the vicinity of the two phase transitions at T_1 and T_2. At each temperature the conductivity may be decomposed into a field-independent part σ_a and a field-dependent part $\sigma_b e^{-E_0/E}$ (suppressing the subscript n, which identifies the transition). From σ_a and σ_b a parameter α is obtained which (at $T = 0$ K) gives the fraction of FS affected by the gap. (In a multiband model the pockets of FS which do not participate in the CDW formation are included in σ_a.) At elevated temperatures (particularly a few K below T_1 and T_2) thermal excitations across the growing gap reduce the value of α from its $T = 0$ K value. Therefore the temperature dependence of α provides information on the temperature dependence of the gap. By applying Fedders and Martin's theory to a CDW system we have theoretically computed the temperature variation of α using a BCS-type gap. Good agreement between the calculations and the data is obtained. This agreement may be interpreted as new evidence for gap formation at the FS at both transitions. The loss of carriers due to gap formation has also been observed directly in recent Hall measurements. From the fit of α to the BCS gap theoretical values for the zero temperature gaps have been calculated. The magnitude is 60 meV (19 meV) for the gap corresponding to the T_1 (T_2) transition. The transport measurements reported here also provide some information on the dimensionality of the electronic band structure. By studying the divergence of the resistivity derivative at T_2 we conclude that the dimensionality is less than three. In conjunction with the large Hall effect and strong galvanomagnetic response at low temperatures, and the absence of a metal-to-insulator (Peierls) transition we believe that the dimensionality is closer to two than to one.

Although some progress has been made in interpreting the non-Ohmic data the actual mechanism for the striking electric breakdown of the anomalies remains a puzzle. A number of theories based on quantum tunneling are successful in explaining the electric-field dependence of the conductivity, but numerical comparison with the experimental data seems to come up against the paradoxical situation that the energy supplied by the electric field is much smaller than the thermal fluctuation energy at T_1 and T_2.

Note added in proof. Electron diffraction evidence of superlattice formation in $NbSe_3$ at T_1 has been reported by Tsutsumi, Takagaki, Yamamoto, Shiozaki, Ido, Sambongi, Yamaya, and Abe, Phys. Rev. Lett. 39, 1675 (1977). X-ray diffraction evidence for a new superlattice at T_2 has also been obtained by Fleming and co-workers [P. A. Lee (private communication)]. Ayrolles and Roucan have also observed the superlattice at T_1 by electron diffraction . [P. Monceau (private communication)].

ACKNOWLEDGMENTS

Illuminating and encouraging discussions with K. Maki and P. Kumar are gratefully acknowledged. The author would like to thank P. Horn for suggesting the critical-divergence measurements and P. Monceau for early communication of results. The sample preparation by J. Savage has been indispensable to the work reported here. This work was supported by the Office of Naval Research Grant No. N00014-77-C-0473.

[1] A. Meerschaut and J. Rouxel, J. Less-Common Metals 39, 197 (1975).
[2] J. Chaussy, P. Haen, J. C. Lasjaunais, P. Monceau, G. Waysand, A. Waintal, A. Meerschaut, P. Moninie, and J. Rouxel, Solid State Commun. 20, 759 (1976).
[3] N. P. Ong and P. Monceau, Phys. Rev. B 16, 3443 (1977).
[4] P. Monceau, N. P. Ong, A. M. Portis, A. Meerschaut, and J. Rouxel, Phys. Rev. Lett. 37, 602 (1976).
[5] M. J. Rice, A. R. Bishop, J. A. Krumhansl, and S. E. Trullinger, Phys. Rev. Lett. 36, 432 (1976).
[6] K. Maki, Phys. Rev. Lett. 39, 46 (1977).
[7] N. P. Ong and P. Monceau, Solid State Commun. (to be published).
[8] J. Bardeen, L. N. Cooper, and J. R. Schrieffer, Phys. Rev. 108, 1175 (1957).
[9] L. P. Kadanoff, W. Götze, D. Hamblen, R. Hecht, E. A. S. Lewis, V. V. Palciauskas, M. Rayl, J. Swift, D. Aspnes and J. Kane, Rev. Mod. Phys. 39, 395 (1967).
[10] P. P. Craig, W. I. Goldburg, T. A. Kitchens, and J. I. Budnick, Phys. Rev. Lett. 19, 1334 (1967).
[11] P. M. Horn and D. Rimai, Phys. Rev. Lett. 36, 809 (1976).
[12] P. M. Horn and D. Guidotti, Phys. Rev. B 16, 491 (1977).
[13] P. Monceau, J. Peyrard, J. Richard, and P. Molinie, Phys. Rev. Lett. 39, 160 (1977).
[14] J. W. Brill and N. P. Ong, Solid State Commun. (to be published).
[15] See, for example, A. L. Fetter and J. D. Walecka, *Quantum Theory of Many-Particle Systems* (McGraw-Hill, New York, 1971), p. 411.
[16] W. Kohn, Phys. Rev. Lett. 2, 393 (1959).
[17] W. M. Lomer, Proc. Phys. Soc. Lond. 80, 489 (1962).
[18] See, for example, C. Herring, in *Magnetism*, edited by G. T. Rado and H. Suhl (Academic, New York, 1966), Vol. IV. See also, S. K. Chan and V. Heine, J. Phys. F 3, 795 (1973).

[19]P. A. Fedders and P. C. Martin, Phys. Rev. 143, 245 (1965).
[20]See Ref. 15, p. 430.
[21]I am indebted to K. Maki for suggesting this analysis.
[22]B. Mühlschlegel, Z. Phys. 155, 313 (1959).
[23]J. M. E. Harper, T. H. Geballe, and F. J. DiSalvo, Phys. Lett. A 54, 27 (1975).
[24]This is the value of the carrier mass observed by Shubnikov–de Haas oscillation measurements. P. Monceau, Solid State Commun. 24, 331 (1977).
[25]A. Larkin and P. A. Lee, Phys. Rev. B 17, 1596 (1978).
[26]M. E. Fisher and J. S. Langer, Phys. Rev. Lett. 20, 665 (1968).
[27]Y. Suezaki and H. Mori, Prog. Theor. Phys. 41, 1177 (1969).
[28]S. Takada, Prog. Theor. Phys. 46, 15 (1971).

Solid State Communications, Vol. 26, pp. 487–491.
0038-1098/78/0522-0487 $02.00/0

HALL EFFECT OF A LINEAR-CHAIN METAL: $NbSe_3$

N.P. Ong

Deparment of Physics, University of Southern California
Los Angeles, California 90007

P. Monceau

Centre de Recerches sur les Tres Basses Temperatures, C.N.R.S.
BP 166 X, 38042
Grenoble Cedex, France

(Received 6 January 1978 by A.A. Maradudin)

We present measurements of the low-field Hall constant R_H as a function of field and temeprature in the linear-chain metal $NbSe_3$. The data range from 2 K to 200 K in temperature and up to 15 kG in field. At the two phase transitions T_1 (142 K) and T_2 (58 K) R_H shows an abrupt increase in magnitude but no change in sign. Below 30 K R_H becomes strongly field dependent. The zero-field-limit R_H changes from n-type to p-type at 15 K. It is argued that the results are consistent with a two-band model in which the difference in population p - n is equal to 3×10^{18} cm^{-3} below T_2. The Hall data are also consistent with a model in which both a loss of carriers and a drastic change in the conductivity anisotropy occur at T_1 and T_2 and lend support to the charge-density-wave hypothesis which has been used to characterize the two transitions.

The linear chain metal niobium triselenide[1] has rather unusual transport properties. The resistivity-temperature profile[2] shows two giant anomalies associated with phase transitions at T_1 (142 K) and T_2 (58 K). The electronic conductivity is highly non-Ohmic[3,4] at temperatures below T_1. The non-Ohmicity manifest itself as a breakdown of the anomalies as the applied E-field is increased. Furthermore the resistivity is a strong function of frequency at microwave frequencies[4]. No trace of the T_2-transition is detected in the resistivity at 9 GH_Z while the T_1 anomaly is sharply reduced in size.

The two phase transitions have been discussed[2,3] in terms of charge-density-wave (CDW) formation[5]. In this model Fermi surface (FS) pathologies cause the electron-phonon interaction to become divergent for a particular phonon mode $\vec{Q}$ which softens. A superlattice of wave vector $\vec{Q}$ appears and induces gaps at points on the FS serparated by the wave vector $\vec{Q}$. The gain in electronic energy due to gap formation stabilizes the new phase. Gap formation also leads to a loss of carriers[4] and accounts for the rise in resistivity at the transitions.

Recently[6] a model based on these ideas has been used to interpret the non-Ohmic data near the phase transitions. Using a modification of Fedders and Martins'[7] calculations on the spin density wave transition we have shown that the temperature dependence of one of the non-Ohmic parameters, α, can be described by a BCS-type gap equation. The parameter α also provides a number for the fraction of FS affected by the transitions at T_1 and T_2. The CDW formation destroys 20% of the FS at T_1 and 60% of the remaining at T_2.

The most direct way to observe a change in carrier concentration in a conductor is to measure the Hall effect as a function of temperature. Recently we have obtained samples with sufficient width to observe the Hall voltage. $NbSe_3$ has a rather large Hall signal at low temperatures. At 2.0 K the Hall constant R_H is 4.1×10^{-7} m^3/C (in the limit of zero field). As the field H increase R_H rapidly saturates to the value of 2.3×10^{-6} m^3/C. The sign of R_H changes from p-type to n-type at 15 K as T is increased. At both T_1 and T_2 R_H shows an abrupt change in magnitude (but not in sign). R_H remains n-type to room temperature where it is of the order of -1.0×10^{-8} m^3/C.

The samples were synthesized by heating stoichiometric proportions of Nb and Se in a quartz tube for 4 weeks at 725°C as discussed in Ref. (1). Four large crystals were found suspended in the middle of the tube away from the walls. Microscopic examination of these samples showed them to be single crystals typically $8 \times 0.40 \times 0.008$ mm^3 in size. Two of these samples were mounted on sapphire substrates and gold leads were attached to them in the standard Hall configuration by means of silver paint. Temperature was monitored and automatically controlled by a capacitance sensor to $\pm$ 20 mK from 2 K to 200 K. A calibrated silicon diode sensor was used to measure the absolute temperature when the magnetic field was off. The longitudinal dc current was maintained at 300μA and the signal from the Hall leads was bucked by a constant voltage, amplified and displayed on an x-y recorder as a function of field. At all temperatures the Hall signal for normal and reversed fields was measured for one direction

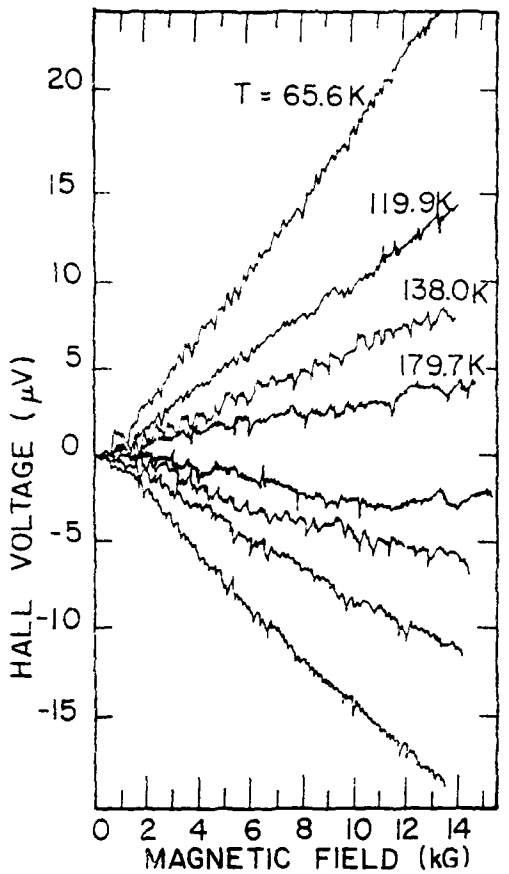

Fig. 1. The Hall voltage of sample 1 at selected temperatures above T_2. The two branches at each temperature correspond to the two directions of the applied magnetic field. The Hall constant R_H is field independent up to 15 kG at temperatures above 40 K.

of the current. At some selected temperatures the current direction was also reversed to correct for the IR drop due to misalignment of the Hall leads. This correction was necessary for only one of the two samples measured. Typical sweep rates were 4 kG/min. At high temperatures the large amplification used required some care in eliminating spurious effects. The sweep rate was varied to detect time dependent emf's due to varying flux threading the Hall leads. In general only those runs were retained, in which both the voltage across the Hall leads and the voltage from the Si cryogenic sensor returned to their initial values after the field was cycled.

In both samples the current I was parallel to the b axis and the Hall voltage V_H was measured along the a axis with the magnetic field either parallel or anti-parallel to $\vec{b} \times \vec{a}$. Figure 1 shows typical runs at selected temperatures

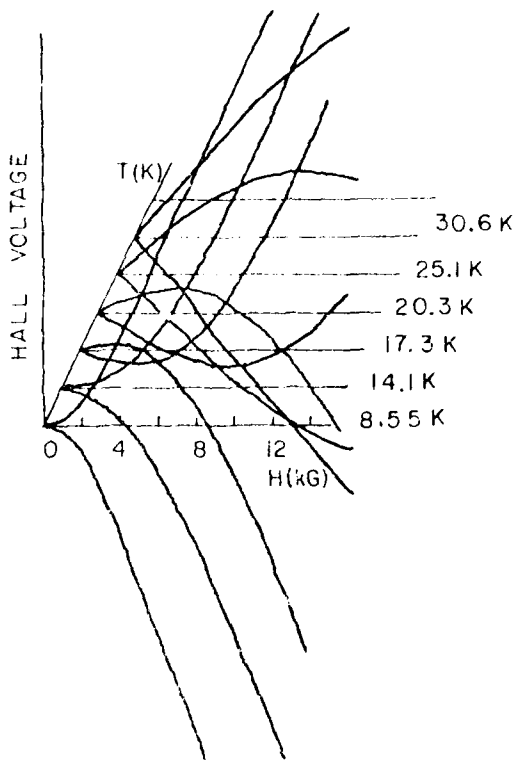

Fig. 2. The Hall voltage of sample 2 at temperatures below 30 K, showing the strong field dependence of the Hall constant and the reversal of sign that occurs below 20 K. Similar behavior is obtained in sample 1.

for sample 1. The Hall constant

$$R_H = (V_H t)/(IH) \qquad (1)$$

(where t is the sample thickness and H the magnetic field) is field independent up to the highest field used (15 kG) for temperatures above 30 K. Below 30 K R_H is strongly field dependent. As shown in Figure 2 (data on sample 2) V_H is strikingly non-linear in the vicinity of 15 K where R_H changes sign.

In Figure 3 we show the temperature dependence of $R_H(0)$ at both T_1 and T_2. Just below T_1 $R_H(0)$ increases at an inital rate of

$$\frac{1}{R_H(0)} \frac{dR_H(0)}{dT} = -0.14\ K^{-1} \quad (T \to T_1^-) \qquad (2)$$

As T decreases R_H continues to rise with a decreasing slope until T crosses the T_2 transition where $R_H(0)$ again undergoes an abrupt increase. Just below the T_2 transition we have

$$\frac{1}{R_H(0)} \frac{dR_H(0)}{d_T} = -0.58\ K^{-1} \quad (T \to T_2^-) \qquad (3)$$

which is four times larger than the fractional increase at T_1. Below 30 K the field-dependence of R_H becomes manifest at the fields we employed. The values displayed in Figure 3 are the values

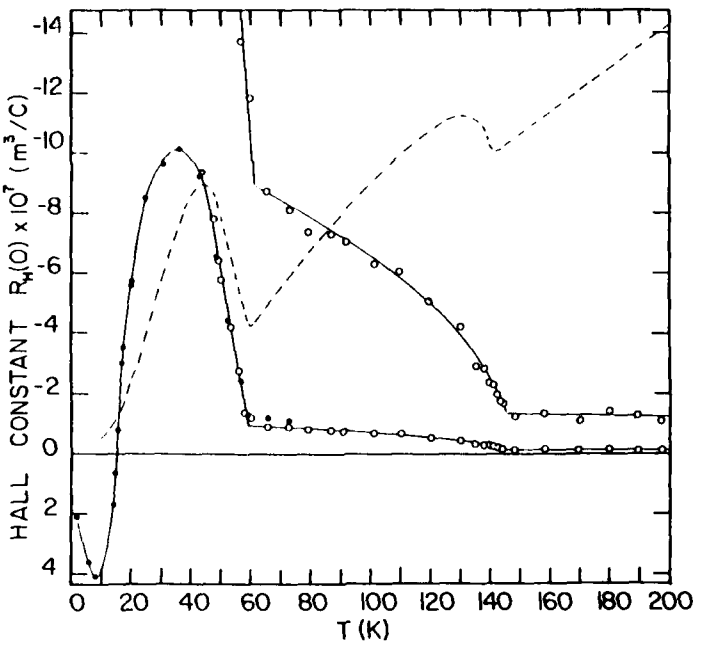

Fig.3. The temperature dependence of $R_H(0)$ (the Hall constant at zero field). The open (solid) circles are data from sample 1 (2). The data above 50 K is also plotted with a factor of ten magnification. The data from the two samples were normalized to agree at 2 K and 14 kG. At both transitions T and T $R_H(0)$ undergoes an abrupt change in magnitude. It changes sign at 15 K, becoming p-type at low temperatures. The jump in magnitude at T and T is consistent with a change in both carrier concentration and mobility ratios at the transitions. The solid lines are drawn to guide the eye and have no further significance. The broken line is the longitudinal resistivity.

of R_H obtained by extrapolating to zero field in a plot of R_H vs. H. $R_H(0)$ changes sign at 15 K and the Hall signal is p-type at low temperatures. The strong field-dependence of R_H at these temperatures is shown in Figure 4 for several temperatures. The qualitative features of $R_H(0)$ may be understood by examining the expression[8] for R_H appropriate to a two-carrier model. We assume that the conductivity matrix is given by

$$\overleftrightarrow{\sigma} = \overleftrightarrow{\sigma_n} + \overleftrightarrow{\sigma_p} \tag{4}$$

$$\overleftrightarrow{\sigma_n} = \frac{ne}{(1 + \mu_1\mu_2H^2)} \begin{pmatrix} \mu_1 & -\mu_1\mu_2H \\ \mu_1\mu_2H & \mu_2 \end{pmatrix} \tag{5}$$

where subscript n (p) refers to electrons (holes), μ_1 (μ_2) is the mobility of electrons in the x(y) direction, and n is the electron concentration. For clarity e and μ_i are considered to be positive quantities.[1] The sign of the carriers will be written out explicitly. The matrix for $\overleftrightarrow{\sigma_p}$ is obtained from Eq. (5) by replacing n by p (the hole concentration) and μ_i by ν_i (the hole mobility). It may be shown[9] that the Hall constant is given by

$$R_H(H) = -N/(A_1A_2 + H^2 N^2) \tag{6}$$

where

$$N = e\left(\frac{n\mu_1\mu_2}{1 + \mu_1\mu_2H^2} - \frac{p\nu_1\nu_2}{1 + \nu_1\nu_2H^2}\right) \tag{7}$$

$$A_i = e\left(\frac{n\mu_i}{1 + \mu_1\mu_2H^2} + \frac{p\nu_i}{1 + \nu_1\nu_2H^2}\right) \tag{8}$$

In the two limits of zero field and infinite field Eq. (6) reduces to

$$R_H\ (H\to 0) = -\frac{(n\mu_1\mu_2 - p\nu_1\nu_2)}{e(n\mu_1+p\nu_1)(n\mu_2+p\nu_2)}\left[1 + O(H^2)\right] \tag{9}$$

$$R_H\ (H\to\infty) = -\frac{1}{e(n-p)}\left[1 - O(\tfrac{1}{H^2})\right] \tag{10}$$

For small values of H, R_H is quadratic in H while in the limit of infinite field R_H approaches the saturation value $R_H(\infty) = 1/(e(n - p))$ as $1/H^2$. These features are evident in all the curves shown in Figure 4. Another prediction of Eq. (6) is that as the mobilities increase (with decreasing T) the characteristic field at which the behavior of R_H switches from H^2 to $(1 - (H^{-2}))$ should

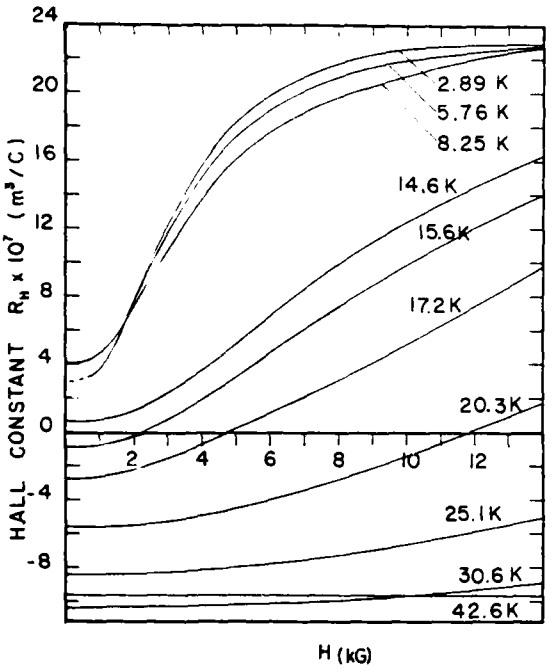

Fig. 4. The field dependence of R_H at low temperatures for fields up to 14 kG. The general features at each temperature are the quadratic increase from its zero field value at low fields, and the asymptotic approach to the infinite-field value $R_H(\infty)$ at high fields. As discussed in the text, these features are consistent with a two band model in which the mobility increases with decreasing temperature. The data are from sample 2.

move to successively lower fields. This is because H scales as $(\mu_1\mu_2)^{-\frac{1}{2}}$ or $(\nu_1\nu_2)^{-\frac{1}{2}}$ in Eq. (7). The low temperature curves in Figure 4 also show this behavior. For example at the lowest temperature R_H saturates at the relatively modest field of 12 kG. Although Eq. (6) can reproduce Figure 4 with a judicious choice of the six unknowns n, p, μ_1, ν_1, a meaningful test of the simple model used in Eqs. (4) and (5) will be possible only if the analysis also agrees with other transport measurements such as conductivity anisotropy and magnetoresistance. A detailed report will be published elsewhere.

We conclude with a few remarks. The saturation value of R_H at high fields provides unambigously the value of 2.7×10^{18} cm^{-3} for the quantity (p - n). Equation (10) implies that at sufficiently high fields R_H attains the same saturation value[10], $R_H(\infty)$, at all temperatures below T_1. This behavior is consistent with the low temperature behavior shown in Figure 4. Above T_2 changes in the FS area alter (p - n) and we obtain a different $R_H(\infty)$. Assuming a characteristic field of $\sim$1 kG at T = 2 K we deduce that the characteristic mobility of the faster carrier is of the order of 10^4 cm^2/Vs at this temperature. Below the T_2 transition the Hall data implies that p is greater than n. However the large value of the ratio $(\mu_1\mu_2/\nu_1\nu_2)$ keeps $R_H(0)$ negative until T decreases below 15 K. The sharp increase of $R_H(0)$ at both transitions is too large to be explained by a change in carrier concentration alone. It is possible that a change in the mobility anisotropies is occuring simultaneously. This will be consistent with the appearance of a superlattice Bragg plane which preferentially scatters the carriers moving parallel to the spanning vector. In fact a comparison of Figure 3 with the prediction of Eq. 9 implies that the conductivity anisotropy $(n\mu_1 + p\nu_1)/(n\mu_2 + p\nu_2)$ should be a strong function of temperature below T_1 and T_2. The reason is that if n and p are temperature independent, a strongly varying $R_H(0)$ implies that $(\mu_1\mu_2)$ and $(\nu_1\nu_2)$ cannot have the same temperature dependence Preliminary conductivty anisotropy measurements using the Montgomery technique have confirmed this inference.

After this work was completed, evidence for superlattice formation at T_1 was reported by Tsutsumi et al.[11]

Acknowledgement - This work was performed under a grant (N00014-17-C-0473) from the office of Naval Research, and was made possible by the expert sample prepartion of Jim Savage.

REFERENCES

1. A. MEERSCHAUT and J. ROUXEL, J. Less Common Metals 39, 197 (1975).
2. J. CHAUSSY, P. HAEN, J.C. LASJAUNAIS, P. MONCEAU, G. WAYSAND, A. WAINTAL, A. MEERSCHAUT, P. MOLINIE, and J. ROUXEL, Solid State Commun. 20, 759 (1976).
3. P. MONCEAU, N.P. ONG, A.M. PORTIS, A. MEERSCHAUT and J. ROUXEL, Phys. Rev. Lett. 37, 602 (1976).
4. N.P. ONG and P. MONCEAU, Phys. Rev. B 16, 3443 (1977).
5. See for example, J.A. WILSON, F.J. DISALVO and S. MAHAJAN, Adv. Phys. 24, 117 (1975).
6. N.P. ONG, Phys. Rev. B, April 15, 1978.
7. P.A. FEDDERS and P.C. MARTIN, Phys. Rev. 143, 245 (1965).
8. See for e.g., A.H. WILSON, The Theory of Metals, (Second edition, Cambridge University Press, 1965), p. 208.
9. Our analysis is similar to that used by B. ABELES and S. MEIBOOM, Phys. Rev. 101, 544 (1956).
10. High-field Hall measurements have been reported by R.M. FLEMING, J.A. POLO, Jr. and R.V. COLEMAN, Phys. Rev. B, (15 Jan. 1978). Their results confirm this aspect of our model. The Hall constant is field independent at 4.2 K between 20 kG and 140 kG. At 30 K, the Hall constant approaches the

4.2 K high-field value asymptotically. This appears to be the case also at 40 K and 50 K. The Hall constant at 77 K and 300 K is of the same sign up to 140 kG. There seems to be a disagreement on the sign of the carriers between our data and that of FLEMING et al.

11. TSUTSUMI, TAKAGAKI, YAMANOTO, SHIOZAKI, IDO, SAMBONGI, YAMAYA, and ABE, Phys. Rev. Lett. 39, 1675 (1977).

PHYSICAL REVIEW B VOLUME 18, NUMBER 10 15 NOVEMBER, 1978

Conductivity anisotropy and transverse magnetoresistance of $NbSe_3$

N. P. Ong and J. W. Brill
Department of Physics, University of Southern California, Los Angeles, California 90007
(Received 10 July 1978)

The first-transverse dc conductivity measurements on a member of the transiton-metal trichalcogenides ($NbSe_3$) are presented. The conductivity anisotropy σ_b/σ_c (where b is the chain axis) was obtained using the Montgomery technique, and varies from 10 to 20 as a function of temperature. The transverse resistivity ρ_c also shows anomalies associated with the charge-density-wave transitions at T_1 (142 K) and T_2 (58 K). However, these anomalies are smaller than the corresponding ones in ρ_b. The quantity $R_H(0)/(\rho_b\,\rho_c)$, where R_H is the Hall constant, demonstrates explicitly the freeze-out of thermally excited quasiparticles below each transition. We show that at both transition gaps appears on the hole surface, and the hole concentration decreases rapidly. The transverse magnetoresistance at low fields has also been measured. Its monotonic power-law decrease with increasing temperature shows explicitly that the resistivity anomalies are due to changes in the carrier concentration, and not in the lifetimes.

I. INTRODUCTION

The transition-metal chalcogenides have proved to be a remarkably fertile series of compounds for the study of instabilities of the electron gas of reduced dimensionality. The MX_2 (where M is a transition metal element and X is one of the chalcogens) compounds form layered structures[1] and the electron gas has a quasi-two-dimensional character. A host of phase transitions into the incommensurate charge-density-wave (ICDW) and commensurate charge-density-wave state (CCDW) occurs in the various poly-types of these compounds. Much theoretical effort has been expended to study the nature of the incommensurate phase and how an ICDW "locks-in" to the underlying host lattice. For instance, McMillan[2] has proposed that the ICDW state in 2H-$TaSe_2$ is in fact one in which the charge-density-wave (CDW) achieves commensurability over microdomains which are separated by domain walls (discommensurations) where the CDW phase undergoes an abrupt change. It remains unclear whether such discommensurations or similar defects occur also in other ICDW systems such as 2H-$NbSe_2$, or whether the canonical CDW theory of Chan and Heine[3] is adequate.

In the last two years compounds of the type MX_3 have been shown to exhibit the same kinds of electronically driven instabilities. Specifically, the compounds $NbSe_3$,[4,5] NbS_3,[6] $TaSe_3$,[5,7] and [8]TaS_3 have been synthesized and studied. The occurrence of CDW's in the MX_3 family is significant because the members generally have a linear-chain structure with high conductivity along the chain direction. In contrast to the layered structure of the MX_2 family where the high conductivity occurs in the basal plane, the MX_3 metals could possibly show quasi-one-dimensional behavior. Indeed, Sambongi *et al.*,[7] have shown that TaS_3 undergoes a transition into the insulating CCDW state, similar to the well-studied quasi-one-dimensional conductors, tetrathiafulvalene tetracyanoquinodimethane[9] (TTF-TCNQ) and the mixed-valence compounds[9] KCP and their numerous derivatives. Another member $TaSe_3$, shows metallic behavior[5] at all temperatures down to 2.2 K where it becomes superconducting.[8] No superlattice formation has been reported for $TaSe_3$.

In many ways the most interesting member of the MX_3 family is $NbSe_3$ which was first structurally characterized by Meerschaut and Rouxel.[4] Monceau and co-workers,[5] first showed the occurence of two giant resistivity anomalies associated with phase transitions at T_1 (~142 K) and T_2 (58 K) which they inferred to be CDW transitions, from the pressure dependence[10] of T_1 and T_2. Support for this hypothesis was provided by measurements on the Hall effect[11] and Young's Modulus[12] which showed respectively a loss of carriers at both T_1 and T_2, and an elastic anomaly at T_1. Furthermore, the growth of a gap at the Fermi surface (FS) at both transitions was inferred[13] by applying the BCS gap equation to data obtained from the non-Ohmic measurements of the longitudinal conductivity. Since then other groups[14-16] have obtained direct supperlattice evidence of ICDW's in both low-temperature phases by electron diffraction and x-ray studies.

The confirmation of the CDW state in $NbSe_3$ is significant because of the anomalous-electronic transport properties which occur below T_1. The giant resistivity anomalies show non-Ohmic breakdown effects[17] under weak dc electric fields.

The conductivity also shows[11] strong frequency dependence in the gigahertz region even when the ac field is much weaker than the value required to observe non-Ohmic behavior at zero frequency. The great difficulties in accomodating these results within the framework of a single-particle picture have been discussed in Refs. 13 and 18. In these papers it was also suggested that the significant enhancement of the conductivity may arise from the depinning of the rigid CDW condensate which is then accelerated by the E field. This possibility has been discussed by many workers[19,20] in the context of one-dimensional "Fröhlich superconductivity." Bardeen[21] recently applied the two-fluid model to account for the temperature dependence of the activation field in $NbSe_3$, and finds that the depinning field should first decrease, then increase as the temperature decreases, in qualitative agreement with the experiment. However, little else is understood, especially quantitatively, regarding the anomalous transport behavior aside from the strong suspicion that a collective mode of the CDW condensate is being excited.

In this paper we present results on the galvanomagnetic and other transport properties of $NbSe_3$ in the zero-frequency-Ohmic regime, restricting current values to below the Ohmic breakdown values. Although the nature of the current-carrying excitations in the non-Ohmic and/or high-frequency regime is of paramount interest, the understanding derived from the analysis of the galvanomagnetic and conductivity anisotropy data in the Ohmic region is a necessary first step towards an understanding of the anomalous behavior. It will be seen in the following paper[22] (II) that the various transport measurements taken together offer a rather complete view of the normal uncondensed electrons and holes in this metal. The galvanomagnetic measurements in the high-frequency and high electric field regimes are currently in progress and will be reported in a later publication.

Hall measurements on $NbSe_3$ from 2 to 300 K, with the B field along a^* and the current parallel to b (the chain axis) have been reported by Ong and Monceau[11] (OM). Monceau[23] has measured the Shubnikov–de Haas oscillations in the magnetoresistance. Fleming, Polo, and Coleman[24] (FPC) have also reported oscillatory magnetoresistance measurements in $NbSe_3$ and $TaSe_3$, as well as high-magnetic-field Hall measurements in $NbSe_3$. A more complete mapping of the Shubnikov frequencies has recently been obtained by Monceau and Briggs[25] (MB). The preceding measurements are all in substantial quantitative agreement except for the disagreement on Hall polarity reported by OM and FPC. Together with the conductivity anisotropy in the b-c plane and the transverse low-field magnetoresistance measurements to be reported here one should have sufficient data to unravel the contributions from the electron and hole pockets. In particular one would hope for a direct observation of the loss of carriers near the CDW transitions, as thermally excited quasiparticles across the developing gaps are frozen out with decreasing temperature. Evidence for this behavior is obtained by combining the Hall and anisotropy measurements. A full analysis of the galvanomagnetic data is presented[22] in II.

II. EXPERIMENTAL DETAILS

Conductivity anisotropy measurements were done using the Montgomery[26] technique. The fibrous morphology of the crystals and the minute transverse dimensions presented the most serious difficulties in measuring the dc transverse conductivity. Samples were mounted on a sapphire substrate and glued to the substrate by four silver paint (du Pont 4922) droplets, which also served as contacts for the gold leads. This mounting configuration is less satisfactory in one respect than some that have been reported[27] in the literature. The differential contraction of the sample and substrate sets up stresses in the sample which lead to cracks parallel to the chain axis. These stress-induced cracks show up as irreproducible jumps in the measured transverse conductivity. Nonetheless, this mounting configuration was used because one could achieve better control over the size of the contacts to the sample. Attempts to use techniques such as that described by Coleman[27] resulted in the droplets completely enveloping the thin sample. The Montgomery configuration requires the contacts to be at the four corners of a rectangular sample. Because the ends of single crystals tend to be frayed the contacts were placed approximately $\frac{1}{2}$ mm away from the ends. Since the transverse dimension in the c direction was typically 300 μm and the diameter of the paint droplets was at least 100 μm great care was required to avoid shorting out contacts on opposite sides of the sample. The technique which proved most successful was to place the sample on the substrate and to wash it with a drop of butyl acetate. This improved adhesion of the sample to the substrate as well as the contact between the sample and paint. When the butyl acetate had evaporated a small droplet of paint was placed on the substrate close to the sample and edged in with a 3-mil wire until contact was achieved. The optimum viscosity was maintained

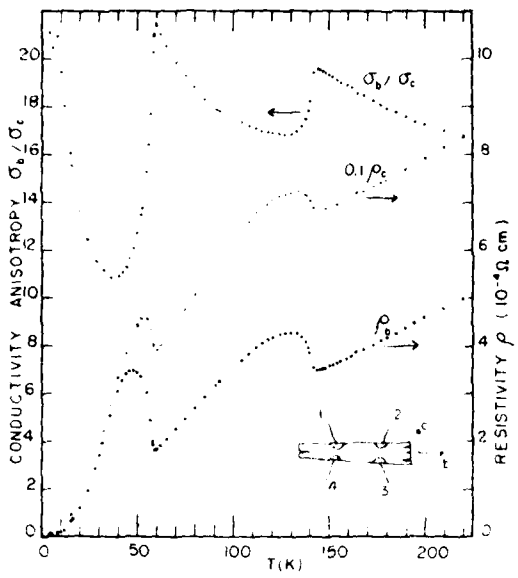

FIG. 1. Conductivity anisotropy (in the b-c plane), the transverse resistivity, and the longitudinal resistivity of $NbSe_3$ (in descending order). The transverse resistivity has been reduced by a factor of 10 for convenience. The longitudinal resistivity profile is in good agreement with previous results obtained by the conventional four-probe technique. Like ρ_b the transverse resistivity ρ_c is also greatly perturbed by the CDW transitions at T_1 and T_2. The inset shows the actual sample orientation in the Montgomery technique used.

by diluting a fresh "pot" of paint with butyl acetate for each contact. To ensure that the sample could withstand the stresses associated with cooling only those crystals with substantial thickness a in the a^* direction (normal to substrate) were used. A successful cool down was judged to be one in which no measurable hysterisis was observed on subsequent warm up. The amount of stress could also be estimated by comparing T_1 and T_2 as well as the size of the two anomalies in the longitudinal resistivity with the ambient pressure results. Chaussy *et al.*[10] have shown that these parameters are sensitive to applied hydrostatic pressure. In the results reported here the longitudinal resistivity and the transition temperatures show no measurable difference from the ambient pressure results. Thus we may safely ignore the effect of these stresses. The substrate was thermally anchored to a copper platform which was surrounded by He gas and enclosed in a double-vacuum jacket. Thermal stability was maintained to ±10 mK while the two measurements were made. The sample whose conductivity anisotropy is shown in Fig. 1 had dimensions 1980×290×50 μm. Since the contact dimensions varied from 30 to 50 μm there is some uncertainty over what the appropriate effective ratio of the sides of the crystal b/c should be. This is discussed in Sec. III.

For the transverse magnetoresistance measurements much thinner fibers can be used (typically 20-μm wide). Leads were mounted in the conventional four-probe configuration with the B field along the a^* axis and the current in the b direction. A quadratic fit to the resistivity at low fields was made at each temperature. This is important below ~12 K where the resistivity starts deviating from quadratic behavior at relatively low fields. The low-field magnetoresistance $\Delta\rho/\rho_0 B^2$ where ρ_0 is the zero-field resistivity is very large at 4.2 K (corresponding to an equivalent mobility of ~40 000 cm^2/V sec), but rapidly decreases to an equivalent mobility of 200 cm^2/V sec at 55 K. No magneto-resistance could be measured to our sensitivity at fields of 70 kG above the T_2 transition. Our highest temperature data is at 55 K. At 15 kG the measured fractional change in the resistivity at 55 K is 7×10^{-4}. Since the temperature-coefficient of the resistivity is very large at this temperature $\rho^{-1}d\rho/dT \simeq -8\times10^{-2}\,K^{-1}$ the fractional increase in ρ would be suppressed by a temperature drift of 9 mK during the time of the field sweep. This represents an upper limit on the cryogenic stability of our apparatus. The temperature of the sample chamber was controlled by a capacitance sensor which, unfortunately, was least sensitive around 60 K. Transients caused by the switching relays in the magnet supply were suppressed by careful screening of the sample leads. Altogether data from three samples were taken. Despite the scatter they are in reasonable agreement with each other.

III. RESULTS AND ANALYSIS

In Montgomery's[26] technique for measuring the conductivity anisotropy of a rectangular sample of sides b and c, the potential drop V_b across contacts 3 and 4 (see Fig. 1) is first measured with the current I going through contacts 1 and 2. Next, the potential drop V_c across contacts 2 and 3 are measured with the same current going through contacts 1 and 4. Specializing to the case where the third dimension a (along the a^* axis) is negligible compared to c, Montgomery and Logan *et al.*[28] show that the resistivity in the b and c directions are given by

$$\rho_b = H(x)a(V_c/I)(cx/b)\,, \tag{1}$$

$$\rho_c = H(x)a(V_c/I)(b/c), \tag{2}$$

where

$$H(x) = \frac{\pi}{4} \ln \frac{1+2q+2q^4\cdots}{1-2q+2q^4\cdots}, \quad q = e^{-\pi x}, \tag{3}$$

and x is the solution to the equation

$$r \equiv \frac{V_b}{V_c} = \frac{\{\pi x/4 - \ln[2(1-q^2+q^6)/(1+2q+2q^4)]\}}{\{\ln[(1+2q+2q^4)/(1-2q+2q^4)]\}}. \tag{4}$$

In practice at each temperature the ratio r is formed from the measured V_b and V_c. Equation (4) is then solved for x, and H computed from Eq. (3). Substitution into Eqs. (1) and (2) gives ρ_b and ρ_c. For reference we note that the product

$$\rho_b\rho_c = H(x)a^2(V_c/I)^2 \tag{5}$$

is independent of b/c. To solve Eq. (4) for x we have found it convenient to use the following series which gives an accuracy of $\pm 0.01\%$ when $1 < r < 30$:

$$x = A + B\ln r + C(\ln r)^2 + D(\ln r)^3\cdots. \tag{6}$$

$A = 0.997229$, $B = 0.160697$, $C = 1.231\,448\times10^{-2}$, $D = -3.797\,40\times10^{-4}$.

Figure 1 shows the computed anisotropy in the b-c plane and the separate resistivities along the two axes. (The transverse resistivity ρ_c has been reduced by a factor of 10.) As mentioned in Sec. I the longitudinal anomaly sizes in ρ_b show good agreement with conventional four-probe measurements on single ribbons. Furthermore, the room temperature value of ρ_b (655 $\mu\Omega$ cm) is in good agreement with previously reported[5] measurements. A rather surprising feature of the transverse resistivity ρ_c is the sizeable anomaly at T_1. This is unexpected from the orientation of the superlattice Bragg plane which is normal to the b axis. Equally unexpected is the fact that the appearance of the CDW at T_2 which has spanning vector[15] (0.5, 0.26, 0.5) seems to disrupt ρ_c less than ρ_b. Below T_2 the transverse resistivity ρ_c decreases much more rapidly than ρ_b but at liquid-helium temperatures the anisotropy has returned to the value it had at 59 K. As mentioned before, the computed anisotropy ρ_c/ρ_b is very sensitive to the choice of the ratio of the sides b/c. Since the contacts have finite size it is not clear what values for b/c is appropriate. The anisotropy shown in Fig. 1 (~16 at 290 K) was computed with a value of b/c equal to 5.0. Room-temperature measurements on two other samples gave values of ρ_c/ρ_b which varied between 10 and 30, again depending on the choice of b/c. Thus the absolute value of the anisotropy is known only to $\pm 50\%$. Nonetheless it may be seen from Eqs. (4) and (5) that the value of x and $(\rho_b\rho_c)$ are unaffected by this uncertainty. It will turn out that in analyzing the anisotropy data in conjunction with the galvanomagnetic data the important quantity is $\rho_b\rho_c$ which does not depend on b/c. The quantity that figures prominently in these analyses is $R_H/\rho_b\rho_c$ which may be shown to be independent of all sample dimensions. (Both R_H and $\rho_b\rho_c$ are linear in a.) Similarly the magnetoresistance is independent of sample dimensions.

Knowing the product $\rho_b\rho_c$ (solid circles in Fig. 2), enables us to proceed one more step in understanding the Hall effect of $NbSe_3$. The puzzling feature of the Hall constant at zero field, $R_H(0)$, is the large increase in $|R_H(0)|$ below T_1 and T_2. Specifically[11] $|R_H(0)|$ undergoes an eightfold increase as the temperature decreases from 145 to 60 K and appears to be still increasing when the T_2 transition is reached. A similar large increase (12-fold) occurs below the T_2 transition (between 59 and 36 K). In a one-band model $R_H(0)$ is in-

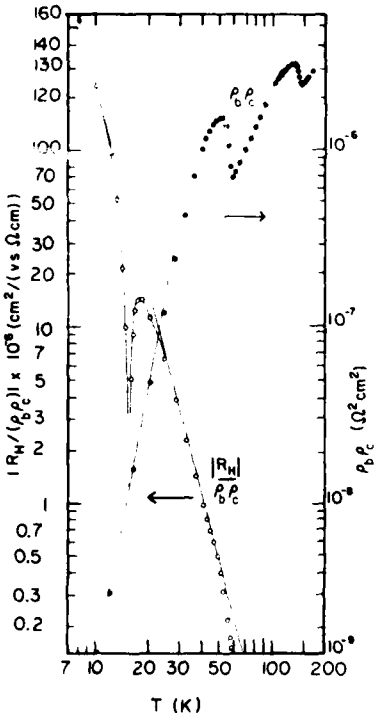

FIG. 2. Product of the resistivities $\rho_b\rho_c$ (solid circles) and the absolute value of the quantity $A \equiv R_H(0)/\rho_b\rho_c$ (open circles) vs temperature in log-log scale. The "resonance" structure in $|A|$ is due to the zero crossing of $R_H(0)$ at 15 K. The straight line through the open circles reflects the dominant power-law behavior $T^{-\alpha}$ of the mobilities.

versely proportional to the carrier concentration. However, it is clear that such large increases in $R_H(0)$ with no sign of saturation is incompatible with this simple interpretation, since the resistivity shows only a 20% and 50% change at T_1 and T_2, respectively. Nevertheless, one would hope that the Hall data would be amenable to a reasonably straight-forward interpretation, and provide experimental evidence of loss of carriers as required by the canonical CDW theory.[3] The change of sign of $R_H(0)$ at 15 K indicates that a two-band model is appropriate for $NbSe_3$. This is also consistent with the very large transverse magnetoresistance observed at low temperatures. The expression for the Hall constant at zero field for the two-band model (assuming a closed simply-connected FS for both holes and electrons) is given by[22]

$$R_H(0) = -(n\mu_1\mu_2 - p\nu_1\nu_2)/e(n\mu_1 + p\nu_1)(n\mu_2 + p\nu_2)\,, \tag{7}$$

where e is the magnitude of the electronic charge, $n(p)$ are the electron (hole) density, $\mu_1(\mu_2)$ is the electron mobility in the $x(y)$ direction and ν_1, ν_2 are the analogous hole mobilities. The form of the denominator suggests that a simpler expression is obtained by dividing Eq. (7) by $(\rho_1\rho_2)$. This gives

$$A \equiv R_H(0)/\rho_1\rho_2 = e(p\nu_1\nu_2 - n\mu_1\mu_2)\,, \tag{8}$$

whose absolute value is plotted in Fig. 2 (open circles) in log-log scale. It becomes immediately apparent that the temperature dependence of A is dominated by that of the mobilities (lifetimes of carriers) which have a power-law dependence. Dividing out this power-law dependence we thus isolate the temperature variation predominantly due to n and p. In Fig. 3 the quantity $A(T)(T/T_2)^{3.875}$ is shown versus temperature. The deviation above 40 K of A from the straight line in Fig. 2 now manifests itself as a sharp change in the hole concentration relative to the electron concentration. To be consistent with the conventional concepts of gap formation at the FS we postulate from Fig. 3 that the gapping occurs at the hole surface. This is because $(p\nu_1\nu_2 - n\mu_1\mu_2)(T/T_2)^{3.875}$ increases algebraically as T_2 is approached from below.

(The reader may question our treatment of the Hall effect due to the thermally excited quasiparticles. On the hole FS the excitation of holes across the CDW gap leaves vacancies behind which are electronlike. These will presumably contribute a negative Hall signal, and to a first approximation, cancel the Hall signal from the excited holes. However, this argument is incorrect. By studying the topology of the constant energy surfaces it may be shown that the vacancies will always have the same galvanomagnetic response as the excited quasiparticles. A more detailed treatment is offered elsewhere.) Much the same analysis can be applied to the Hall data above T_2. Again we find that A vs T in a log-log scale falls on a straight line of slope -2.792 except near T_1. Dividing out this power-law dependence shows the same carrier freeze-out phenomenon below T_1 (see Fig. 4) rather more clearly than in Fig. 3 because $R_H(0)$ has no zero crossing above T_2. Above T_1, $A(T/T_1)^{1.744}$ is temperature independent indicating no relative changes in the electron and hole concentrations. Thus the slight decrease in $R_H(0)$ above 145 K that is evident in Fig. 3 of Ref. 11 is entirely due to the temperature dependence of $\rho_b\rho_c$. Similar to the T_2 transition we conclude that at T_1 the loss of carriers occurs on the hole FS. From the foregoing the picture that emerges is that above T_1, R_H is negative $(n\mu_1\mu_2 > p\nu_1\nu_2)$. At T_1 a gap occurs on the hole FS associated with a CDW with spanning vector[14] (0, 0.24, 0). The decrease in p relative to n drives R_H more negative. However, A (with the temperature dependence of the lifetime divided out) decreases smoothly before saturating instead of dropping abruptly to its sat-

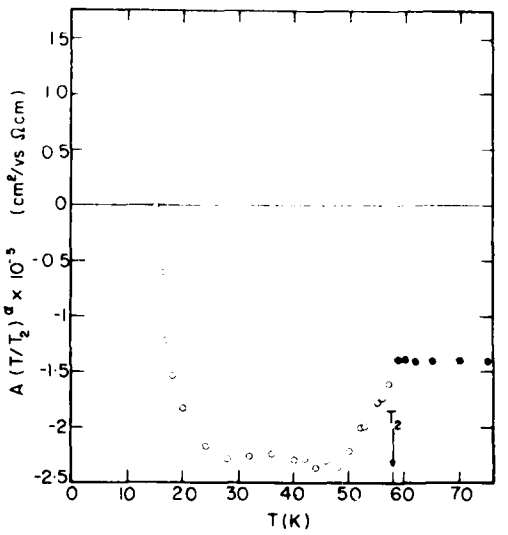

FIG. 3. Temperature dependence of A with the power-law dependence $T^{-\alpha}$ divided out. Below T_2 (open circles) α equals 3.875. Above T_2 (solid circles) α has the value 2.792. It argued in the text that the increase in A as the temperature increases towards T_2 is due to the thermal excitation of quasi-particles across the CDW gap.

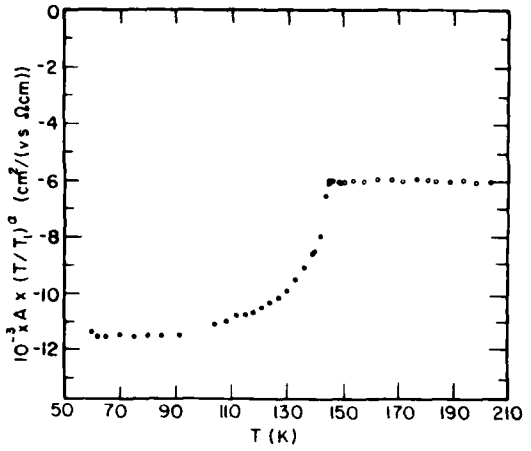

FIG. 4. Temperature dependence of $A(T/T_1)^{\alpha}$ around the upper transition. Below T_1 (solid circles) α equals 2.792 while above T_1 (open circles) α equals 1.774. Between ~100 and 145 K the steep rise in $A(T/T_1)^{\alpha}$ is ascribed to the thermal generation of quasiparticles across the CDW gap on the hole Fermi surface. Note that $A(T/T_1)^{\alpha}$ is temperature independent above T_1 and below 100 K.

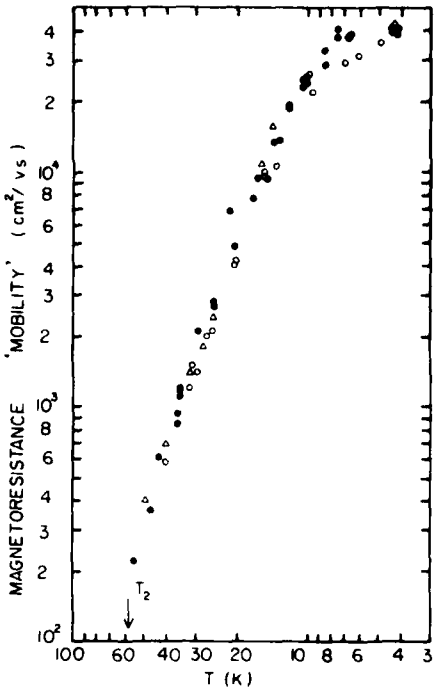

FIG. 5. Transverse magnetoresistance expressed as an effective mobility μ_M vs temperature in log-log scale [see Eq. (9)]. Data from three samples are shown. Note that the mobility μ_M continues to decrease with increasing temperature between 40 and 58 K whereas the longitudinal conductivity is rapidly rising in this temperature interval. This implies a steep increase in carrier concentration as discussed in the text.

uration value. This is due to the thermal excitation of quasiparticles (which are holes) across the developing gap. Below ~90 K these quasiparticles have been frozen out and $A(T/T_1)^{+2.792}$ becomes temperature independent until T_2 where a new gap—again associated with the hole surface—appears in conjunction with a CDW of spanning vector[15] (0.5, 0.26, 0.5). A is again driven to more negative values and the appearance of thermally excited quasiparticles (again holes) is shown in Fig. 3. At ~40 K the freeze out of these carriers is complete. No further change in carrier population occurs below 40 K. The reversal of sign of A is presumably due to the steady increase of the hole mobility versus the electron mobility at low temperatures. This picture is borne out by the analysis presented in II.

Figure 5 presents the transverse magnetoresistance data at low magnetic fields. We have defined the effective magnetoresistance mobility μ_M as the square root of the coefficient of B^2 in the expansion of the resistivity in a Taylor's series,

$$\rho(B) = \rho(0)(1 + \mu_M^2 B^2 + \cdots). \tag{9}$$

Figure 5 shows the temperature dependence of μ_M in log-log scale. The striking feature of the data, in view of the model sketched above, is the monotonic power-law decrease of μ_M as T_2 is approached from below. Significantly, whereas $|R_H|$ and $\rho_b \rho_c$ attain a maximum before decreasing to their value at T_2, μ_M shows no such structure. Insofar as μ_M measures the lifetime of the carriers (in an averaged way) this immediately implies that the steep rise in conductivity in both b and c directions as the temperature increases from 40 K to T_2 is *not* due to any increase in carrier lifetimes. Taken together with the change in carrier concentration shown by the data on A, the data in Fig. 5 give strong support to the conventional picture of FS gapping at a CDW transition.

IV. CONCLUSION

The first measurements on the transverse dc resistivity of a transition-metal trichalcogenide are presented. Although the linear-chain crystal structure of $NbSe_3$ suggests the possibility of quasi-one-dimensional behavior the measured anisotropy (~20) is several orders of magnitude smaller than the best one-dimensional conductors. Nonetheless, the peculiar transport properties of this metal make it directly relevant to

the issues of interest in the field of highly anisotropic conductors, particularly the question of the depinning of the CDW condensate and the sliding Fröhlich mode. Some clarification of the electronic instabilities have been obtained by studying the conductivity anisotropy in relation to the Hall constant and transverse magnetoresistance. In particular it is demonstrated that the gapping occurs on the hole FS at both transitions. Furthermore, the giant resistivity anomalies in the longitudinal resistivity are shown to be a consequence of loss of carriers at T_1 and T_2 due to the slow freeze-out of thermally excited quasiparticles across a developing gap. This confirms the previously published[13] analysis of the non-Ohmic data which also showed that the decrease in conductivity was consistent with carrier freeze-out across a gap which could be described by the BCS equation. In particular, by combining the product $\rho_b \rho_c$ with previously published[11] data on the zero-field Hall constant $R_H(0)$ which shows a surprisingly large change at T_1 and T_2 we obtain an expression which shows more transparently the decrease in the hole concentration below T_1 and T_2. Finally, the transverse magnetoresistance provides complementary information on the averaged lifetime of the carriers and shows explicitly that the resistivity anomaly at T_2 is not due to pathological changes in carrier mobilities, as has been suggested by other workers.[24]

ACKNOWLEDGMENT

We are grateful to J. Savage for sample preparation work and Dr. J. C. Woo for help with the measurements. This work was supported by a grant from the Office of Naval Research No. N00014-77-C-0473.

[1]J. A. Wilson, F. J. DiSalvo, and S. Mahajan, Adv. Phys. 24, 117 (1975).
[2]W. L. McMillan, Phys. Rev. B 14, 1496 (1976).
[3]S. K. Chan and V. Heine, J. Phys. F 3, 795 (1973).
[4]A. Meerschaut and J. Rouxel, J. Less Common Metals 39, 197 (1975).
[5]P. Haen, P. Monceau, B. Tissier, G. Waysand, A. Meerschaut, P. Molinie, and J. Rouxel, *Proceedings of the Fourteenth International Conference on Low Temperature Physics* (North-Holland, Amsterdam, 1975), Vol. 5, p. 445.
[6]J. Rijnsdorp and F. Jellinek, J. Solid State Chem. (to be published).
[7]T. Sambongi, K. Tsutsumi, Y. Shiozaki, M. Yamamoto, K. Yamaya, and Y. Abe, Solid State Commun. 22, 729 (1977).
[8]T. Sambongi, M. Yamamoto, K. Tsutsumi, Y. Shiozaki, K. Yamaya, and Y. Abe, J. Phys. Soc. Jpn. Lett. 42, 1421 (1977).
[9]A review appears in *One-Dimensional Conductors*, edited by H. G. Shuster (Springer-Verlag, Berlin, 1975).
[10]J. Chaussy, P. Haen, J. C. Lasjaunais, P. Monceau, G. Waysand, A. Waintal, A. Meerschaut, P. Molinie, and J. Rouxel, Solid State Commun. 20, 759 (1976).
[11]N. P. Ong and P. Monceau, Solid State Commun. 26, 487 (1978). The *c* axis is mislabeled as the *a* axis in this reference.
[12]J. W. Brill and N. P. Ong, Solid State Commun. 25, 1075 (1978).
[13]N. P. Ong, Phys. Rev. B 17, 3243 (1978).
[14]T. Tsutsumi, T. Takagaki, M. Yamamoto, Y. Shiozaki, M. Ido, and T. Sambongi, Phys. Rev. Lett. 39, 1675 (1977).
[15]R. M. Fleming, D. E. Moncton, and D. B. McWhan, Bull. Am. Phys. Soc. 23, 425 (1978).
[16]S. Nakamura, and R. Aoki, Solid State Commun. 27, 151 (1978).
[17]P. Monceau, N. P. Ong, A. M. Portis, A. Meerschaut, and J. Rouxel, Phys. Rev. Lett. 37, 602 (1976).
[18]N. P. Ong and P. Monceau, Phys. Rev. B 16, 3443 (1977).
[19]P. A. Lee, T. M. Rice, and P. W. Anderson, Solid State Commun. 14, 703 (1974).
[20]D. Allender, J. W. Bray, and J. Bardeen, Phys. Rev. B 9, 119 (1974)
[21]J. Bardeen, "Recent Developments and Comments," in *Highly Conducting One-Dimensional Solids*, edited by J. T. Devresse (Plenum, New York, to be published).
[22]N. P. Ong, Phys. Rev. B 18, 5272 (1978) (following paper, referred to as II).
[23]P. Monceau, Solid State Commun. 24, 331 (1977).
[24]R. M. Fleming, J. A. Polo, and R. V. Coleman, Phys. Rev. B 17, 1634 (1978).
[25]P. Monceau and A. Briggs, J. Phys. C 11, L465 (1978).
[26]H. C. Montgomery, J. Appl. Phys. 42, 2971 (1971).
[27]L. B. Coleman, Rev. Sci. Instrum. 46, 1125 (1975).
[28]B. F. Logan, S. O. Rice, and R. F. Wick, J. Appl. Phys. 42, 2975 (1971).

PHYSICAL REVIEW B VOLUME 18, NUMBER 10 15 NOVEMBER, 1978

Two-band model for $NbSe_3$ (Ohmic regime)

N. P. Ong
Department of Physics, University of Southern California, Los Angeles, California 90007
(Received 10 July 1978)

The charge-density-wave (CDW) linear-chain metal $NbSe_3$ shows striking non-Ohmic behavior when the applied electric field exceeds ~ 0.1 V/cm. Hall effect, transverse magnetoresistance, conductivity anisotropy, and Shubnikov–de Haas measurements using sufficiently low current densities to avoid Ohmic breakdown have been published. We propose a simple two-band model to account for the temperature dependence of these quantities as well as the (magnetic) field dependence of the Hall constant in the Ohmic regime below 58 K. The model has six unknowns (carrier concentrations and mobilities) that are fixed by six experimental numbers at each temperature T. The solution shows that all the mobilities obey a power-law behavior versus T, whereas the carrier concentrations are both T independent up to 40 K. Above 40 K the hole population rises sharply, analogous to the theoretical predictions for an excitonic insulator. This implies that the CDW gap occurs on the hole surface. Using the parameters of the model, we have recomputed the resistivities, Hall constant, and magnetoresistance, and they have been shown to agree with all the available experimental data. Thus the conventional single-particle picture with the additional hypothesis of a BCS-type gap on the hole surface is adequate for understanding the transport properties of $NbSe_3$ in the zero-frequency-Ohmic regime. We also interpret the SdH data in terms of the two-band model.

I. INTRODUCTION

Below the transition temperature T_1 (~142 K) the transport properties of the charge-density-wave (CDW) metal[1] $NbSe_3$ are conveniently divided into three regimes for the purpose of analysis. These are, (i) the zero-frequency low-current (Ohmic) regime; (ii) the zero-frequency high-current (non-Ohmic) regime; (iii) the high-frequency (above ~100 MHz) low-current regime. (There clearly exists a fourth regime: the high-frequency non-Ohmic regime, but no experimental data exist in this regime.) Strong interest has been generated by the study of regimes (ii) and (iii) because of the possibility of studying experimentally the dynamics of a sliding CDW in a real metal. Such studies will shed light on (a) the nonlinear dynamics associated with a drifting CDW,[2] (b) the nature of the pinning forces impeding its motion, and (c) the feasibility of realizing a system in which the sliding Fröhlich mode leads to superconductivity. With regard to (b) the ease with which the pure compound is alloyed[3] or intercalated[4,5] with Li makes it an attractive system in which to study the pinning effects of the CDW condensate due to impurities. Such impurity studies are presently underway and show[3] that the behavior in regimes (ii) and (iii) are exceedingly sensitive to impurity concentrations.

Most of the galvanomagnetic[1,6] as well as Fermiology[7–9] studies done to date have been in regime (i) where the applied electric fields are sufficiently low to avoid Ohmic breakdown. Although regime (i) is of less interest as compared to (ii) and (iii) it is essential to obtain a picture of the "normal" regime that is as complete as experimentally feasible so that the intriguing additional effects (conductivity enhancement) in regimes (ii) and (iii) can be isolated and analyzed. In this paper we construct a simple two-band model that will account for the galvanomagnetic and conductivity anisotropy data [regime (i)] presented in Refs. 1, 6, and 8. Single crystals of $NbSe_3$ usually grow in the shape of long ribbons with the long side along the (chain) b axis and the wider transverse dimension along the c axis. Low-magnetic-field Hall measurements with $\boldsymbol{H}$ along a^* have been reported by Ong and Monceau (OM).[6] High-field-Hall measurements in the same geometry have been presented by Fleming, Polo, and Coleman (FPC).[8] Transverse magnetoresistance ($H||a^*$) were presented in the preceding paper[1] as well as conductivity anisotropy measurements. In addition, extensive Shubnikov–de Haas (SdH) measurements have been carried out by Monceau (M),[7] Fleming *et al.* (FPC)[8], and Monceau and Briggs (MB).[9] It will be seen that a two-band model can satisfactorily account for much of the data in these studies below the T_2 transition. Out of this analysis we obtain the temperature dependence of the four mobilities in the b-c plane as well as the carrier concentration in both bands. In support of the conventional CDW model,[10,11] our analysis shows that the carrier concentrations are temperature independent below ~40 K. Above 40 K the hole population rises dramatically in analogy with the increase in thermally excited quasiparticles across the Fermi surface (FS) gap of an excitonic insulator.[12] In contrast the electron population remains con-

stant up to 58 K. Persuasive evidence identifies the electron pocket with the ellipsoidal pocket seen in the SdH oscillations of M, FPC, and MB. The evidence for a hole pocket is unclear at present. This two-band analysis enables us to disentangle the individual contributions of the four mobilities to the conductivity anisotropy, the Hall signal and the transverse magnetoresistance. It will be shown for instance that the twelve-fold increase in $|R_H(0)|$ at T_2 is compatible with the twofold rise in the longitudinal resistivity and the still smaller rise in the transverse resistivity. The zero crossing of $R_H(0)$ at ~15 K is due to the faster increase of the hole mobilities relative to the electron mobilities as the temperature drops, and not to any change in the carrier population. On the other hand, the giant anomaly in the resistivities is due to the rapid change in hole concentration between ~40 K and T_2. No anomalous structure is reflected in any of the mobilities. This is also presumably the case at the upper transition, although the lack of sufficient galvanomagnetic data and theoretical considerations preclude the extension of our analysis beyond 58 K.

II. TWO-BAND MODEL

The single-particle picture with a semiclassical treatment of the transport properties[13] has been remarkably successful when applied to ordinary metals and semiconductors. To make the analysis manageable we have assumed the simplest Boltzmann equation-relaxation time approach in computing the galvanomagnetic response. Since the details are found in many text books[14] we will present results only. The assumptions intrinsic to the model are as follows. (a) At low-temperatures there exist two closed FS pockets containing electrons and holes, respectively. (b) These pockets are ellipsoids with their principal axes along a^*, b, and c. (c) The relaxation time is assumed isotropic and independent of magnetic field and complications such as intense scattering from "hot spots" on the FS will be disregarded. Assumptions (a) and (b) are indicated by the SdH data which show two branches. The prominent branch is consistent with an ellipsoid of moderate anisotropy with principal axes along a^*, b, and c. Less conclusive evidence is available for the other pocket which we take to be ellipsoidal as well. The third assumption will be discussed together with the computed magnetoresistance. No further justification of the assumptions will be discussed except to appeal to the comparison of the computations with the experiments.

In the Boltzmann equation approach the current is given by[14]

$$\vec{J} = \sum_{\vec{k}} \left(-\frac{\partial f}{\partial \epsilon} \right) e^2 \tau \vec{v}_{\vec{k}} \cdot \vec{A} \vec{v}_{\vec{k}} = \frac{2e^2\tau}{(2\pi)^3} \int_{\epsilon_F} \frac{dS_F}{|\hbar v_{\vec{k}}|} \vec{v}_{\vec{k}} \cdot \vec{A} \vec{v}_{\vec{k}} . \tag{1}$$

$$\vec{A} \equiv \left(\vec{E} - \frac{e\tau}{(m_1 m_2)^{1/2}} \vec{H} \times \vec{E} \right) \Big/ \left(1 + \frac{e^2\tau^2}{m_1 m_2} H^2 \right) , \tag{2}$$

where $\vec{v}_{\vec{k}} = \hbar^{-1} \partial \epsilon_{\vec{k}} / \partial \vec{k}$ is the velocity of the carrier at $\vec{k}$, f is the Fermi-dirac distribution, τ the isotropic relaxation time, m_i the effective mass along the i axis and the integral in (1) is over the FS. In general the relaxation time may be anisotropic as well, aspecially if the system is highly anisotropic. However, the galvanomagnetic measurements analyzed here cannot distinguish between mass and relaxation time anisotropy. In the spirit of the model we will describe all the observed anisotropy in terms of the mobilities. Assuming a quadratic dispersion it is straightforward to reduce Eq. (1) to the familiar conductivity matrix for electrons (with $\vec{H}$ along the three axis)

$$\bar{\sigma}_n = \frac{ne}{[1 + (\mu_1\mu_2 H)^2]} \begin{pmatrix} \mu_1 & -\mu_1\mu_2 H \\ \mu_1\mu_2 H & \mu_2 \end{pmatrix} , \tag{3}$$

where the mobility $\mu_i \equiv e\tau / m_i$ has been introduced and n the carrier concentration is given by

$$n = \frac{2}{(2\pi)^3} \int_0^{\epsilon_F} d\epsilon \int_{\epsilon} \frac{dS_F}{|\hbar v|} . \tag{4}$$

Calling the hole concentration p and the hole mobilities ν_i we have for the total conductivity matrix

$$\bar{\sigma} = \frac{n}{[1 + (\mu_1\mu_2 H)^2]} \begin{pmatrix} \mu_1 & -\mu_1\mu_2 H \\ \mu_1\mu_2 H & \mu_2 \end{pmatrix} + \frac{p}{[1 + (\nu_1\nu_2 H)^2]} \begin{pmatrix} \nu_1 & +\nu_1\nu_2 H \\ -\nu_1\nu_2 H & \nu_2 \end{pmatrix} . \tag{5}$$

For convenience we have absorbed e into n and p. All quantities in Eq. (5) are assumed positive. The sign difference in the off-diagonal elements has been shown explicitly. In the experimental situation[15,16] it is actually the resistivity matrix $\bar{\rho} = \bar{\sigma}^{-1}$ which is measured. Explicitly, if the constant current is along the two-axis (b axis) and the magnetic field along the three-axis (a^* axis) the electric field along the one and two axes is given by $\vec{E} = \bar{\rho} \cdot \vec{J}$ where $\vec{J} = (0, J_0)$. The Hall voltage is proportional to $E_1 = \rho_{12} J_0$ whereas the transverse magnetoresistance is measured by $E_2 = \rho_{22} J_0$. Inverting the matrix in Eq. (5) we may show that the Hall constant $R_H \equiv E_1/(HJ_0)$ is given by

$$R_H(H) = -A(H)/(B_1 B_2 + A^2 H^2) , \tag{6}$$

where

$$A(H) \equiv n\mu_1\mu_2 [1 + (\mu_1\mu_2 H)^2] - p\nu_1\nu_2 [1 + (\nu_1\nu_2 H)^2] \tag{7}$$

and

$$B_i \equiv n\mu_i/[1+(\mu_1\mu_2H)^2]+p\nu_i/[1+(\nu_1\nu_2H)^2]. \quad (8)$$

In the limits of zero field and infinite field Eq. (6) reduces to

$$R_0 \equiv R_H(0) = -(n\mu_1\mu_2 - p\nu_1\nu_2)/(n\mu_1+p\nu_1)(n\mu_2+p\nu_2) \quad (9)$$

and

$$R^\infty \equiv R_H(\infty) = -1/(n-p). \quad (10)$$

We have adopted the convention that R_H is negative if there are no holes present ($p=0$). From Eqs. (9) and (10) it is clear that whereas the sign of R^∞ is determined by the more populous carrier type the sign of R_H at low fields is also influenced by the relative sizes of the mobilities and the anisotropy in each band. The longitudinal resistance in the presence of a weak magnetic field behaves as $\rho(H)=\rho_0(1+\mu_M^2H^2)$ where μ_M is the effective magnetoresistance mobility. From the diagonal element of the resistivity matrix we calculate

$$\mu_M^2 = \frac{\rho_{22}(H)-\rho_{22}(0)}{H^2} = \frac{np\mu_1\nu_1(\mu_2+\nu_2)^2}{(n\mu_1+p\nu_1)(n\mu_2+p\nu_2)}. \quad (11)$$

We note that μ_M vanishes if either n or p is zero. This is the expected result in a single band where the relaxation time is energy independent. The Hall field prevents any deflection of the carriers and the measured longitudinal resistance is unaffected by a transverse magnetic field. Furthermore μ_M vanishes if $\mu_2=-\nu_2$, i.e., if the two bands have the same sign of charge and the same longitudinal mobility. The longitudinal mobility is responsible for this cancellation because the longitudinal velocity sets up the Lorentz force. As mentioned above the mobilities themselves are assumed to be field independent. In principle the relaxation time can have a field dependence such as $\tau^{-1}=\tau_0^{-1}+\alpha^2H^2$. However, since the observed magnetoresistance at low temperatures is very large we shall assume that the dominant effect is due to the deflection of carrier trajectories arising from mutual (partial) cancellation of the Hall field of the holes and electrons. The existance of hot spots on the FS where electron-phonon interaction is enhanced can also affect the magnetoresistance. But in the low-field limit where the carriers sample only a limited portion of the FS before being scattered we may neglect such complications.

In the model described by Eq. (5) there are six unknowns, n, p, μ_1, ν_1, μ_2, and ν_2. At each temperature there are four measured quantities: the Hall constant $R_H(0)$, the transverse magnetoresistance, and the zero-field resistivities

$$\rho_i \equiv (n\mu_i+p\nu_i)^{-1}. \quad (12)$$

The Hall constant at infinite field R^∞ which can be measured only at very low temperatures provides a constraint through Eq. (10). Finally, the field dependence of R_H at each temperature provides the sixth equation to determine the six unknowns, leaving no adjustable parameters. Although the analytical inversion of the six equations is rather difficult the numerical solution may be readily accomplished by first forming the dimensionless constants

$$C_1 \equiv \mu_M(\rho_1\rho_2)^{1/2}/(R^\infty - R_0), \quad (13)$$

$$C_2 \equiv \mu_M(\rho_1\rho_2)^{1/2}/R^\infty. \quad (14)$$

(It turns out that C_1 and C_2 may be measured very accurately even if the sample dimensions are unknown. This is because $(\rho_1\rho_2)^{1/2}$ (determined by Montgomery's[17] technique) is independent[1] of b and c, and is linear in a (the dimension along $\vec{H}$). This is also true of $R_H(H)$. μ_M is independent of sample dimensions. Thus C_1 and C_2 are the ratio of voltmeter readings). A closed subset of three equations can be formed which expresses C_1, C_2, and $R_H(H)/R^\infty$ in terms of the three dimensionless parameters

$$r = n/p, \quad \eta = \mu_1/\nu_1, \quad \text{and } \xi = \mu_2/\nu_2. \quad (15)$$

Finally, these three equations can be solved numerically for r, ξ, and η. Details of the solution are presented in the appendix. We note that insofar as C_1, C_2, and R_H/R^∞ do not depend on sample dimensions the values r, η, and ξ will not be influenced by uncertainties in sample dimensions. However, to compute μ_1, ν_1, μ_2, and ν_2 separately we need to use the anisotropy ρ_1/ρ_2 which, of course, depends on the ratio b/c.

In the foregoing analysis we have assumed that the carrier concentrations are temperature dependent. This enables us to use the value of R^∞ measured at 2 K to fix the value of $(p-n)$. (It is not possible to measure R^∞ at elevated temperatures with currently available magnetic fields.) This assumption is justified in a self-consistent fashion by the solutions below 36 K which show that r in Eq. (15) is temperature independent. However, this assumption is invalid at temperatures above ~40 K where a previous analysis[18] of the non-Ohmic conductivity data shows that substantial thermal excitation of quasiparticles across the CDW gap occurs. This is also clearly demonstrated by Hall data in Figs. 3 and 4 of the previous paper.[1] In addition the field dependence of $R_H(H)$ has not been measured for temperatures above 36 K. Thus we are deprived of two pieces of experimental information. To continue the analysis to higher temperatures we need to introduce a fourth assumption: (d) the electron con-

centration n remains temperature independent from 36 to 58 K. This implies that the electron mobility μ_2 decreases with the same power law. The remaining four unknowns μ_1, ν_1, ν_2, and p are then computed from the measured ρ_1, ρ_2, $R_H(0)$, and μ_M. With this fourth assumption we find that (Fig. 1) the computed μ_1 (and ν_1) deviates only very slightly from its previous behavior; and p rises dramatically to four times its value at 36 K. The computed behavior of μ_1 provides justification for assumption (d) (that the electron pocket is not affected by the T_2 transition) while the exponential rise in p agrees with the gap analysis of Ref. 18. It is easy to see from the measured temperature behavior of $R_H/\rho_1\rho_2$ that, as the temperature approaches T_2 from below, either p rises rapidly or n decreases rapidly. Since the conductivity in both directions is also rising in this temperature range the first case is the obvious choice. (We have repeated the computation with the different assumption that p is held constant between 36 and 58 K and found that all the mobilities turn around and increase with temperature as T_2 is approached. This picture is certainly harder to justify.) Thus assumption (d) is the simplest one that provides physically reasonable behavior for the mobilities and carrier concentrations, under the four constraints provided by $R_H(0)$, ρ_1, ρ_2, and μ_M.

III. RESULTS AND DISCUSSION

Figure 1 shows the temperature dependence below T_2 of the four mobilities obtained by the solution of Eqs. (6)–(12). (For compactness the transverse hole mobility ν_c has been multiplied by 100.) All four mobilities show power-law behavior in this range before saturating at low temperatures. The longitudinal mobilities are surprisingly large at liquid-helium temperatures (270 000 cm^2/V sec). However, we note that at 40 K where the non-Ohmic effects are the most dramatic[18,19] μ_b and ν_b are only of the order of 3 000 cm^2/V sec. At 4 K the electron pocket anisotropy is 15 compared to 23.8 for the hole pocket. The carrier concentration n and p obtained from this analysis is shown in Fig. 2. As mentioned above both n and p are temperature independent below 40 K. Above 40 K, p rises rapidly, reflecting the thermal excitation of quasiparticles across a diminishing CDW gap on the hole surface. The solid line is the least-squares fit which provides the values of p used in all subsequent computations. The broken line indicates the assumed temperature-independent value of n above 40 K.

To check the validity of the solution we have made a least-squares fit to the calculated values in Fig. 1 and then used these values to recompute ρ_1, ρ_2, R_H, and μ_M. The electron concentration is taken to be fixed at 1.088×10^{18} cm^{-3} and p is taken from Fig. 2. Figure 3 shows the comparison of the computed ρ_1, ρ_2, and $R_H(0)$ with the experimental data while Fig. 4 shows the comparison for μ_M. The largest discrepancy occurs for $R_H(0)$, especially at temperatures below 12 K. This is to be expected for two reasons. Whereas ρ_1, ρ_2, and μ_M measure the additive effect of the two pockets the Hall constant measures the competition between the mobilities of the two pockets. Also R_H cannot be measured with the same precision as that of ρ_1 and ρ_2. At low temperatures where all

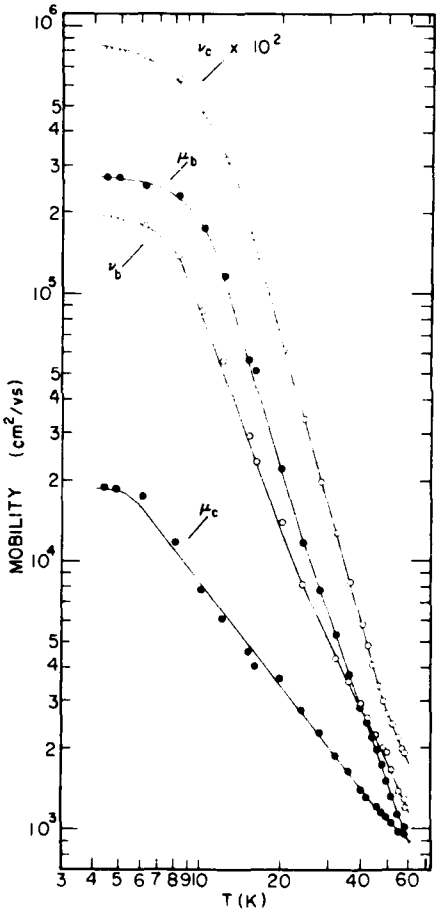

FIG. 1. Temperature dependence of the electron (solid circles) and hole (open circles) mobilities below 58 K. The data points are calculated from the experimental data using Eqs. (6)–(12). The lines are a least-squares fit to the data. In all cases the mobilities obey a power-law behavior except at low temperatures where they saturate. At 4 K the electron mobility ratio μ_b/μ_c equals 15, and the hole mobility ratio is 23.8. Note that the transverse hole mobility ν_c has been multiplied by 100.

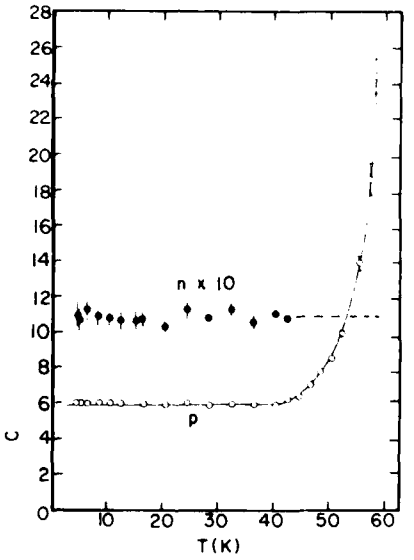

FIG. 2. Temperature dependence of the electron (solid circles) and hole (open circles) concentration. The data points below 40 K are computed from Eqs. (6)–(12) of text, and the error bars reflect the uncertainty in the measurements. Above 40 K the broken line indicates the assumed temperature-independent value of the electron concentration (1.09×10^{18} cm^{-3}). The open circles above 40 K are the computed values of p using this assumption. The solid line is the least-squares fit to the computed data on p.

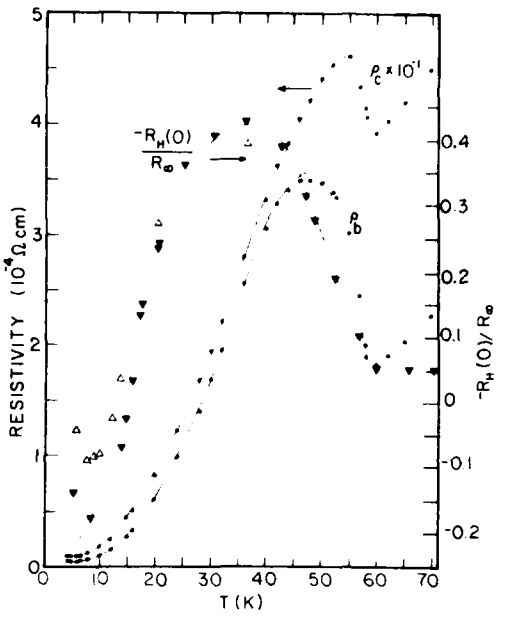

FIG. 3. Comparison of the experimental data for the resistivities ρ_b and ρ_c (circles), and the zero-field Hall constant $R_H(0)$ (triangles) with the two-band model calculation. The lines represent the values of $R_H(0)$, and ρ_b and ρ_c calculated using Eqs. (9) and (12). The values of the mobilities used are given by the full lines in Fig. 1. The electron concentration is assumed fixed at 1.09×10^{18} cm^{-3} and the hole concentration is given by the full line in Fig. 2. Values of $R_H(0)$ at low temperatures appear to be sample dependent. (The open and solid triangles are data from two samples normalized to the same value at infinite field.)

the mobilities are large R_H becomes very sensitive to the values of r, η, and ξ. At the same time, the zero-field value of R_H cannot be measured accurately due to the narrow range of fields over which R_H is field independent. Thus the computed values of r, η, and ξ below 12 K are accurate to only 20%. We have found also that the values of $R_H(0)$ and R^∞ at 2 K have a slight variation from sample to sample.[20]

The computed field dependence of R_H is shown in Figs. 5 (low fields) and 6 (high fields). (The experimental data in Fig. 6 are from FPC.) While the agreement in Fig. 5 is excellent except at very low temperatures, in Fig. 6 we have had to adjust the temperature of the sample to improve the fit at high fields. At low fields (~20 kG) the disagreement is larger. The value of $R_H(0)$ (the slope in Fig. 6) at 30 K is approximately equal and opposite in sign to R^∞ at 4.2 K in FPC's data whereas in the data used for this analysis the same quantity is only 40%. This accounts for the large discrepancy in Fig. 6 at low fields. The disagreement may be sample dependent.

We now turn to the SdH data and see to what extent the model described here is supported by the FS mapping obtained by means of the Shubnikov oscillations. The most extensive measurements on $NbSe_3$ are those of MB whose measurements indicate the presence of two branches and possibly a third. Along directions of the magnetic field where the oscillations are strong the data of MB agree with the preliminary data of M and FPC. The first branch which is the most well defined in MB's data corresponds to an approximately ellipsoidal surface with its principal axes along a^*, b, and c. The shortest dimension is along b and the longest is along c. If the semiaxis dimensions are k_{a^*}, k_b, and k_c the volume of the ellipsoid is $V=\frac{1}{3}S_c\times(S_a/4\pi\epsilon)^{1/2}$ where $S_a=4\pi k_b k_c$, $S_c=4\pi k_{a^*}k_b$, and $\epsilon=k_b/k_c$. From the SdH data of M, FPC, and MB, $S_c=0.3$ MG (2.86×10^{13} cm^{-2}), $S_a=1.05$ MG (1.00×10^{14} cm^{-2}). The carrier density within this FS pocket is thus equal to $n=2.17\times10^{17}/\sqrt{\epsilon}$ cm^{-3}. FPC find that $\epsilon\simeq\frac{1}{8}$ gives the best fit to the angular dependence of the frequency as the magnetic field is rotated towards the b axis. MB's data favor a smaller ϵ. In any case the carrier concentration is of the order of 6×10^{17}cm^{-3} which is in order-

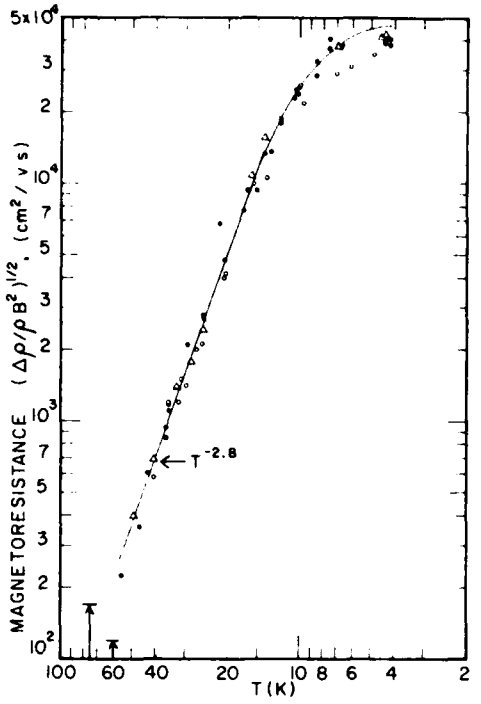

FIG. 4. Comparison of the experimental data for the magnetoresistance mobility with the two-band model calculation. The full line is calculated from Eq. (11) with the model parameters given by the full lines in Figs. 1 and 2. Data from three samples (Ref. 1) are displayed.

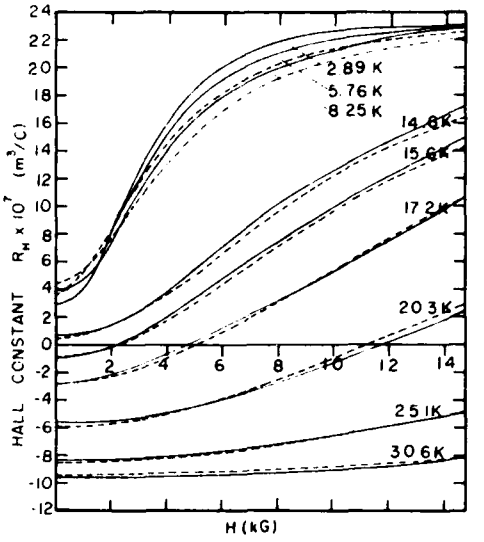

FIG. 5. Field dependence below 14 kG of the Hall constant at various temperatures below 40 K. The full lines are the experimental curves from Ref. 6 and the broken lines are calculated from Eqs. (6)–(8) using model parameters given by the full lines in Figs. 1 and 2. The computed R_H has been adjusted by a scale factor for comparison with the measurements (see Ref. 20). Agreement is excellent except at low temperatures where R_H is very sensitive to model parameters.

of-magnitude agreement with the electron concentration computed here (1.09×10^{18} cm^{-3}). Hence the ellipsoidal surface measured in the SdH data is probably the electron pocket. However, there are several difficulties in a careful comparison of the detailed SdH measurements of MB and FPC with our conclusions. First, the value of $\frac{1}{8}$ for ϵ would imply a mobility ratio of 64 (assuming a parabolic band) in the electron pocket. This is four times larger than the computed anisotropy in Fig. 1. This disagreement is probably due to the fact that this FS pocket resembles more a briefcase than an ellipsoid. MB's data agree with a cylindrical trajectory ($\epsilon \simeq 0$) with the magnetic filed tilted up to an angle of 70° from the a^*c plane.

Secondly, MB's data show other branches of the same order of magnitude in frequency which merge abruptly with the main branch. Over a certain angular range when the magnetic field is in the a^*c plane the main branch fades dramatically, leaving a ghost image of its original sec θ trajectory, while continuing with undiminished intensity into the new branch. These complications suggest that a simply connected ellipsoidal pocket is prob-

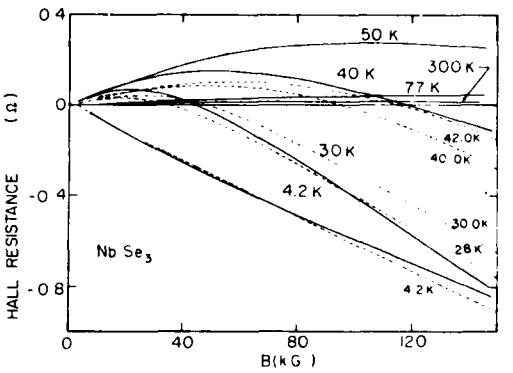

FIG. 6. Field dependence at high fields of the Hall resistance at various temperatures. The full lines are from Fleming, Polo, and Coleman (Ref. 8). The broken lines are calculated from the two-band model using parameters given by the solid lines in Figs. 1 and 2. The calculated Hall resistance has been normalized to agree with the experimental data at 4.2 K. The temperature of the sample has also been adjusted to give a better fit at high fields. There is a disagreement in the measured Hall polarity between Ref. 6 and Fleming *et al*. However, for the purpose of comparison we have changed the sign of the carriers in this figure.

ably too naive a picture. A possible explanation of these intriguing patterns is the intersection of the original pocket by higher-order superlattice Bragg planes. Indeed it may be shown[21] that several second-order images of the T_2-CDW Bragg plane oriented at 45° to the b-axis intersect the center of the Brillouin zone where the electron pocket would presumably be located. The faint ghost spots may be the result of magnetic breakdown[22] across these small gaps in analogy with the case[23] in Cr, while the abrupt appearance of a new branch may be the deflection of the electron trajectory into a new external orbit by the second-order gap.

The separation of the contributions of the two bands to the transport properties enables us to justify the argument used in the preceding paper with respect to $R_H(\rho_b\rho_c)^{-1}$. There it was argued that the quantity $A \equiv R_H(0)/(\rho_b\rho_c)$ had a temperature dependence which was dominated by the lifetime of the carriers. Dividing out the power-law behavior of the lifetimes enables us to observe the relative change in carrier concentration. From Fig. 1 the temperature dependence of the mobilities above 20 K is $T^{-1.2}(\mu_1)$, $T^{-2.8}(\mu_2)$, $T^{-3.5}(\nu_1)$, and $T^{-2.0}(\nu_2)$. Thus the quantity $A(T) = -(n\mu_1\mu_2 - p\nu_1\nu_2)$ has the temperature dependence $-(nT^{-4.0} - cpT^{-5.5})$ where c is a constant. Within the calculated parameters of the model the second term is 21% of the first at 50 K and increases to 61% at 58 K. Thus the first term dominates the behavior of A in this temperature range. We would then expect the quantity

$$A(T/T_1)^{3.875} \propto T^{-0.1}(n - cpT^{-1.4}),$$

to measure the relative change in carrier concentrations. The residual power law dependence $T^{-1.4}$ multiplying p unfortunately distorts the actual temperature dependence of p. However this is not serious near the transition because of the exponential increase in p. (A comparison of the data in Fig. 3 of the preceding paper with that in Fig. 2 here shows the slight difference between the temperature behavior of $A(T/T_1)^{3.875}$ and p.)

IV. CONCLUSION

The galvanomagnetic, conductivity and Shubnikov data obtained to date on $NbSe_3$ provide a rather complete picture of the low-temperature phase. To sort out the different components which contribute to the observed quantities we have adopted the simplest two-band model and used the experimental data to calculate the six unknowns in the model. Enough parameters are fixed by the measurements to leave no free parameters below 40 K. Above 40 K we have had to assume that the electron concentration remains temperature independent and shown that this is borne out self-consistently by the results. The picture that we obtain is that just below T_2 a CDW gap occurs on the hole surface. As the hole carriers are frozen out across the developing CDW gap, the total hole concentration decreases by a factor of 4. This results in only a factor of 2 rise in the longitudinal resistivity and an even smaller increase in the transverse resistivity because the electron mobilities are higher at this temperature. Below 40 K the carrier freeze out is complete, leaving 6.0×10^{18} cm^{-3} holes and 1.09×10^{18} cm^{-3} electrons. The remaining holes are from portions of the same FS which are not destroyed by the gap or may possibly belong to an entirely separate pocket. Below 36 K the Hall constant at zero field increases to more positive values and changes sign at 15 K because of the rapidly increasing hole mobilities. At very low temperatures the longitudinal mobilities become so large (~250 000 cm^2/V sec) that the Hall signal is rapidly driven to its infinite field value with the relatively modest field of 10 kG. In contrast to the Hall and resistivity data which show peak structures the transverse magnetoresistance obeys a smooth power-law behavior. This model also accounts for the strong field dependence of R_H (Fig. 6). The presence of the electron pocket is strongly indicated by the SdH data although the possibility of superlattice Bragg planes intersecting the electron FS may complicate the full interpretation of the SdH data. Evidence for the hole pocket is not apparent in the SdH data. Based on the parameters of this model, the resistivities, Hall constant, and magnetoresistance are calculated and good agreement is obtained with the experimental data.

The number of carriers participating in the T_2 transition is approximately 2×10^{19} cm^{-3} (16 times the electron concentration). This number, based on Fig. 2 is not meaningful if the gapping portion of the hole surface is not closed [since Eq. (5) is then no longer valid]. In fact the value of the transverse components of the spanning vector at T_2 $(0.5a^*, 0.5c^*)$[24] suggests that the FS that nests may be a cosine band[25] which intersects the Brillouin zone face. In this case Eq. (5) is clearly inadequate to describe contributions from all three sources. A third matrix obtained from a current term such as

$$\vec{J}_3 \cong \frac{2}{(e^{\beta\Delta}+1)} \frac{2e^2\tau}{(2\pi)^3} \int_{\text{gap}} \frac{dS_F}{|\hbar\vec{v}_{\vec{k}}|} \hat{v}_{\vec{k}} \cdot \hat{A}\hat{v}_{\vec{k}}$$

(where the integral is over the gapped portion of the FS) should be included. In spite of this qualification it is remarkable that the temperature dependence of p computed from Eq. (5) shows explicitly the exponential rise in quasiparticles as the

T_2 transition is approached. The number 2×10^{19} cm^{-3} should serve adequately as an order-of-magnitude estimate of the FS destroyed by the gap at T_2.

ACKNOWLEDGMENT

A useful discussion with Leo Falicov is gratefully acknowledged. This work was supported by the Office of Naval Research Contract No. N00014-77-C-0473. We wish to thank P. Monceau for sending a preliminary version of Ref. 9 prior to publication.

APPENDIX

Equations (6) and (9)–(12) may be reduced to a single equation involving only r as the unknown as follows. First, five of the equations are rewritten in terms of the dimensionless parameters [see Eq. (15)] r, ξ, and η, as

$$1/\rho_1 = p\nu_1(r\eta+1), \quad 1/\rho_2 = p\nu_2(r\xi+1), \quad R^\infty = 1/p(1-r). \tag{A1}$$

$$\mu_H/(\rho_1\rho_2)^{1/2} = p\nu_1\nu_2\sqrt{r\eta}(\xi+1), \tag{A2}$$

$$(R^\infty - R_0)/\rho_1\rho_2 = [rp\nu_1\nu_2/(1-r)](\xi+1)(\eta+1). \tag{A3}$$

By forming the dimensionless constants C_1 and C_2 we eliminate p, ν_1, and ν_2. Thus we have

$$C_1 \equiv \frac{\mu_H(\rho_1\rho_2)^{1/2}}{(R^\infty - R_0)} = \frac{(1-r)}{\sqrt{r}} \frac{\sqrt{\eta}}{(1+\eta)}, \tag{A4}$$

$$C_2 \equiv \frac{\mu_H(\rho_1\rho_2)^{1/2}}{R^\infty} = \frac{\sqrt{r\eta}(1-r)(\xi+1)}{(r\xi+1)(r\eta+1)}. \tag{A5}$$

With r as the independent variable η and ξ can be expressed in terms of r through Eqs. (A4) and (A5). The mobilities ν_1 and ν_2 can then be found from Eq. (A1) in terms of r. Finally $R_H(H)/R^\infty$ can be computed as a function of H by Eq. (6) with r as an adjustable parameter. The value of r which provides the best fit of R_H/R^∞ to the experimental data (Fig. 5) is taken to be the correct solution.

[1]See references in preceding paper, N. P. Ong and J. W. Brill, Phys. Rev. B 18, 5265 (1978).

[2]See, for example, M. L. Boriack and A. W. Overhauser, Phys. Rev. B 16, 5206 (1977); D. Allender, J. W. Bray, and J. Bardeen, Phys. Rev. B 9, 119 (1974).

[3]N. P. Ong, J. W. Brill, J. Eckert, and J. Savage, S. K. Khanna, and R. B. Somoano (unpublished).

[4]R. R. Chianelli and M. B. Dines, Inorg. Chem. 14, 2417 (1975).

[5]D. W. Murphy, F. A. Trumbore, and J. N. Carides, J. Electro-Chem. Soc. 124, 325 (1977).

[6]N. P. Ong and P. Monceau, Solid State Commun. 26, 487 (1978). The c axis is mislabeled as the a axis in this reference.

[7]P. Monceau, Solid State Commun. 24, 331 (1977).

[8]R. M. Fleming, J. A. Polo, and R. V. Coleman, Phys. Rev. B 17, 1634 (1978).

[9]P. Monceau and A. Briggs, J. Phys. C 11, L465 (1978).

[10]S. K. Chan and V. Heine, J. Phys. F 3, 795 (1973).

[11]M. J. Rice and S. Strässler, Solid State Commun. 13, 125 (1973).

[12]J. Zittartz, Phys. Rev. 164, 575 (1967); 165, 605 (1968).

[13]See, for example, *The Fermi Surface*, edited by W. A. Harrison and M. B. Webb (Wiley, New York, 1962).

[14]See, for example, J. M. Ziman, *Principles of the Theory of Solids*, (Cambridge University, Cambridge, England, 1964), Chap. 7.

[15]See, for example, A. H. Wilson, *The Theory of Metals*, 2nd ed. (Cambridge University, Cambridge, England, 1965), p. 208.

[16]B. Abeles and S. Meiboom, Phys. Rev. 101, 544 (1956).

[17]H. C. Montgomery, J. Appl. Phys. 42, 2971 (1971).

[18]N. P. Ong, Phys. Rev. B 17, 3243 (1978).

[19]N. P. Ong and P. Monceau, Phys. Rev. B 16, 3443 (1977).

[20]Measurements of R^∞ on three samples give 2.37×10^{-6}, 1.41×10^{-6}, and 1.28×10^{-6} m^3/C. The values of n, p and the mobilities reported here as well as the data on the anisotropy apply to the third sample. In Fig. 5 the computed Hall constant has been multiplied by a scale factor of 1.85 to compare with the previously published measurements on sample 1 (Ref. 6).

[21]N. P. Ong (unpublished).

[22]L. M. Falicov, A. B. Pippard, and P. R. Sievert, Phys. Rev. 151, 498 (1966).

[23]L. M. Falicov and M. J. Zuckermann, Phys. Rev. 160, 372 (1967).

[24]R. M. Fleming, D. E. Moncton, and D. B. McWhan, Bull. Am. Phys. Soc. 23, 425 (1978).

[25]B. Horovitz, H. Gutfreund, and M. Weger, Phys. Rev. B 12, 3174 (1975).

Effect of Impurities on the Anomalous Transport Properties of $NbSe_3$

N. P. Ong, J. W. Brill, J. C. Eckert, and J. W. Savage[a]
Department of Physics, University of Southern California, Los Angeles, California 90007

and

S. K. Khanna and R. B. Somoano
Jet Propulsion Laboratory, California Institute of Technology, Pasadena, California 91103

(Received 17 October 1978)

Studies on the effect of charged (Ti) and uncharaged (Ta) impurities on the non-Ohmic behavior of and microwave absorption in $NbSe_3$ show that (1) the characteristic field E_0 increases as c^2 (c = Ta concentration), in agreement with a recent calculation by Lee and Rice; (2) the microwave absorption is suppressed by impurities; and (3) charged impurities are strikingly more effective in supressing the anomalous properties. These conclusions provide very strong evidence for Fröhlich sliding-mode conductivity in the nominally pure compound.

The central question[1] in the study of charge-density-wave (CDW) or Peierls systems may very well be whether collective modes are significant in the conductivity in the CDW phase. The striking, anomalous transport properties[2,3] discovered in $NbSe_3$ below the two phase transitions at T_1 (142 K) and T_2 (58 K) have aroused much interest in this regard. Recent electron[4] and x-ray[5] diffraction measurements have confirmed superlattice formation at both T_1 and T_2, and it now appears certain that these anomalous properties are due to excitations in the CDW condensate. Below T_1 and T_2 $NbSe_3$ is non-Ohmic. It also shows a strong absorption mode at micro-

wave frequencies.[3] The small dc fields E (50 mV/cm near T_2; 1 V/cm near T_1) required to suppress the anomalies as well as the small photon energies (4×10^{-5} eV) absorbed in the microwave measurements have defied all theoretical analyses[3,6] unless it is postulated that a macroscopic number of charges couples coherently to the applied fields.

As first discussed by Fröhlich,[7] the condensation of an incommensurate CDW breaks the translational symmetry. The zero-energy excitation associated with this broken symmetry is rigid motion of the CDW. In a real crystal, however, defects will pin[8] the CDW. The application of a sufficiently high electric field will depin the condensate leading to non-Ohmic conductivity. Also weak ac fields will cause segments of the CDW to oscillate about the pinning centers, leading to an absorption mode near the resonance frequency. This model predicts that increasing the impurity concentration c will increase the characteristic depinning field E_0, as well as the pinning frequency (by stiffening the spring constant). Charged impurities are also expected to pin the condensate more strongly than uncharged ones. Recently Lee and Rice (LR)[9] have applied this model in detail to $NbSe_3$, and predict that E_0 increases as c^2 in the weak-pinning (uncharged impurities) case. The first test of these ideas is the study of the effects of impurities on the anomalous properties. Our data confirm all the qualitative arguments described above, and provide experimental verification of the c^2 dependence of E_0 as well.

Impurities were introduced by first forming the master alloy $Nb_{1-x}M_x$ (M = Ta or Ti). Several remelting and cutting cycles were performed to achieve good homogeneity. The alloyed compound $Nb_{1-x}M_xSe_3$ was then grown as described by Meerschaut and Rouxel.[10] The starting Nb metal had a nominal concentration of 180 ppm Ta. We have used the residual resistivity ratio (RRR, denoted also as $\mathcal{R}$) to monitor sample purity. [A plot of $\mathcal{R}$ versus the nominal concentration of Ta impurities c_1 shows that $1/\mathcal{R}$ obeys the equation $1/\mathcal{R} = (5.2\pm0.2)\times10^{-3} + (19\pm2)c_1 (c_1 < 3\times10^{-3})$. In general[11] we may write $1/\mathcal{R} \propto c$, where c ($= c_0 + c_1$) is the *total* concentration of impurities and defects, and c_0 the concentration of defects excluding Ta impurities.] Details of the non-Ohmic[3] and microwave experiments[12] have previously appeared.

Below both T_1 and T_2 the dc conductivity obeys the empirical behavior[3] $\sigma(E,T) = \sigma_a(T) + \sigma_b(T) \times \exp[-E_0(T)/E]$. This equation is valid in all samples studied. The characteristic field E_0 is strongly temperature dependent (Fig. 1, inset), attaining a minimum value E_0^{min} a few degrees below T_2. This minimum provides a convenient and unambiguous quantity for comparison from sample to sample.[13] For each sample E_0^{min} is determined by measuring E_0 at four temperatures bracketing the minimum. We have plotted in Fig. 1, E_0^{min} vs $\mathcal{R}^{-1}$ for each Ta-doped sample. Since $\mathcal{R}^{-1}$ is linear in c, E_0^{min} varies as c^2 (solid line). A least-squares fit to the data gives $E_0^{min} = 447\mathcal{R}^{-1.87}$ V/cm. Also apparent in Fig. 1 is that in the low-c limit the data for E_0 show *no* sign of saturation. Annealing of the purest samples may produce a further decrease in E_0. (Our results indicate that a RRR much larger than 200 cannot be obtained by further removal of Ta impurities.) It should be very interesting to see how low a depinning field one can attain in a real solid. The effect of charged impurities (Ti) has also been studied. A concentration of 1000 ppm Ti

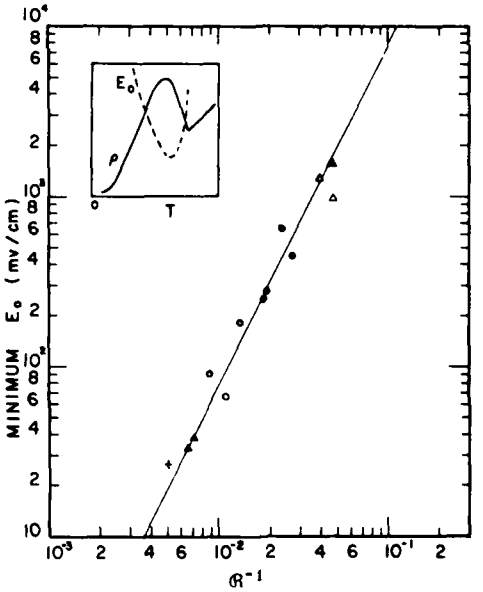

FIG. 1. The minimum characteristic field E_0 for each sample vs the reciprocal of its residual resistivity ratio (RRR). The nominal Ta impurity concentration c_1 is 1900 ppm (open triangles), 1300 ppm (closed circles), 300 ppm (open circles), and 180 ppm (closed triangles). Values for a sample quoted in Ref. 5 are shown as plus sign. The solid line has slope 2.0. Since $\mathcal{R}^{-1}$ is linear in c, E_0^{min} varies as c^2, in agreement with calculations in Ref. 9. The inset shows the temperature dependence of E_0 below T_2 (58 K).

nails down the condensate to the extent that no Ohmic breakdown could be observed (although a lower bound of 6 V/cm may be inferred.) This is to be compared to a typical value of 300 mV/cm for Ta impurities in the same concentration. The variation of E_0 with the RRR in two samples has also been reported by Fleming, Moncton, and McWhan.[5]

The effects of both Ta and Ti impurities on the microwave absorption mode are shown in Fig. 2. The absorption strength is proportional to the difference between the dc and ac data for each sample. As the Ta concentration increases (moving up in the figure) one sees the suppression of the anomalous absorption mode. The data are consistent with the pinning frequency changing monotonically with the increasing impurity concentration. Again it is also clear that Ti impurities have a more drastic effect on the microwave absorption than a similar concentration of Ta (samples *B* and *D*). No dc Ohmic breakdown was observed (up to a field of 6 V/cm) in samples *A* (50 000 ppm Ta), *B* (1000 ppm Ti), and *C* (5000 ppm Ta).

Since claims on anomalous effects which are highly sensitive to sample purity have been controversial in the past, it appears essential that an independent monitor of sample purity be used. For each sample studied we have measured the width of the critical divergence of $d\ln\rho/dT$ (ρ is the low-field resistivity) at T_2 as well as T_2 itself. In Fig. 3 data from five samples show the monotonic correlation between the RRR on the one hand, and the width and T_2 on the other. The latter thus provide an independent measure of the sample purity.

The failure of the usual Drude model (to explain the anomalous transport properties in the CDW phase) can be quantitatively discussed using energy considerations. Equating the minimum field energy ($E_0 \sim 40$ mV/cm) picked up by an electron to the thermal fluctuation energy at 50 K we find that the mean free path must be of the order of 0.1 cm—a truly macroscopic distance. (This is indefensible, particularly when a two-band analysis[14] of $NbSe_3$ based on all available galvanomag-

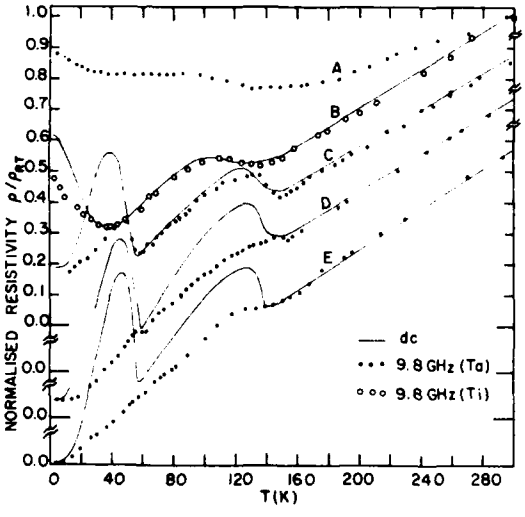

FIG. 2. The temperature dependence of the resistivity at 9.8 GHz for various samples of $Nb_{1-x}M_xSe_3$ (M = Ta or Ti). The solid line is the dc resistivty for each sample. As discussed in the text the absorption mode is suppressed with increasing impurity concentration (moving up in figure). The nominal concentrations/RRR are (50 000 ppm Ta)/1.14 (curve *A*), (1000 ppm Ti)/1.58 (curve *B*), (5000 ppm Ta)/2.99 (curve *C*), (1900 ppm Ta)/ 18.2 (curve *D*), and (300 ppm Ta)/115 (curve *E*). Ti impurities are more effective in suppressing the absorption mode than Ta. For clarity the data for curves *C*, *D*, and *E* have been displaced downwards.

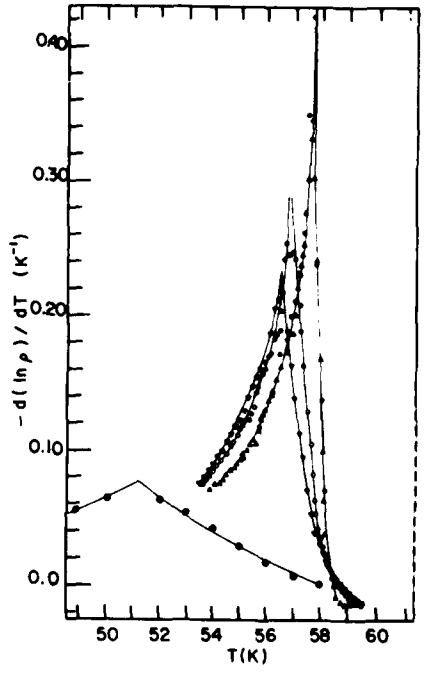

FIG. 3. Critical divergence of $d\ln\rho/dT$ at T_2 for five samples showing the decrease in T_2 and the broadening of the transition with increasing c_1. The Ta concentrations/RRR are (5000 ppm)/3 (circles within circles), (1900 ppm)/25 (inverse triangles), (1300 ppm)/42 (open circles), (300 ppm)/91 (closed circles), and (180 ppm)/111 (triangles).

netic data shows that the uncondensed carriers have a rather ordinary mobility of 3000 $cm^2/V\,s$ at 50 K comparable to that in Ge at 300 K.) Similar attempts using single-particle theory to explain the extra microwave absorption (for example, by the photogeneration of carriers across minigaps or out of traps) lead to gap or trap sizes which are $(1/100)kT$, which is clearly untenable. Models based on the partial destruction of the CDW state by the applied E field can also be ruled out experimentally. The transition temperatures T_1 and T_2 are not affected by the highest applied fields.[2] More significantly, direct observation of the superlattice spot intensity by Fleming, Moncton, and McWhan[5] shows no change in intensity under fields strong enough to suppress the T_2 anomaly by half.

In Ref. 9, one of the mechanisms for non-Ohmic behavior discussed by LR is the depinning of a rigid CDW domain of length L by an applied field. Equating the energy gained from the field to the pinning energy of a domain, LR get the estimate (in the weak-pinning case)

$$E_0 = \frac{1}{e\bar{\rho}\rho_{eff}2\pi/Q}\,\frac{1}{|\psi|^2}\,\frac{(\rho_i V)^4 c^2}{f_0^3(\xi_x\xi_y\xi_z)^2}.$$

Here ψ is the order parameter, $\rho_i V$ the impurity potential, ξ_i the coherence length along i, and Q the spanning vector. The c^2 dependence is verified by our data. Using reasonable numbers, LR calculate E_0 to be 10 mV/cm for $c = 10^{-5}$, which corresponds to $\mathcal{R}^{-1} \sim 5.2\times10^{-3}$. This is in order-of-magnitude agreement with the data in Fig. 1. However, neither the nonmonotonic temperature dependence of E_0 nor the field dependence of $\sigma(E,T)$ is accounted for in LR's zero-temperature calculation. These remain serious problems in the model.

In conclusion our results show that the non-Ohmic behavior at dc and the strong absorption mode at 9.8 GHz are intrinsic to the nominally pure compound, and easily suppressed by weak concentrations of impurities. Charged impurities (Ti) are strikingly more effective in suppressing these anomalous properties than uncharged ones (Ta). The measured c^2 dependence of E_0^{min} agrees with LR's calculations based on the depinning of a CDW domain. These results provide the strongest evidence to date for the Fröhlich mechanism in a CDW metal.

We have benefitted from discussions with P. A. Lee, T. M. Rice, S. E. Trullinger, and K. Maki. This work was supported in part by the U. S. Office of Naval Research (N00014-77-C0473) and in part by the National Aeronautics and Space Administration (NAS7-100).

---

[a] Also at Materials Science Department, University of Southern California.

[1] See Proceedings of the Conference on Quasi-One-Dimensional Conductors, Dubrovnik, Yugoslavia, 1978 (to be published).

[2] P. Monceau, N. P. Ong, A. M. Portis, A. Meerschaut, and J. Rouxel, Phys. Rev. Lett. 37, 602 (1976).

[3] N. P. Ong and P. Monceau, Phys. Rev. B 16, 3443 (1977).

[4] T. Tsutsumi, T. Takagaki, M. Yamamoto, Y. Shiozaki, M. Ido, and T. Sambongi, Phys. Rev. Lett. 39, 1675 (1977).

[5] R. M. Fleming, D. E. Moncton, and D. B. McWhan, Bull. Am. Phys. Soc. 23, 425 (1978), and Phys. Rev. B 18, 5560 (1978).

[6] N. P. Ong, Phys. Rev. B 17, 3243 (1978).

[7] H. Fröhlich, Proc. Roy. Soc. London, Ser. A 223, 296 (1954).

[8] P. A. Lee, T. M. Rice, and P. W. Anderson, Solid State Commun. 14, 703 (1974).

[9] P. A. Lee and T. M. Rice, Phys. Rev. B (to be published).

[10] A. Meerschaut and J. Rouxel, J. Less-Common Met. 39, 197 (1975).

[11] At 4.2 K galvanomagnetic and Shubnikov measurements show that the uncondensed carriers in $NbSe_3$ are highly degenerate (Fermi energy $\gg \hbar/\tau$). This rules out diffuse hopping as a conductivity mechansim. Thus the dominant effect of Ta impurities on the carriers is to shorten their lifetimes τ. This implies that $\mathcal{R}^{-1}$ is linear in c.

[12] S. K. Khanna, E. Ehrenfreund, A. B. Garito, and A. J. Heeger, Phys. Rev. B 10, 2205 (1974).

[13] E_0 varies smoothly with respect to both c and T. In all the samples studied the E_0 vs T curves are qualitatively similar, all ataining a minimum a few degrees below T_2. Insofar as E_0^{min} isolates the c dependence of E_0 (with temperature effects contributing to second order only) we may use the zero-temperature Lee-Rice result. In practice this is justified since E_0^{min} varies by two orders of magnitude whereas the temperature at which E_0^{min} occurs varies by only a few percent.

[14] N. P. Ong, Phys. Rev. B 18, 5272 (1978).

Electric-Field-Dependent Thermopower of $NbSe_3$

R. H. Dee and P. M. Chaikin
Department of Physics, University of California, Los Angeles, California 90024

and

N. P. Ong
Department of Physics, University of Southern California, Los Angeles, California 90007

(Received 31 October 1978)

We have measured the thermoelectric power of $NbSe_3$ in the temperature range, 10–70 K, where charge-density-wave formation and strongly nonlinear conductivity has been reported. We report the first observation of an electric-field–dependent thermopower. Our results for $NbSe_3$ show that in the presence of an electric field there is an additional negative contribution to the thermopower. Possible mechanisms which may account for this are discussed.

There has been a great deal of recent interest in the non-Ohmic behavior observed in systems which undergo charge-density-wave (CDW) instabilities.[1,2] Upon application of an electric field, the electrical conductivity is found to rise dramatically when a certain threshold is surpassed. This effect is often found in quasi-one-dimensional conductors with tetrathiafulvalene tetracyanoquinodimethane[2] (TTF-TCNQ) and $NbSe_3$ (Ref. 1) as primary examples. A variety of models have been proposed to explain the nonlinear characteristics.[3-5] Since the models predict different types of charge carriers, thermoelectric power (TEP) measurements can contribute to the understanding of the nature of the carriers.

In this Letter we report on TEP measurements performed on $NbSe_3$ in the presence of an electric field. This is the first time that thermopower has been used to probe nonlinear effects in any material and consequently the first time that an electric-field–dependent TEP has been observed. Below the 59-K CDW transition the measurements show an increase in the magnitude of the TEP as electric field is increased, the limiting value approaching the TEP observed above the 59-K transition. Since a collective mode (i.e., sliding CDW) by itself would produce a reduced (or zero) TEP, the present work implies that some other mechanism is responsible for the observed increase in TEP and conductivity.

In the experiments we have measured both the electrical resistance and the TEP of $NbSe_3$ as a function of both temperature and electric field. The experimental situation is governed by the transport equation

$$\vec{E} = \vec{J}\rho(E) + S(E)\nabla T,$$

where $\vec{E}$ is the electric field, $\vec{J}$ is the electric current density, ∇T is the temperature gradient, and for $NbSe_3$ both $\rho(E)$ and $S(E)$ are dependent on the electric field at temperatures below 142 K.[1] In order to measure the TEP in a high electric field we have to superimpose a heat current onto an electric current passing through the sample and measure the incremental voltage caused by the subsequent temperature difference. Use of a steady current $\vec{J}$ to produce the electric field proved to be difficult, as a large dc voltage is produced if the mean temperature of the sample changes. This is due to the strong temperature dependence of the resistance in $NbSe_3$. On applying heat to produce a temperature gradient in the sample even small changes in temperature cause this voltage to be much larger than the thermoelectric voltage. To eliminate this problem a low-frequency ac current was applied to the sample via a dc blocking capacitor. The dc voltages across the sample were measured after the ac background was eliminated by passing the signal through a PAR-113 amplifier set at dc with a suitable rolloff filter. Use of ac electric fields give similar experimental conditions to dc as the same breakdown effects are observed. However, measured values of $\rho(E)$ would differ slightly as the ac measurement would take a different average over the nonlinear region. Any incremental dc effect superimposed on the ac field would be made in the nonlinear region although the actual value of the effective applied electric field would depend on the characteristics of the current-versus-voltage (I-V) curve. These conditions were checked by superimposing a small dc current (10 μA) upon the applied ac current and the observed dc voltage was reduced above the threshold current as expected. Thus for a thermoelectric measurement we can be confident that we are in the nonlinear region and the observed effects confirm this.

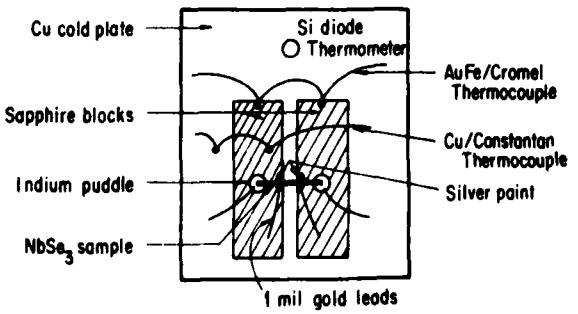

FIG. 1. The experimental arrangement used.

The experimental configuration is shown in Fig. 1. A needle of $NbSe_3$ was thermally anchored to two sapphire blocks with indium solder and silver paint which acted as current and voltage contacts, respectively. The thermoelectric measurements were made differentially by switching heat from one sapphire block to the other alternately in the presence of a constant ac current. This enabled the thermoelectric voltage to be distinguished from any dc offsets. The resulting voltages and temperature differences were measured using conventional nanovoltmeters and thermocouples. The low temperatures were achieved by attaching the assembly to an Air Products Dixplex refrigeration system.

Initially, measurements of the non-Ohmic resistance were made in the region of the low-temperature CDW transition. This was documented in three forms (i) by measuring the I-V characteristic at various temperatures; (ii) by measuring the dc resistance using a small constant current (10 μA) at various values of the applied ac current; and (iii) by sweeping the temperature with various ac sample currents and monitoring the ac voltage. The resulting R-vs-T data [using method (iii)] are shown in Fig. 2(a). As can be

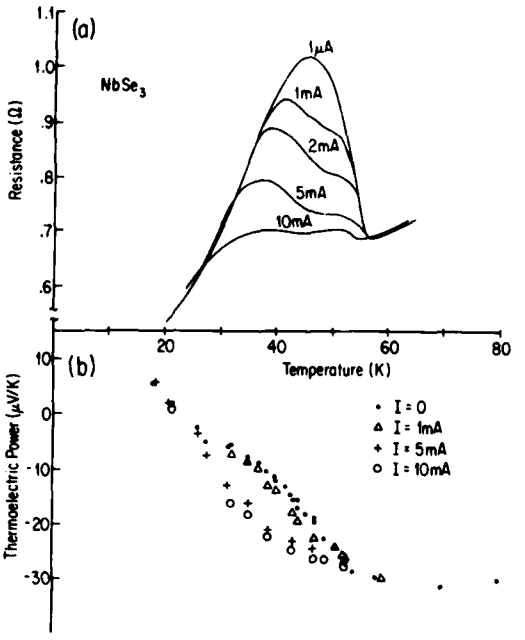

FIG. 2. (a) The electrical resistance and (b) the thermoelectric power of $NbSe_3$ as a function of temperature between 10 and 80 K at several values of the applied ac current.

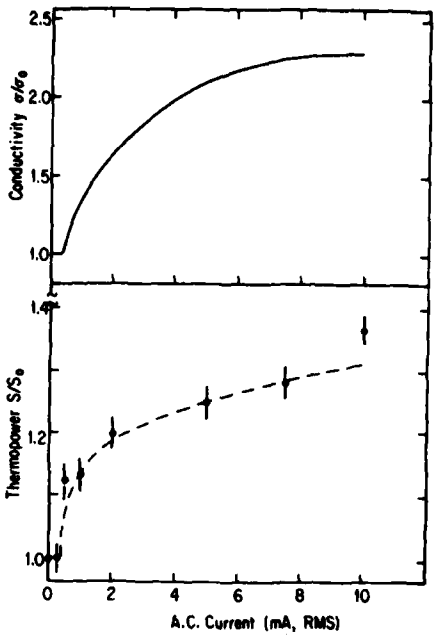

FIG. 3. The electrical conductivity and thermoelectric power of $NbSe_3$ as a function of applied current at $T = 47$ K, normalized to values in the limit of zero current.

seen the electric field breakdown is similar to that observed previously,[1] and for the current levels used sample heating is only evident in the highest current level used (i.e., 10 mA).

The TEP data in this non-Ohmic region is shown in Fig. 2(b). The zero-applied-electric-field data shown as the closed circles are similar to those obtained by others.[6] As the sample current (i.e., the applied electric field) is increased, the TEP increases for electric fields above some threshold value in similar fashion to the electrical conductance. This is illustrated in Fig. 3 which shows the dependence of both R and S on the applied current at $T = 47$ K and the threshold value is the same in each case. The resistance curves in Figs. 2(a) and 3 are similar to the data of Monceau *et al.*,[1] and both R and S tend to saturate to values consistent with an extrapolation of data above the CDW transition to lower temperatures.

Attempts were also made to observe similar effects at the higher-temperature CDW transition in this material, but due to the higher sample currents required to see the breakdown effects, sample heating was a greater problem. However, a few measurements in this region indicated a decrease in TEP toward the value obtained above 145 K although no accurate data were obtained.

Several models have been proposed to explain the non-Ohmic conductivity in $NbSe_3$. In the original experimental papers[1,3] the nonlinear characteristics were fitted to a Zener tunneling model with the unphysically small gap value inferred from the breakdown field. The possibility that hot-electron effects may be responsible for such effects has been discussed for TTF-TCNQ,[2] but since these materials have undergone a charge-density-wave transition, several groups[2-4,7] have suggested that the electric field effects are related to excitations of the CDW. If the incommensurate CDW is weakly pinned, an electric field should be able to depin it, and a contribution to the conductivity would result from the sliding CDW in a manner similar to that proposed by Fröhlich.[8] If the CDW is more strongly pinned, it may still be possible to observe nonlinear effects due to the creation of low-energy charged excitations such as solitons.[5]

The TEP rules out some of these models. In the case of Zener tunneling or hot-electron effects, the added carriers are in energy states considerably above the Fermi energy. They would therefore transport a good deal of heat and produce a large contribution to the TEP similar to that observed in semiconductors. The magnitude of the TEP increases with electric field only to the value of $-30\ \mu V/K$ which was found above the CDW transition and no higher. It is then unlikely that the Zener tunneling or hot electron models are appropriate.

Recent x-ray measurements[9] show that the lattice distortion in $NbSe_3$ remains unchanged in the presence of electric fields high enough to show non-Ohmic behavior, which implies that the CDW remains intact under such conditions. This means that models involving solitons or depinning charge density waves can be discussed.

In a soliton model, the electric field creates charged soliton-antisoliton pairs which are mobile and increase the conductivity. While the TEP of a soliton gas has not yet been calculated, the probable result would be similar to that of a semiconductor whose gap is the sum of the soliton-antisoliton rest mass and whose mobilities are given by the soliton dispersion relations and scattering rates. Since these calculations have not been performed, it is possible that a soliton model may explain our results. It is, however, unusual that in an electric field the TEP tends to return to the value obtained above the CDW transition. This would imply that the mobility and energy distribution of the solitons is similar to that

of the electrons above the transition, or that some fortuitous cancelation has occurred.

If the additional conductivity in the non-Ohmic region is due to a depinned sliding charge-density wave, the carriers involved are in a condensate. This condensed state of electron-hole pairs results from a situation in which a finite fraction of conduction electrons occupy their ground-state configuration. The condensate has no entropy and can transport no heat and therefore produces no TEP. The situation is similar to that which arises in conventional superconductors where the TEP drops to zero at the transition temperature, the supercurrent arising from a condensate with no entropy. Therefore a sliding charge-density wave *by itself* will not contribute to the measured TEP which means that some other mechanism must exist in order to explain the observed contribution to the TEP.

The most direct interpretation of the TEP data is that the applied field is freeing the single-particle carriers which have been frozen at the CDW transition. This would result in the TEP returning to a value consistent with the pretransition value (which is observed) and also be consistent with the observed saturation of the conductivity. However, this implies that the CDW is being depleted by the electric field which appears incompatible with the interpretation of the x-ray data mentioned earlier.

In conclusion, we have reported the first observation of a nonlinear or electric-field–dependent thermopower. Our results suggest that sliding charge-density waves alone, Zener tunneling, or hot-electron effects are not responsible for the observed thermopower. The simplest interpretation involves the electric-field breakdown of the charge-density–wave state. In the light of recent x-ray studies on $NbSe_3$ it is clear that further work is required to resolve this.

We would like to acknowledge useful discussions with S. Alexander, A. J. Berlinsky, J. W. Brill, T. Holstein, P. Monceau, R. Orbach, and P. Pincus. This research was supported in part by the National Science Foundation, Grant No. DMR 76-83421 and in part by the U. S. Office of Naval Research, under Grant No. N00014-77-C-0473. One of us (P.M.C.) acknowledges receipt of an A. P. Sloan Foundation Fellowship.

[1]P. Monceau, N. P. Ong, A. M. Portis, A. Meerschaut, and J. Rouxel, Phys. Rev. Lett. 37, 602 (1976).

[2]M. J. Cohen, P. R. Newman, and A. J. Heeger, Phys. Rev. Lett. 37, 1500 (1976).

[3]N. P. Ong and P. Monceau, Phys. Rev. B 16, 3443 (1977).

[4]M. J. Rice, S. Strassler, and N. R. Scheider, in *One-Dimensional Conductors*, edited by H. G. Schuster (Springer, Berlin, 1975), Chap. 19.

[5]M. B. Fogel, S. E. Trullinger, A. R. Bishop, and J. A. Krumhansl, Phys. Rev. Lett. 36, 1411 (1976).

[6]J. K. Dwak, R. L. Greene, P. M. Chaikin, and N. P. Ong, to be published; T. Takagaki, M. Ido, and T. Sambongi, J. Phys. Soc. Jpn. Lett. 45, 2039 (1978).

[7]P. Haen, J. M. Mignot, P. Monceau, and M. Núñez Regueiro, J. Phys. (Paris), Colloq. 2, Suppl. No. 8, C6-703 (1978).

[8]H. Fröhlich, Proc. Roy. Soc. London, Ser. A 223, 296 (1954).

[9]R. M. Fleming, D. E. Moncton, and D. B. McWhan, Phys. Rev. B 18, 5560 (1978).

thus the addition of Ta must do more than just squeeze the $NbSe_3$ lattice.

In conclusion, we have seen that by adding 5% Ta to $NbSe_3$ we obtain a three dimensional, anisotropic superconductor with a $T_c = 1.55 \pm 0.2K$. The addition of Ta suppresses the low temperature CDW by slightly lowering its transition temperature and greatly reducing its amplitude, thus allowing superconductivity.

Acknowledgement - We would like to thank P. Pincus and R. Dee for stimulating discussions.

REFERENCES

1. CHAUSSY, J., HAEN, P., LASJAUNIAS, J.C., MONCEAU, P., WAYSAND, G., WAINTAL, A., MEERSCHAUT, A., MOLINIÉ, P. and Rouxel, J., Solid State Commun. 20, 759 (1976).
2. WILSON, J.A., DISALVO, F.J. and MAHAJAN, S., Adv. Phys. 24, 117 (1975).
   TSUTSUMI, T., TAKAGAKI, T., YAMMAMOTO, M., SHIOZAKI, Y., IDO, M. and SAMBONGI, T., Phys. Rev. Lett. 39, 1675 (1977).
   FLEMING, R.M., MONCTON, D.E. and McWHAN, D.B., Bull. Am. Phys. Soc. 23, No. 3, 425 (1978); Phys Rev. B., Nov. 15, 1978, to appear.
3. MONCEAU, P., ONG, N.P., PORTIS, A.M., MEERSCHAUT, A. and ROUXEL, J., Phys Rev. Lett. 37, 602 (1976).
4. ONG, N.P. and MONCEAU, P., Phys. Rev. B 16, 3443 (1977).
5. MONCEAU, P., PEYRARD, J., RICHARD, J. and MOLINIÉ, P., Phys. Rev. Lett. 39, 161 (1977).
6. HAEN, P., MIGNOT, J.M., MONCEAU, P. and NÚÑEZ REGUEIRO, M., Journal de Physique C-6, 703 (1978).
7. FLEMING, R.M., POLO JR., J.A. and COLEMAN, R.V., Phys. Rev. 17, 1634 (1978).
8. SAMBONGI, T., YAMAMOTO, M., TSUTSUMI, K., SHIOZAKI, Y., YAMAYA, K. and ABE, Y., J. Phys. Soc. Japan 42, 1421 (1977).
9. BILBRO, G. and McMILLAN, W.L., Phys. Rev. B 14 1887 (1976).
   BERTHIER, C., MOLINIÉ, P. and JÉROME, DL, Solid State Commun. 18, 1393 (1976).
   CHU, C.W., DIATSCHENKO, V., HUANG, C.Y. and DISALVO, F.J., Phys. Rev. B 15, 1340 (1977).
10. HAEN, P., WAYSAND, G., BOCH, G., WAINTAL, A., MONCEAU, P., ONG, N.P. and PORTIS, A.M., Journal de Physique 37, 179 (1976).
11. ONG, M.I., BRILL, G.W., ECKERTS, J.C., SAVAGE, K.W., KHANNA, S.K. and SOMOANO, R.B., unpublished.
12. KWAK, J.F., GREENE, R.L., CHAIKIN, P.M. and ONG, N.P., unpublished.
13. MEERSCHAUT, A. and ROUXEL, J., Journal of the Less Common Metals 39, 197 (1977).
14. AZEVEDO, L.J., CLARK, W.G., DEUTSCHER, G., GREENE, R.L., STREET, G.B. and SUTTER, L.J., Solid State Commun. 19, 197 (1976).
15. KWAK, J.F., GREENE, R.L. and FULLER, W.W., to be published.
16. ONG, N.P. and BRILL, J.W., Phys. Rev. B, Nov. 15, 1978, to appear.
17. HAEN, P., LA PIERRE, F., MONCEAU, P., NÚÑEZ REGUEIRO, M. and RICHARD, J., to be published.
18. DEE, R.H., DOLLARD, D.H., TURRELL, B.G. and CAROLAN, J.F., Solid State Commun. 24, 469 (1977).

the coherence lengths from figure 3. One finds that $\xi_{\parallel}(0) \sim 230\text{Å}$ and $\xi_{\perp}(0) \sim 98\text{Å}$. This leads to an anisotropy, $\varepsilon^{-1} = \xi_{\parallel}/\xi_{\perp} = H_{\parallel}/H_{\perp}$ of 2.37. The anisotropic effect mass theory predicts that ε^{-1} is independent of temperature as long as $\xi(T)$ is larger than the interchain distance. In $NbSe_3$ the interchain distance is ~ 4Å from X-ray data.[13] $TaSe_3$ has a similar interchain distance[8] therefore one would expect the same for $Nb_{.95}Ta_{.05}Se_3$. Thus the condition is fulfilled for all T. As can be seen in Table 1, ε^{-1} is independent of temperature with a value of 2.39 ± 0.02. This is consistent with the anisotropic effective mass theory. Another check of the applicability of this model is to check the angular dependence of the critical field. This study is currently underway.

Table 1 The anisotropy of the critical fields of $Nb_{.95}Ta_{.05}Se_3$ as a function of temperature. The points below 0.6K are from the extrapolated data. $H_{\parallel}$ and $H_{\perp}$ are the parallel and perpendicular critical fields respectively.

T	$H_{\parallel}$	$H_{\perp}$	$\varepsilon^{-1} = H_{\parallel}/H_{\perp}$
1.2	4.55	1.88	2.42
1.0	8.78	3.69	2.38
0.8	12.75	5.35	2.38
0.6	16.25	6.82	2.38
0.4	19.34	8.05	2.40
0.2	21.50	9.06	2.37
0.	22.30	9.38	2.38

$Nb_{.95}Ta_{.05}Se_3$ is not like the anisotropic superconductor $(SN)_x$ where the anisotropy is due to $(SN)_x$'s filamentary nature.[14] In $Nb_{.95}Ta_{.05}Se_3$ the Hc_2 versus T curve does not show the anomalous concave behaviour near $T = T_c$ that was observed in $(SN)_x$.[14] The Hc_2 versus T curve comes in linearly to the axis at T_c for both parallel and perpendicular fields in $Nb_{.95}Ta_{.05}Se_3$ (figure 3). It has been seen in $(SN)_x$ that the perpendicular critical field loses its concave behaviour near T_c when bromine is added. This has been interpreted as being due to more coupling between the fibers.[15] The anisotropic effective mass model is not applicable to $(SN)_x$[14] since ε^{-1} is not independent of temperature.

The addition of Ta appears to cause the $NbSe_3$ to become more three dimensional. Ong and Brill[16] have found an anisotropy in the conductivity of $NbSe_3$ of $\sigma_{\parallel}/\sigma_{\perp} = 20 \pm 5$; while from our critical field measurements we find an anisotropy of 2.39 ± 0.02 for $Nb_{.95}Ta_{.05}Se_3$. This shows the Ta doped samples are less anisotropic than the pure $NbSe_3$. Another sign of the Ta making $NbSe_3$ more three dimensional is the fact that in three dimensional materials CDW's do not have as pronounced an effect on the resistance as they do in one dimensional ones, and we see a decrease in the CDW in the Ta doped samples. The superconducting transition is sharp, ~ 10% T_c or ~ 30% Hc_2, which is another characteristic of three dimensional superconductors. Thus the difference in anisotropy between $NbSe_3$ and $Nb_{.95}Ta_{.05}Se_3$ could be due to the fact that $NbSe_3$ is quasi one-dimensional while the Ta doped material is three dimensional.

In pure $TaSe_3$ Haen et al[17] report a T_c of less than 1.5K. Fleming et al[7] and Sambongi et al[8] report a T_c of 2.1K in $TaSe_3$. Thus, the T_c of $Nb_{.95}Ta_{.05}Se_3$ is of the same order as that of $TaSe_3$. Sambongi et al[8] also say that at 1.25K or 0.6 T_c, Hc_2 is 1.3 kOe while 10 kOe parallel to the chain only recovers one fourth of the normal state. This leads to an anisotropy of greater than 7.7. Thus it appears that $Nb_{.95}Ta_{.05}Se_3$ is less anisotropic than $TaSe_3$. From looking at Hc_2 for 0.6 T_c = .92K one sees that $Hc_{2\perp}$ in $Nb_{.95}Ta_{.05}Se_3$ is three times the $Hc_{2\perp}$ in $TaSe_3$, whereas $Hc_{2\parallel}$ is smaller. From this one can say that we are not seeing strands of $TaSe_3$ undergoing the superconducting transition.

It is possible that the Ta in $Nb_{.95}Ta_{.05}Se_3$ is squeezing the $NbSe_3$ lattice. From pressure studies[5] it is known that $NbSe_3$ goes superconducting under pressure; the CDW are also suppressed under pressure. Haen et al[10] find that $dT_{CDW}/dP = -4\text{K/kbar}$. We see a change in the temperature of the higher temperature CDW of 7.5 ± 2K in $Nb_{.95}Ta_{.05}Se_3$ (figure 1). This would correspond to a pressure of 1.9 ± 0.5 kbar. According to Monceau et al[5] $NbSe_3$ goes superconducting at ~ 1.1K under a pressure of ~ 2 kbar. This is in rough agreement with our T_c for $Nb_{.95}Ta_{.05}Se_3$ of 1.5K. Monceau et al[5] measured the magnetic susceptibility to see the superconducting transition whereas we have measured the transition resistively, and this may account for the difference.[18] There can be a difference in T_c due to the two methods of measureing T_c. However a pressure of 2 kbar is not enough to completely smear out the lower CDW in $NbSe_3$,

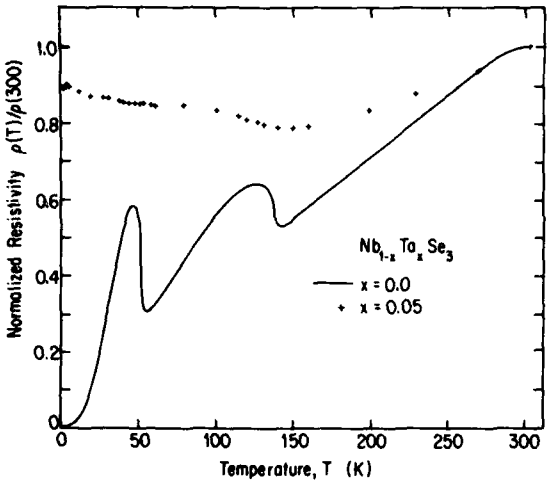

Figure 1 The resistivity normalized to the room temperature value as a function of temperature for representative $NbSe_3$ and $Nb_{.95}Ta_{.05}Se_3$ samples.

~ 125 in the pure $NbSe_3$ to 1 - 1.7 in the Ta doped samples. It is expected that the actual Ta doping is 5 ± 1%. This can account for the differences in the Ta doped samples. The thermopower studies[12] also indicate slight variations in Ta concentration in samples from the nominal 5% Ta batch.

The resistivity of the pure and doped samples for T < 4.2K, normalized to the 4.2K values, is shown in figure 2. The pure $NbSe_3$ displays no transition (to 0.5K) just a low temperature tail which levels off at about 3.5K. The Ta doped samples show a superconducting transition with T_c = 1.55 ± .2K, where T_c is the midpoint of the resistive transition and the error represents 10 to 90% of the transition as well as deviations from sample to sample. Two of our samples did not have their resistances go completely to zero, although their residual resistance was less than 10% of their resistance at 4.2K. This is probably due to sample inhomogeneities. There was no observable hysteresis in the transition when the samples were cooled and warmed through T_c.

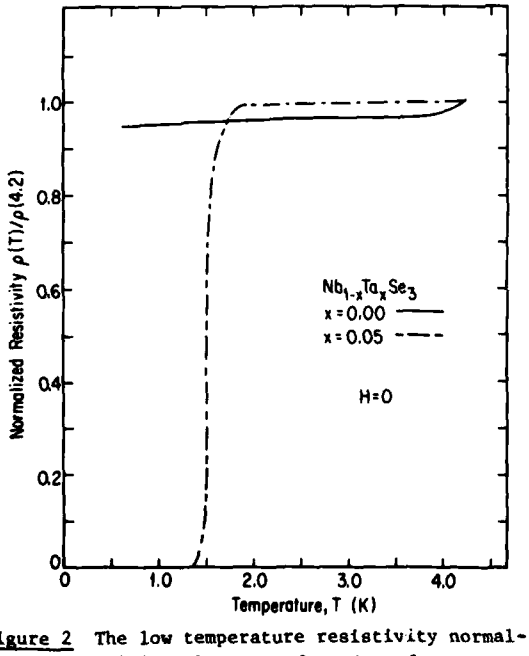

Figure 2 The low temperature resistivity normalized to the 4.2K value as a function of temperature in zero magnetic field. The samples are the same as those in figure 1.

In figure 3 we have plotted the upper critical field, Hc_2, versus T for two Ta doped samples. Hc_2 was taken as the midpoint in the resistive transition. The fields were approximately (± 5°) perpendicular and parallel to the chain direction. The bars represent the 10 - 90% transition width. The sharpness of the transition can be seen in the insert in figure 3.

From the data one can estimate the critical field at zero temperature $Hc_2(0)$. One finds

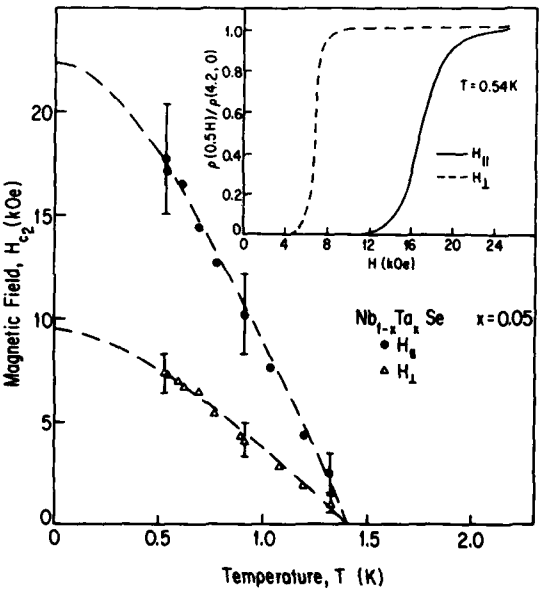

Figure 3 The upper critical field Hc_2, parallel and perpendicular, as a function of temperature for $Nb_{.95}Ta_{.05}Se_3$. The dashed lines are a least squares fit of the data to the Abrikosov-Gor'kov universal function. The resistive transitions as a function of magnetic field at T = 0.54K are shown in the insert.

$Hc_{2\parallel}(0)$ ~ 22 kOe while $Hc_{2\perp}$ ~ 9 kOe. For an anisotropic superconductor, the Ginsburg-Landau (GL) theory of superconductivity gives

$$\frac{dH_{\parallel}}{dT} = \frac{\phi_o}{2\pi\xi_{\perp}^2 T_c} \quad \text{and} \quad \frac{dH_{\perp}}{dT} = \frac{\phi_o}{2\pi\xi_{\parallel}\xi_{\perp} T_c},$$

where $\phi_o = 2 \times 10^{-7}$ Oe-cm^2, $\xi_{\parallel}$ is the GL coherence length along the chain direction and $\xi_{\perp}$ is the coherence length in the transverse direction. Using these expressions one can calculate

Solid State Communications, Vol.30, pp.689-692.
Pergamon Press Ltd. 1979. Printed in Great Britain.

SUPERCONDUCTIVITY IN $Nb_{.95}Ta_{.05}Se_3$

W.W. Fuller,[+] P.M. Chaikin[*]

Department of Physics, University of California[**]
Los Angeles, California 90024, USA

and

N.P. Ong
Department of Physics, University of Southern California[++]
Los Angeles, California 90007, USA

(Received 20 February by A.A. Maradudin)

We have measured the resistivity of $NbSe_3$ doped with 5% Ta from room temperature down to 0.5K and compared our results with similar measurements on pure $NbSe_3$. The pure sample remains normal to the lowest temperature (0.5K), whereas the doped sample has a sharp transition to the superconducting state with $T_c = 1.5 \pm 0.2$K. Measurements of the critical magnetic field indicate that the Ta doped samples are homogeneous, anisotropic three dimensional superconductors.

The transition metal trichalcogenides, $NbSe_3$ and $TaSe_3$, are highly anisotropic metals. $NbSe_3$ has two anomalies in its resistivity as a function of temperature, one at 145K and the other at 59K. The anomalies have been identified as charge density wave (CDW) transitions.[1,2] Below these transitions, $NbSe_3$ shows striking nonohmic behaviour.[3,4] From magnetization measurements Monceau et al[5] do not see any sign of superconductivity down to 50 mK under atmospheric pressure in $NbSe_3$, however a drop in its resistance between 2.2K and 1.5K to a plateau and then a linear drop below 0.4K is seen by Haen et al.[6]

In $TaSe_3$ there are no resistive anomalies.[7,8] Two groups, Fleming et al[7] and Sambongi et al,[8] report that $TaSe_3$ is superconducting at atmospheric pressure with a transition temperature, T_c of ~ 2.0 - 2.1K.

It has previously been suggested[9] that CDW formation and superconductivity are antagonistic, both competing for states near the Fermi surface. The $NbSe_3$-$TaSe_3$ system is therefore interesting for studying this competition. Pressure measurements[5] on pure $NbSe_3$ have shown an increase in superconductivity from $T_c = 0$ to T_c ~ 2.5K with a pressure of 7 kbar. Pressure also suppresses the CDW.[10] It both lowers the temperature at which the resistive anomalies occur and diminishes the size of the anomalies. Thus it appears, from the measurements on $NbSe_3$, that by suppressing the CDW one is able to obtain superconductivity.

In the present study we have used the alloying of $NbSe_3$ with $TaSe_3$ to suppress the CDW transition in a quite separate way. The addition of 5% $TaSe_3$ to $NbSe_3$ is sufficient to smear the CDW transition and produce a T_c comparable to that of $TaSe_3$.

We have measured the resistivity, ρ, versus temperature, T, for several samples of $Nb_{.95}Ta_{.05}Se_3$ and $NbSe_3$. The samples were ribbon like with typical dimensions being 4.5 mm long, 0.01 - 0.02 mm wide for those samples with Ta, 0.02 - 0.04 mm wide for $NbSe_3$, and ~ 0.006 mm thick. The resistance was measured along the chain direction using the usual four probe method with 1 mil gold leads silver painted to the sample. The low temperatures were achieved in a He^3 cryostat, the samples being either in gaseous He^3 or submerged in liquid He^3 depending on the temperature. Both DC and low frequency (< 100 Hz) AC measurements were taken with a current through the samples of 1 μA. The AC measurements were performed with a lock-in voltmeter. Critical field measurements were made on the superconducting samples by monitoring the resistance while sweeping a magnetic field at constant temperature (± 2 mk).

The resistivity, normalized to its room temperature value, is shown in figure 1 for both the pure $NbSe_3$ and Ta doped samples. Here one can see that the CDW's smear out with the addition of the Ta impurity. The lower temperature CDW anomaly is almost nonexistent. Ong et al[11] have done a much more detailed study of this transition. In thermopower measurements Kwak et al[12] have also seen that the 145K transition is less affected than the 59K transition for the 5% doping. Those samples with Ta are much more disordered than the pure $NbSe_3$ samples. The resistivity ratio, $\rho(300)/\rho(4.2)$, changes from

---

+ IBM Predoctoral Fellow
* A.P. Sloan Foundation Fellow
** Work supported by the Office of Naval Research under grant # N00014-76-C-1078
++ Work supported by the Office of Naval Research under grant # N0014-77-0473